TWO-DIMENSIONAL OSCILLATING FLOW OVER A STEP

By

DOUGLAS CARL HOFER

A THESIS PRESENTED TO THE GRADUATE SCHOOL
OF THE UNIVERSITY OF FLORIDA IN
PARTIAL FULFILLMENT OF THE REQUIREMENTS
FOR THE DEGREE OF MASTER OF SCIENCE

UNIVERSITY OF FLORIDA

1987

TWO-DIMENSIONAL OSCILLATING FLOW OVER A STEP

By

DOUGLAS CARL HOFER

A THESIS PRESENTED TO THE GRADUATE SCHOOL
OF THE UNIVERSITY OF FLORIDA IN
PARTIAL FULFILLMENT OF THE REQUIREMENTS
FOR THE DEGREE OF MASTER OF SCIENCE

UNIVERSITY OF FLORIDA

1987

ACKNOWLEDGMENTS

I first express gratitude to Dr. Tom I-P. Shih for his invaluable guidance and essential encouragement during the course of my research. I also thank Dr. Shih for his exceptional help in preparing this manuscript. I am grateful to Dr. R. A. Gater and Dr. U. H. Kurzweg for serving on my master's committee. In particular, I am indebted to Dr. Gater for his editorial completeness.

Finally, I thank my wife whose patience, encouragement, moral support and hard work made this study possible.

TABLE OF CONTENTS

LIST OF TABLES

NOMENCLATURE

A_1 - amplitude of oscillation for left piston

A_2 - amplitude of oscillation for right piston

d - see Eq. (4.4-2)

e - total energy--see Eq. (3.1-5)

H_1 - height of left piston--see Fig. 2-1

H_2 - height of right piston--see Fig. 2-1

IL - number of grid points in the ξ-direction--see Fig. 4-2

IP - grid point corresponding to $\xi = \xi(0,t)$--see Fig. 4-2

JL - number of grid points in the η-direction--see Fig. 4-2

JP - grid point corresponding to $\eta = \eta(H_2)$--see Fig. 4-2

k - thermal conductivity

L_1 - position about which left piston moves

L_3 - position about which right piston moves

L_η - operator--see Eq. (4.2-15)

L_ξ - operator--see Eq. (4.2-14)

m - ρu

n - ρv

P - pressure

q''_x - heat flux in the x-direction

q''_y - heat flux in the y-direction

R - universal gas constant

T - temperature

t - time coordinate in the physical domain

u - x-component of velocity

$\hat{u}$ - internal energy

v - y-component of velocity

V_{LP} - velocity of left piston--see Eq. (2-6)

V_{RP} - velocity of right piston--see Eq. (2-7)

x - coordinate in physical domain--see Figs. 2-1 and 4-1

x_{LP} - position of left piston--see Fig. 2-1 and Eq. 2-1

x_{RP} - position of right piston--see Fig. 2-1 and Eq. 2-2

y - coordinate in physical domain--see Figs. 2-1 and 4-1

Greek

α_1 - phase shift for left piston--see Eqs. (2-1) and (2-6)

α_2 - phase shift for right piston--see Eqs. (2-2) and (2-7)

β - stretching parameter--see Eqs. (4.1-5) and (4.1-7)

γ - ratio of specific heats

η - spatial coordinate in transformed domain--see Fig. 4-2

μ - dynamic viscosity

ξ - spatial coordinate in transformed domain--see Fig. 4-2

ρ - density

τ - time coordinate in transformed domain

τ_{xx} - shear stress defined by Eq. (3.1-6)

τ_{yy} - shear stress defined by Eq. (3.1-7)

τ_{xy} - shear stress defined by Eq. (3.1-8)

τ_{yx} - shear stress defined by Eq. (3.1-8)

ω_2 - frequency of oscillation for left piston--see Eq. (2-1)

ω_1 - frequency of oscillation for right piston--see Eq. (2-2)

Subscripts

i - grid point location in the ξ-direction

j - grid point location in the η-direction

LP - left piston

RP - right piston

^{0} - initial position

x - differentiation with respect to x

y - differentiation with respect to y

t - differentiation with respect to t

ξ - differentiation with respect to ξ

η - differentiation with respect to η

τ - differentiation with respect to τ

Superscripts

n - n^{th} time level

$\overline{n+1}$ - $(n+1)^{th}$ time level

n+1 - a fictitious $(n+1)^{th}$ time level

* - dummy time index corresponding to n

** - dummy time index corresponding to n+1

Abstract of Thesis Presented to the Graduate School
of the University of Florida in Partial Fulfillment of the
Requirements for the Degree of Master of Science

TWO-DIMENSIONAL
OSCILLATING FLOW OVER A STEP

By

DOUGLAS CARL HOFER

December 1987

Chairman: Dr. Tom I-P. Shih
Major Department: Mechanical Engineering

A computer program was developed that can be used to study oscillating flows past a two-dimensional step in which the oscillation is induced by two oscillating pistons, one on each side of the step. The computer program was based on the conservation equations of mass momentum, and total energy valid for unsteady, laminar flow of an ideal gas. The computer program generated numerical solutions to the conservation equations by using the time-split method of MacCormack.

To demonstrate the usefulness of the computer program for studying oscillating flows past a two-dimensional step, the computer program was used to study the velocity field of three different types of flows past a step. The three types of flows studied were

1. Steady flows past a step
2. Oscillating flows past a step with the pistons oscillating in phase

3. Oscillating flows past a step with pistons oscillating out of phase

It is noted that the two types of oscillating flows investigated here have never been studied by previous investigators.

The velocity fields generated by the computer program for these three types of flows are presented in graphical form, to illustrate the flow patterns. Analysis of the flow patterns indicated that the computer program is useful for studying oscillating flows past a two-dimensional step.

CHAPTER I

INTRODUCTION

The physics of oscillating flows past solid surfaces have attracted the attention of many investigators. Stokes and Rayleigh studied the oscillating flow induced by a flat plate undergoing sinusoidal oscillations in a plane parallel to the plate [1]. Rayleigh [2], Andrade [3], Schlicting [4], and Davidson [5] studied the oscillating flow induced by a circular cylinder oscillating in a plane perpendicular to its axis. Roy [6] performed a similar study except instead of oscillating a circular cylinder, he oscillated an axially symmetric ellipsoid in a plane perpendicular to its major axis. Lin [7] studied an oscillating flow past a stationary flat plate in which the free stream velocity far away from the wall oscillated about some mean value. Steger [8] and Chyu et al. [9] studied dynamic stall from oscillating airfoils. Sexl [10], Uchida [11], Brocher [12], Watson [13], and Kurzweg [14, 15] studied oscillating flows inside very long pipes. Finally, references 16 to 37 report studies of the oscillating flow inside piston-cylinder configurations that resemble reciprocating-piston engines.

The above account of previous studies on oscillating flows is far from complete. However, it does indicate the wide interest displayed toward such flows.

To date, the author knows of no study reporting the physics of oscillating flow past a two-dimensional step induced by two oscillating pistons, one on each side of the step. A good understanding of the physics of such oscillating flows is important to the design of certain types of heat exchangers [14, 15].

The objectives of this investigation are as follows:

1. Develop a computer program based on the conservation equations of mass, momentum, and energy that can be used to study the physics of oscillating flows past a step.
2. Vectorize the computer program so that it will run efficiently on a pipelined computer such as the CRAY XMP.
3. Use the computer program developed to study the flow patterns in the vicinity of the step as a function of amplitude and phase shift of the piston oscillation.

In the next chapter, the problem of oscillating flows past a step that will be investigated here is described. In Chapter III, the governing equations for this problem are presented. Afterwards, Chapter IV describes the numerical method employed to obtain solutions. Chapter V presents the results obtain by the numerical method. Finally, in Chapter VI, a brief summary is given.

CHAPTER II

DESCRIPTION OF PROBLEM

A schematic diagram of the two-dimensional step region considered in this study is shown in Fig. 2-1. As shown in the figure, the boundaries for this region consist of three fixed solid walls (surfaces 2,3, and 4), two movable pistons (surfaces 1 and 5), and a plane of symmetry (surface 6). Oscillating flow is induced in the region by sinusoidal movement of the pistons.

The position of the left piston (surface 1) at time t is given by the following equation:

$$x_{LP} = -L_1 - A_2 * \cos(\omega_2 t + \alpha_1) \qquad (2\text{-}1)$$

$$0 \leq y \leq H_1$$

Please refer to the nomenclature for the definition of the terms in Eq. (2-1). The position of the right piston (surface 5) at time t is given by:

$$x_{RP} = L_3 - A_2 * \cos(\omega_2 t + \alpha_2) \qquad (2\text{-}2)$$

$$0 \leq y \leq H_2$$

The locations of the three fixed walls (surfaces 2, 3, and 4) are defined by the following expressions

$$\text{Surface 2:} \quad y = H_1, \quad x_{LP} \leq x \leq 0 \qquad (2\text{-}3)$$

$$\text{Surface 3:} \quad x = 0, \quad H_1 \leq y \leq H_2 \qquad (2\text{-}4)$$

$$\text{Surface 4:} \quad y = H_2, \quad 0 \leq x \leq x_{RP} \qquad (2\text{-}5)$$

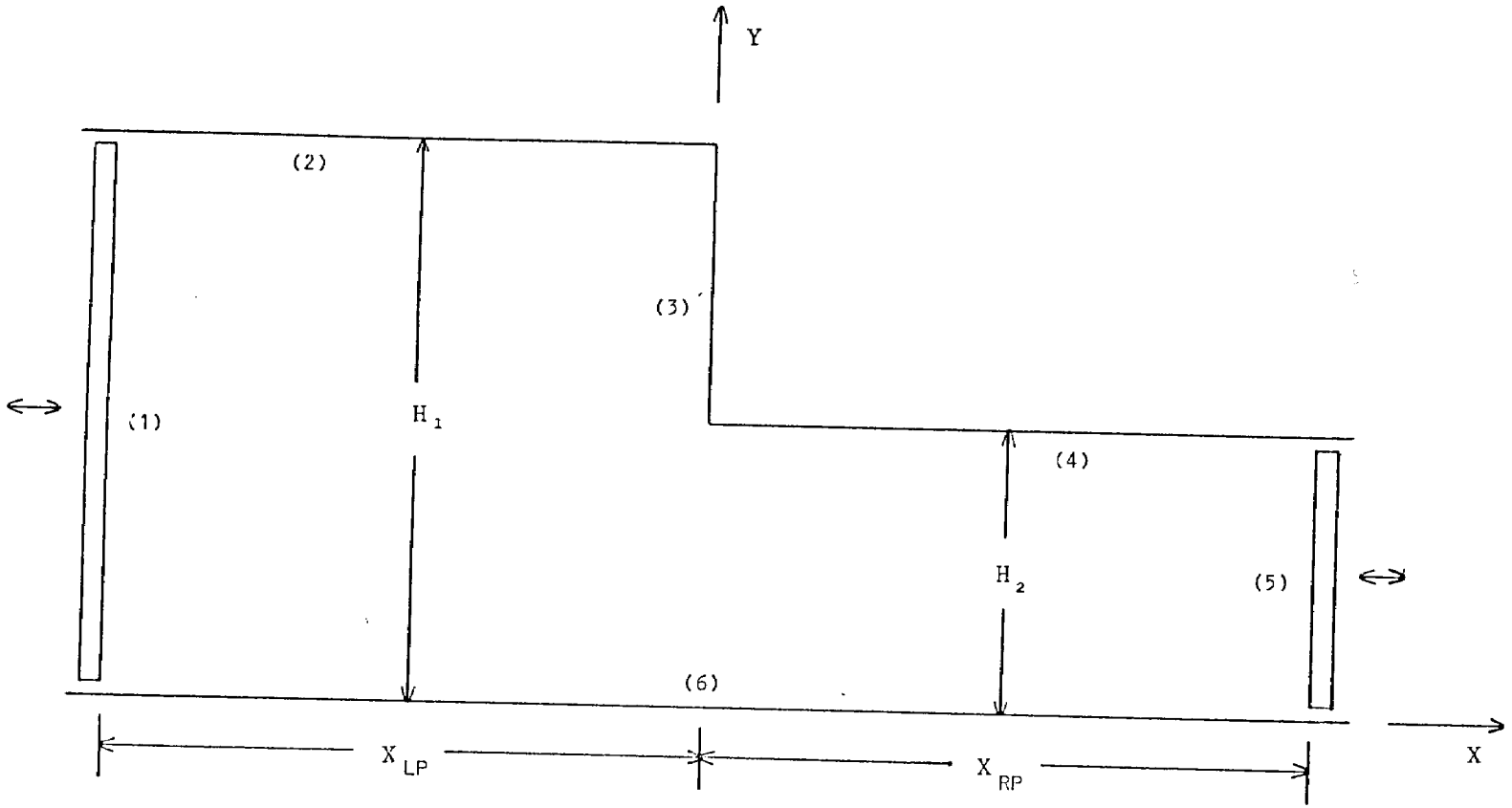

Figure 2-1. Schematic diagram of region studied

The velocities of the two pistons (surfaces 1 and 5) are given by

$$V_{LP} = A_1 * \omega_1 * \sin(\omega_1 t + \alpha_1) \qquad (2\text{-}6)$$

$$V_{RP} = A_2 * \omega_2 * \sin(\omega_2 t + \alpha_2) \qquad (2\text{-}7)$$

The above two equations are derived by differentiating Eq. (2-1) and (2-2) with respect to time. The values of A_1, A_2, ω_1, and ω_2 are chosen so that the maximum Reynolds number is less than 400, i.e.:

$$Re = \frac{\rho UH}{\mu} < 400$$

where:

ρ = density at t=0 (see Section 3.2)

U = maximum velocity of the small piston

H = height of the smaller piston

This ensures that the flow in the region will be laminar [38].

The three fixed walls (surfaces 2, 3, and 4 in Fig. 2-1) are adiabatic, while the two piston faces (surfaces 1 and 5) are maintained at a constant temperature of 300 K. There was no leakage around the pistons so the mass of the gas in the region remains fixed.

Initially, the two pistons are located as specified by Eqs. (2-1) and (2-2) with t set equal to zero and the region is filled with a stagnant gas at a uniform temperature of 300 K and a uniform pressure of 1 atm. At time t equal to zero, the two pistons begin to move according to Eqs. (2-6) and (2-7) resulting in oscillating flow past a step (the step is formed by surfaces 2, 3, and 4).

CHAPTER III

FORMULATION OF PROBLEM

The equations that govern the problem described in Chapter II are the conservation equations of mass, x-momentum, y-momentum, and total energy valid for unsteady, compressible flow of a viscous and thermally conducting ideal gas. In this numerical study, the following simplifications were made to the conservation equations: (i) all thermodynamic and transport properties were taken to be constants, (ii) gravity force was not considered and, (iii) bulk viscosity was taken to be zero. Below, the governing equations and corresponding initial and boundary conditions in Cartesian coordinates are first presented. These equations are then cast in generalized coordinates to facilitate the numerical method of analysis.

3.1 Governing Equations in Cartesian Coordinates

The conservation equations in cartesian coordinates and an inertial reference frame are summarized in Table 3-1. Equations (3.1-1) to (3.1-4) constitute a closed system in four dependent variables: density (ρ), x-momentum (ρu), y-momentum (ρv), and total energy per unit volume (e). The definition of total energy per unit volume (e) is given by Eq. (3.1-5). The relationships for the shear stress terms in Eqs. (3.1-1) to (3.1-4) are given by Eqs. (3.1-6) to (3.1-8). Expressions for pressure and temperature in terms of the four dependent variables are given by Eqs. (3.1-9) and (3.1-10). These expressions were derived by

Table 3-1. Conservation equations in cartesian coordinates

Continuity equation

$$\frac{\partial \rho}{\partial t} + \frac{\partial \rho u}{\partial x} + \frac{\partial \rho v}{\partial y} = 0 \qquad (3.1\text{-}1)$$

X-momentum equation

$$\frac{\partial \rho u}{\partial t} + \frac{\partial}{\partial x}\rho u^2 + \frac{\partial}{\partial y}\rho uv = -\frac{\partial P}{\partial x} + \frac{\partial \tau_{xx}}{\partial x} + \frac{\partial \tau_{yx}}{\partial y} \qquad (3.1\text{-}2)$$

Y-momentum equation

$$\frac{\partial \rho v}{\partial t} + \frac{\partial}{\partial x}\rho uv + \frac{\partial}{\partial y}\rho v^2 = -\frac{\partial P}{\partial y} + \frac{\partial \tau_{xy}}{\partial x} + \frac{\partial \tau_{yy}}{\partial y} \qquad (3.1\text{-}3)$$

Total energy equation

$$\frac{\partial e}{\partial t} + \frac{\partial}{\partial x}(e+P)u + \frac{\partial}{\partial y}(e+P)v = \frac{\partial}{\partial x}(\tau_{xx}u + \tau_{xy}v) + \frac{\partial}{\partial y}(\tau_{yx}u + \tau_{yy}v) - \frac{\partial}{\partial x}q''_x - \frac{\partial}{\partial y}q''_y \qquad (3.1\text{-}4)$$

Definition of total energy

$$e = \rho\left(\hat{u} + \frac{v^2}{2} + \frac{u^2}{2}\right) \qquad (3.1\text{-}5)$$

Shear stress relations

$$\tau_{xx} = 2\mu\frac{\partial u}{\partial x} - \frac{2}{3}\mu\left(\frac{\partial u}{\partial x} + \frac{\partial v}{\partial y}\right) \qquad (3.1\text{-}6)$$

$$\tau_{yy} = 2\mu\frac{\partial v}{\partial y} - \frac{2}{3}\mu\left(\frac{\partial u}{\partial x} + \frac{\partial v}{\partial y}\right) \qquad (3.1\text{-}7)$$

$$\tau_{xy} = \tau_{yx} = \mu\left(\frac{\partial u}{\partial y} + \frac{\partial v}{\partial x}\right) \qquad (3.1\text{-}8)$$

Expression for pressure

$$P = (\gamma-1)[e - \tfrac{1}{2}(\rho u^2 + \rho v^2)] \qquad (3.1\text{-}9)$$

Expression for temperature

$$T = \frac{\gamma-1}{\rho R}[e - \tfrac{1}{2}(\rho u^2 + \rho v^2)] \qquad (3.1\text{-}10)$$

using the ideal gas equation of state and the assumption of constant specific heats. For convenience, the conservation equations [Eqs. (3.1-1) to 3.1-4)] combined with the shear stress relations [Eqs. (3.1-6) to (3.1-8)] are cast in vector form. The vector form of these equations are summarized in Table 3-2.

3.2 Boundary and Initial Conditions in Cartesian Coordinates

Boundary and initial conditions must be specified before a solution can be obtained from the governing equations [Eqs. (3.1-1) to (3.1-4)]. The boundary and initial conditions for the problem described in Chapter II are given below.

The no-slip condition for a viscous fluid requires that the fluid velocity immediately adjacent to a solid wall be equal to the wall velocity. For the present problem, this condition can be expressed mathematically as (see Fig. 2-1)

$$u=0,\ v=0 \qquad x=0, \quad H_1 \leq y \leq H_2 \tag{3.2-1}$$

$$y=H_1, \quad x_{LP} \leq x \leq 0 \tag{3.2-2}$$

$$y=H_2, \quad 0 \leq x \leq x_{RP} \tag{3.2-3}$$

$$u=V_{LP},\ v=0 \qquad x=x_{LP}, \quad 0 \leq y \leq H_1 \tag{3.2-4}$$

$$u=V_{RP},\ v=0 \qquad x=x_{RP}, \quad 0 \leq y \leq H_2 \tag{3.2-5}$$

The heat flux on the stationary solid walls (surfaces 2, 3, and 4 in Fig. 2-1) is equal to zero. This condition results in the spatial derivative of temperature in the direction normal to the wall being equal to zero, i.e.,

$$\frac{\partial T}{\partial y}=0 \qquad y=H_1, \quad x_{LP} \leq x \leq 0 \tag{3.2-6}$$

$$y=H_2, \quad 0 \leq x \leq x_{RP} \tag{3.2-7}$$

$$\frac{\partial T}{\partial x}=0 \qquad x=0, \quad H_1 \leq y \leq H_2 \tag{3.2-8}$$

Table 3-2. Conservation equations in vector form

$$\frac{\partial}{\partial t}\underset{\sim}{U} + \frac{\partial}{\partial x}\underset{\sim}{F}(\underset{\sim}{U}) + \frac{\partial}{\partial y}\underset{\sim}{G}(\underset{\sim}{U}) = \frac{\partial}{\partial x}\underset{\sim}{V}_1(\underset{\sim}{U},\underset{\sim}{U}_x) + \frac{\partial}{\partial x}\underset{\sim}{V}_2(\underset{\sim}{U},\underset{\sim}{U}_y) + \frac{\partial}{\partial y}\underset{\sim}{W}_1(\underset{\sim}{U},\underset{\sim}{U}_x) + \frac{\partial}{\partial y}\underset{\sim}{W}_2(\underset{\sim}{U},\underset{\sim}{U}_y) \qquad (3.1\text{-}11)$$

$$\underset{\sim}{U} = \begin{bmatrix} \rho \\ \rho u \\ \rho v \\ e \end{bmatrix} = \begin{bmatrix} \rho \\ m \\ n \\ e \end{bmatrix} \qquad (3.1\text{-}12)$$

$$\underset{\sim}{F}(\underset{\sim}{U}) = \begin{bmatrix} \rho u \\ \rho u^2 + P \\ \rho uv \\ (e+P)u \end{bmatrix} = \begin{bmatrix} m \\ \frac{m^2}{\rho} + P \\ \frac{mn}{\rho} \\ (e+P)\frac{m}{\rho} \end{bmatrix} \qquad (3.1\text{-}13)$$

$$\underset{\sim}{G}(\underset{\sim}{U}) = \begin{bmatrix} \rho v \\ \rho uv \\ \rho v^2 + P \\ (e+P)v \end{bmatrix} = \begin{bmatrix} n \\ \frac{nm}{\rho} \\ \frac{n^2}{\rho} + P \\ (e+P)\frac{n}{\rho} \end{bmatrix} \qquad (3.1\text{-}14)$$

$$\underset{\sim}{V}_1(\underset{\sim}{U},\underset{\sim}{U}_x) = \begin{bmatrix} 0 \\ \frac{4}{3}\mu\frac{\partial u}{\partial x} \\ \mu\frac{\partial v}{\partial x} \\ \frac{2}{3}\mu\frac{\partial}{\partial x}u^2 + \frac{1}{2}\mu\frac{\partial}{\partial x}v^2 + k\frac{\partial T}{\partial x} \end{bmatrix} = \begin{bmatrix} 0 \\ \frac{4}{3}\mu\frac{\partial}{\partial x}\frac{m}{\rho} \\ \mu\frac{\partial}{\partial x}\frac{n}{\rho} \\ \frac{2}{3}\mu\frac{\partial}{\partial x}\left(\frac{m}{\rho}\right)^2 + \frac{1}{2}\mu\frac{\partial}{\partial x}\left(\frac{n}{\rho}\right)^2 + k\frac{\partial T}{\partial x} \end{bmatrix} \qquad (3.1\text{-}15)$$

Table 3-2. Continued

$$\underset{\sim}{V}_2(\underset{\sim}{U},\underset{\sim}{U}_y) = \begin{bmatrix} 0 \\ -\frac{2}{3}\mu\frac{\partial v}{\partial y} \\ \mu\frac{\partial u}{\partial y} \\ \mu v\frac{\partial u}{\partial y} - \frac{2}{3}\mu\frac{\partial v}{\partial y} \end{bmatrix} = \begin{bmatrix} 0 \\ -\frac{2}{3}\mu\frac{\partial}{\partial y}\frac{n}{\rho} \\ \mu\frac{\partial}{\partial y}\frac{m}{\rho} \\ \mu\frac{n}{\rho}\frac{\partial}{\partial y}\frac{m}{\rho} - \frac{2}{3}\mu\frac{\partial}{\partial y}\frac{n}{\rho} \end{bmatrix} \qquad (3.1\text{-}16)$$

$$\underset{\sim}{W}_1(\underset{\sim}{U},\underset{\sim}{U}_x) = \begin{bmatrix} 0 \\ \mu\frac{\partial v}{\partial x} \\ -\frac{2}{3}\mu\frac{\partial u}{\partial x} \\ \mu u\frac{\partial v}{\partial x} - \frac{2}{3}\mu v\frac{\partial u}{\partial x} \end{bmatrix} = \begin{bmatrix} 0 \\ \mu\frac{\partial}{\partial x}\frac{n}{\rho} \\ -\frac{2}{3}\mu\frac{\partial}{\partial x}\frac{m}{\rho} \\ \mu u\frac{\partial}{\partial x}\frac{n}{\rho} - \frac{2}{3}\mu v\frac{\partial}{\partial x}\frac{m}{\rho} \end{bmatrix} \qquad (3.1\text{-}17)$$

$$\underset{\sim}{W}_2(\underset{\sim}{U},\underset{\sim}{U}_y) = \begin{bmatrix} 0 \\ \mu\frac{\partial u}{\partial y} \\ \frac{2}{3}\mu\frac{\partial v}{\partial y} \\ \frac{2}{3}\mu\frac{\partial}{\partial y}v^2 + \frac{1}{2}\mu\frac{\partial}{\partial y}u^2 + k\frac{\partial T}{\partial y} \end{bmatrix}$$

$$= \begin{bmatrix} 0 \\ \mu\frac{\partial}{\partial y}\frac{m}{\rho} \\ \frac{2}{3}\mu\frac{\partial}{\partial y}\frac{n}{\rho} \\ \frac{2}{3}\mu\frac{\partial}{\partial y}\left(\frac{n}{\rho}\right)^2 + \frac{1}{2}\mu\frac{\partial}{\partial y}\left(\frac{m}{\rho}\right)^2 + k\frac{\partial T}{\partial y} \end{bmatrix} \qquad (3.1\text{-}18)$$

Where T and P in terms of the dependent variables are

$$P = (\gamma - 1)\left[e - \frac{1}{2}\left(\frac{m^2}{\rho} + \frac{n^2}{\rho}\right)\right] \qquad (3.1\text{-}19)$$

$$T = \frac{(\gamma - 1)}{\rho R}\left[e - \frac{1}{2}\left(\frac{m^2}{\rho} + \frac{n^2}{\rho}\right)\right] \qquad (3.1\text{-}20)$$

On the piston faces the temperatures are fixed. For these boundaries, the temperature of the gas next to the wall equals the temperature of the wall. This condition yields

$$T=T_{LP} \qquad x=x_{LP}, \quad 0 \leq y \leq H_1 \tag{3.2-9}$$

$$T=T_{RP} \qquad x=x_{RP}, \quad 0 \leq y \leq H_2 \tag{3.2-10}$$

Along the plane of symmetry (surface 6 in Fig. 2-1), the following symmetry conditions apply

$$\frac{\partial \rho}{\partial y}=0 \qquad \frac{\partial u}{\partial y}=0 \tag{3.2-11}$$

$$\frac{\partial e}{\partial y}=0 \qquad v=0$$

Initially, the pistons are located as specified by Eqs. (2-1) and (2-2) with t=0, and the stagnant gas inside the region is at uniform temperature, T_0 and pressure, P_0. The initial conditions corresponding to the above constraints are

$$\rho = \frac{P_0}{RT_0} \qquad e = \frac{P_0}{\gamma-1} \tag{3.2-12}$$

$$u=0 \qquad v=0$$

3.3 Governing Equations in Transformed Coordinates

Solutions to the governing equations summarized in Table 3-2 will be obtained by using a numerical method. In order to allow the numerical method to be implemented more easily, the governing equations will be transformed from the x-y-t coordinate system to the ξ-η-τ coordinate system by the following coordinate transformations

$$\xi = \xi(x,t) \tag{3.3-1}$$

$$\eta = \eta(y) \tag{3.3-2}$$

$$\tau = t \tag{3.3-3}$$

The x-, y-, and t-derivatives can be related to the ξ-, η-, and τ-derivatives as follows:

$$\frac{\partial}{\partial x} = \frac{\partial \xi}{\partial x}\frac{\partial}{\partial \xi} \tag{3.3-4}$$

$$\frac{\partial}{\partial y} = \frac{\partial \eta}{\partial y}\frac{\partial}{\partial \eta} \tag{3.3-5}$$

$$\frac{\partial}{\partial t} = \frac{\partial \xi}{\partial t}\frac{\partial}{\partial \xi} + \frac{\partial}{\partial \tau} \tag{3.3-6}$$

The coordinate system corresponding to ξ, η, and τ constitutes a noninertial frame of reference since ξ is a function of time. Substituting Eqs. (3.1-1) to (3.1-6) into Eqs. (3.1-11) to (3.1-18) yields the governing equations in transformed coordinates which are given in Table 3-3.

3.4 Boundary Conditions in Transformed Coordinates

The boundary conditions must also be transformed according to the transformation given by Eqs. (3.3-1) to (3.3-6). Under this transformation, the no-slip conditions on the solid walls given by Eqs. (3.2-1) to (3.2-5) become

$$u=0, \quad v=0 \qquad \xi=\xi(0,t), \quad \eta(H_1) \leq \eta \leq \eta(H_2) \tag{3.4-1}$$

$$\eta=\eta(H_1), \quad \xi(x_{LP},t) \leq \xi \leq \xi(0,t) \tag{3.4-2}$$

$$\eta=\eta(H_2), \quad \xi(0,t) \leq \xi \leq \xi(x_{RP},t) \tag{3.4-3}$$

$$u=V_{LP}, v=0 \qquad \xi=\xi(x_{LP},t), \quad \eta(0) \leq \eta \leq \eta(H_1) \tag{3.4-4}$$

$$u=V_{RP}, v=0 \qquad \xi=\xi(x_{RP},t), \quad \eta(0) \leq \eta \leq \eta(H_2) \tag{3.4-5}$$

The zero heat flux condition at the solid walls given by Eqs. (3.2-6) to (3.2-8) becomes

$$\frac{\partial T}{\partial \eta}=0 \qquad \eta=\eta(H_1), \quad \xi(x_{LP},t) \leq \xi \leq \xi(0,t) \tag{3.4-6}$$

$$\eta=\eta(H_2), \quad \xi(0,y) \leq \xi \leq \xi(x_{RP},t) \tag{3.4-7}$$

$$\frac{\partial T}{\partial \xi}=0 \qquad \xi=\xi(0,t), \quad \eta(H_1) \leq \eta \leq \eta(H_2) \tag{3.4-8}$$

Table 3-3. Governing equations in transformed coordinates

$$\frac{\partial}{\partial \tau}\underset{\sim}{U} + \xi_t \frac{\partial}{\partial \xi}\underset{\sim}{U} + \xi_x \frac{\partial}{\partial \xi}\underset{\sim}{F}(\underset{\sim}{U}) + \eta_y \frac{\partial}{\partial \eta}\underset{\sim}{G}(\underset{\sim}{U}) = \xi_x \frac{\partial}{\partial \xi}\underset{\sim}{V}_1(\underset{\sim}{U},\underset{\sim}{U}_\xi)$$

$$+ \xi_x \frac{\partial}{\partial \xi}\underset{\sim}{V}_2(\underset{\sim}{U},\underset{\sim}{U}_\eta) + \eta_y \frac{\partial}{\partial \eta}\underset{\sim}{W}_1(\underset{\sim}{U},\underset{\sim}{U}_\xi) + \eta_y \frac{\partial}{\partial \eta}\underset{\sim}{W}_2(\underset{\sim}{U},\underset{\sim}{U}_\eta) \qquad (3.3\text{-}7)$$

Where

$$\underset{\sim}{V}_1(\underset{\sim}{U},\underset{\sim}{U}_\xi) = \begin{bmatrix} 0 \\ \frac{4}{3}\mu \xi_x \frac{\partial u}{\partial \xi} \\ \mu \xi_x \frac{\partial v}{\partial \xi} \\ \frac{2}{3}\mu \xi_x \frac{\partial}{\partial \xi} u^2 + \frac{1}{2}\mu \xi_x \frac{\partial}{\partial \xi} v^2 + k \xi_x \frac{\partial T}{\partial \xi} \end{bmatrix}$$

$$= \begin{bmatrix} 0 \\ \frac{4}{3}\mu \xi_x \frac{\partial}{\partial \xi}\frac{m}{\rho} \\ \mu \xi_x \frac{\partial}{\partial \xi}\frac{n}{\rho} \\ \frac{2}{3}\mu \xi_x \frac{\partial}{\partial \xi}\left(\frac{m}{\rho}\right)^2 + \frac{1}{2}\mu \xi_x \frac{\partial}{\partial \xi}\left(\frac{n}{\rho}\right)^2 + k \xi_x \frac{\partial T}{\partial \xi} \end{bmatrix} \qquad (3.3\text{-}8)$$

$$\underset{\sim}{V}_2(\underset{\sim}{U},\underset{\sim}{U}_\eta) = \begin{bmatrix} 0 \\ -\frac{2}{3}\mu \eta_y \frac{\partial v}{\partial \eta} \\ \mu \eta_y \frac{\partial u}{\partial \eta} \\ \mu v \eta_y \frac{\partial u}{\partial \eta} - \frac{2}{3}\mu u \eta_y \frac{\partial v}{\partial \eta} \end{bmatrix}$$

$$= \begin{bmatrix} 0 \\ -\frac{2}{3}\mu \eta_y \frac{\partial}{\partial \eta}\frac{n}{\rho} \\ \mu \eta_y \frac{\partial}{\partial \eta}\frac{m}{\rho} \\ \mu \frac{n}{\rho} \eta_y \frac{\partial}{\partial \eta}\frac{n}{\rho} \frac{2}{3}\mu \frac{n}{\rho} \eta_y \frac{\partial}{\partial \eta}\frac{n}{\rho} \end{bmatrix} \qquad (3.3\text{-}9)$$

Table 3-3. Continued

$$\underset{\sim}{W}_1(\underset{\sim}{U},\underset{\sim}{U}_\xi) = \begin{bmatrix} 0 \\ \mu\,\xi_x \dfrac{\partial v}{\partial \xi} \\ -\dfrac{2}{3}\,\mu\,\xi_x \dfrac{\partial u}{\partial \xi} \\ \mu\,u\,\xi_x \dfrac{\partial v}{\partial \xi} - \dfrac{2}{3}\,\mu v\,\xi_x \dfrac{\partial u}{\partial \xi} \end{bmatrix}$$

$$= \begin{bmatrix} 0 \\ \mu\,\xi_x \dfrac{\partial}{\partial \xi}\ \dfrac{n}{\rho} \\ -\dfrac{2}{3}\,\mu \xi_x \dfrac{\partial}{\partial \xi}\ \dfrac{m}{\rho} \\ \mu\,\dfrac{m}{\rho}\,\xi_x \dfrac{\partial}{\partial \xi}\ \dfrac{n}{\rho} - \dfrac{2}{3}\,\mu\,\dfrac{n}{\rho}\,\xi_x \dfrac{\partial}{\partial \xi}\ \dfrac{m}{\rho} \end{bmatrix} \qquad (3.3\text{-}10)$$

$$\underset{\sim}{W}_2(\underset{\sim}{U},\underset{\sim}{U}_\eta) = \begin{bmatrix} 0 \\ \mu\,\eta_y \dfrac{\partial u}{\partial \eta} \\ \dfrac{2}{3}\,\mu\,\eta_y \dfrac{\partial v}{\partial \eta} \\ \dfrac{2}{3}\,\mu\,\eta_y \dfrac{\partial}{\partial \eta}\,v^2 + \ \dfrac{1}{2}\,\mu\,\eta_y \dfrac{\partial}{\partial \eta}\,u^2 + \ k\,\eta_y\ \dfrac{\partial T}{\partial \eta} \end{bmatrix}$$

$$= \begin{bmatrix} 0 \\ \mu\,\eta_y \dfrac{\partial}{\partial \eta}\ \dfrac{m}{\rho} \\ \dfrac{2}{3}\,\mu\,\eta_y \dfrac{\partial}{\partial \eta}\ \dfrac{n}{\rho} \\ \dfrac{2}{3}\,\mu\,\eta_y \dfrac{\partial}{\partial \eta}\left(\dfrac{n}{\rho}\right)^2 + \dfrac{1}{2}\,\mu\,\eta_y \dfrac{\partial}{\partial \eta}\left(\dfrac{m}{\rho}\right)^2 + \ k\,\eta_y \dfrac{\partial T}{\partial \eta} \end{bmatrix} \qquad (3.3\text{-}11)$$

and $\underset{\sim}{U}$, $\underset{\sim}{F}$, and $\underset{\sim}{G}$ are given by Eqs. (3.1-12) to (3.1-14) in Table 3-2.

The temperature boundary condition given by Eqs. (3.2-9) to (3.2-10) becomes

$$T=T_{LP} \qquad \xi=\xi(x_{LP},t) \qquad \eta(0) \leq \eta \leq \eta(H_1) \tag{3.4-9}$$

$$T=T_{RP} \qquad \xi=\xi(x_{RP},t) \qquad \eta(0) \leq \eta \leq \eta(H_2) \tag{3.4-10}$$

The symmetry conditions at the plane of symmetry given by Eqs. (3.2-11) become

$$\frac{\partial}{\partial \eta}=0 \qquad \frac{\partial u}{\partial \eta}=0 \tag{3.4-11}$$

$$\frac{\partial e}{\partial \eta}=0 \qquad v=0$$

The initial condition given by Eq. (3.2-12) remains the same in the transformed coordinates.

CHAPTER IV

NUMERICAL METHOD OF SOLUTION

Solutions to the governing equations described in the previous section can only be obtained by using a numerical method. Here, an explicit finite-difference method was used to obtain solutions.

In order to use finite-difference methods, two types of approximations must be made. First, it is necessary to replace the continuous domain of the problem with a system of grid points and time levels. Second, the governing partial differential equations (PDE's) must be replaced by a system of algebraic equations known as finite-difference equations (FDE's).

The two types of approximations mentioned above are described in the next three sections (Section 4.1-4.3). In section 4.4, the procedures used to obtain solutions are given. Finally, in Section 4.5, efforts made to vectorize the computer program are briefly described.

4.1 Grid Points and Time Levels

As noted earlier, in order to apply finite-difference methods, the continuous domain of the problem must be replaced by a system of grid points (grid points are located at the intersections of grid lines) and time levels. Numerical solutions will be found only at grid points and time levels.

Finite-difference methods are most readily applied when the grid points are stationary and uniformly distributed. The purpose of grid

generation is to map moving and nonuniformly distributed grid points in the physical domain (Fig. 4-1) onto a transformed domain (Fig. 4-2) where the grid points are stationary and uniformly distributed. This mapping is accomplished through the appropriate choice of the transformation functions $\xi(x,t)$ and $\eta(y)$ given by Eqs. (3.3-1) and (3.3-2).

In this study, the transformation functions were chosen so that ξ and η vary between 0 and 1. This results in the following grid spacings in the transformed domain

$$\Delta\xi = \frac{1}{IL-1} \qquad \Delta\eta = \frac{1}{JL-1} \tag{4.1-1}$$

where IL denotes the number of grid points between $\xi=0$ and $\xi=1$ along a line of constant η and JL denotes the number of grid points between $\eta=0$ and $\eta=1$ along a line of constant ξ.

For this study, the spacing between adjacent grid lines parallel to the x-axis in the physical domain was constant. This allowed the shearing transformation to be used to determine $\eta(y)$ as follows

$$\eta = \frac{y}{y_{max}} = \frac{y}{H_1} \tag{4.1-2}$$

In order to facilitate finding the function $\xi(x,t)$, the physical domain is divided into three regions as shown in Fig. 4-1. For the center region (region II in Fig. 4-1), the grid spacing in the x-direction is constant and the shearing transformation is used to map this region onto the transformed domain as follows

$$\xi = \xi_1 + \frac{x-x_1}{x_2-x_1}(\xi_2-\xi_1) \qquad x_1 < x < x_2 \tag{4.1-3}$$

The transformations for regions I and III in Fig. 4-1 are similar and only the details for region III will be given here. Region III undergoes two transformations. The first is a shearing transformation

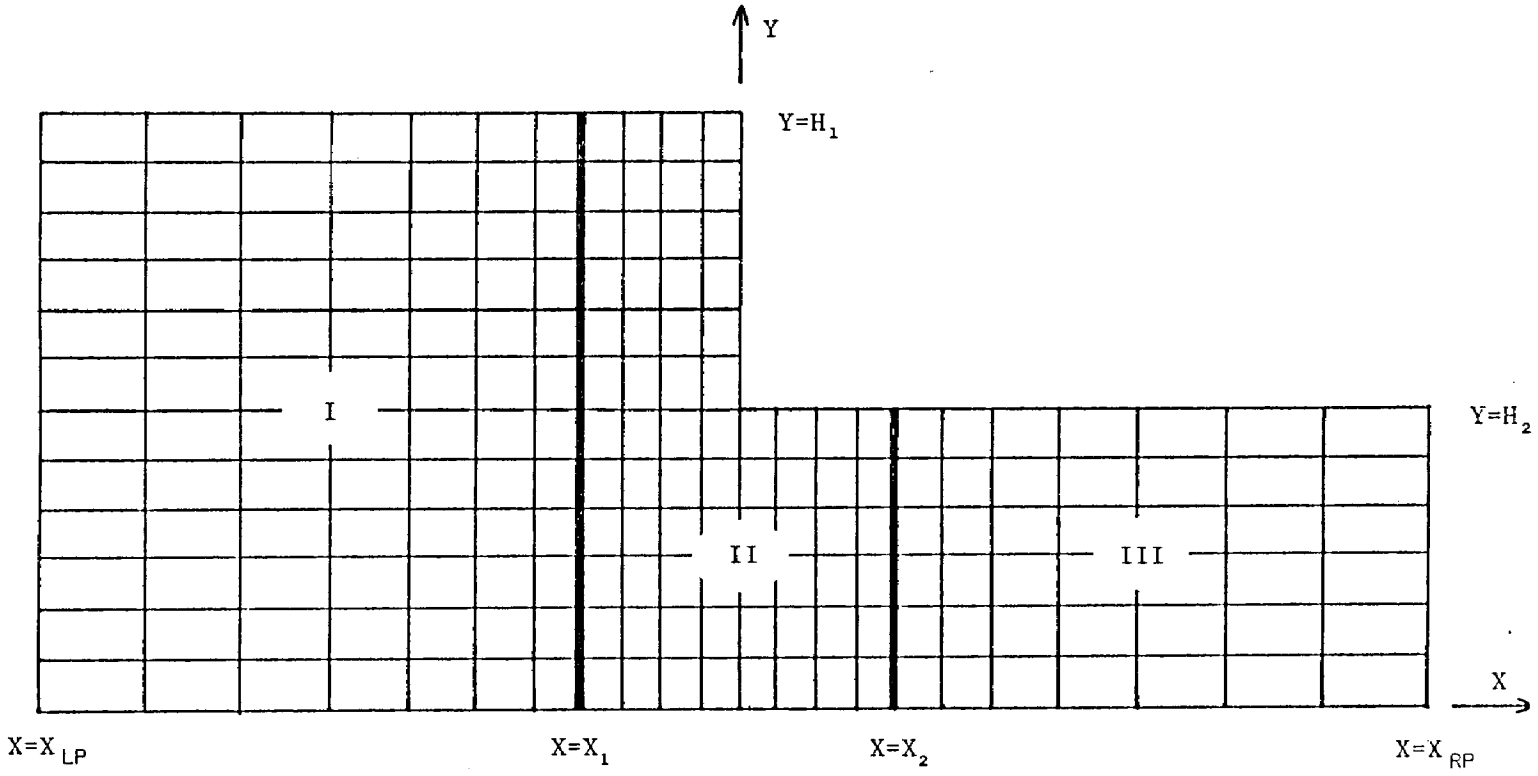

Figure 4-1. Grid system in the physical domain. In the physical domain, grid points (located at intersection of grid lines) are nonuniformly distributed and they move as the two pistons move.

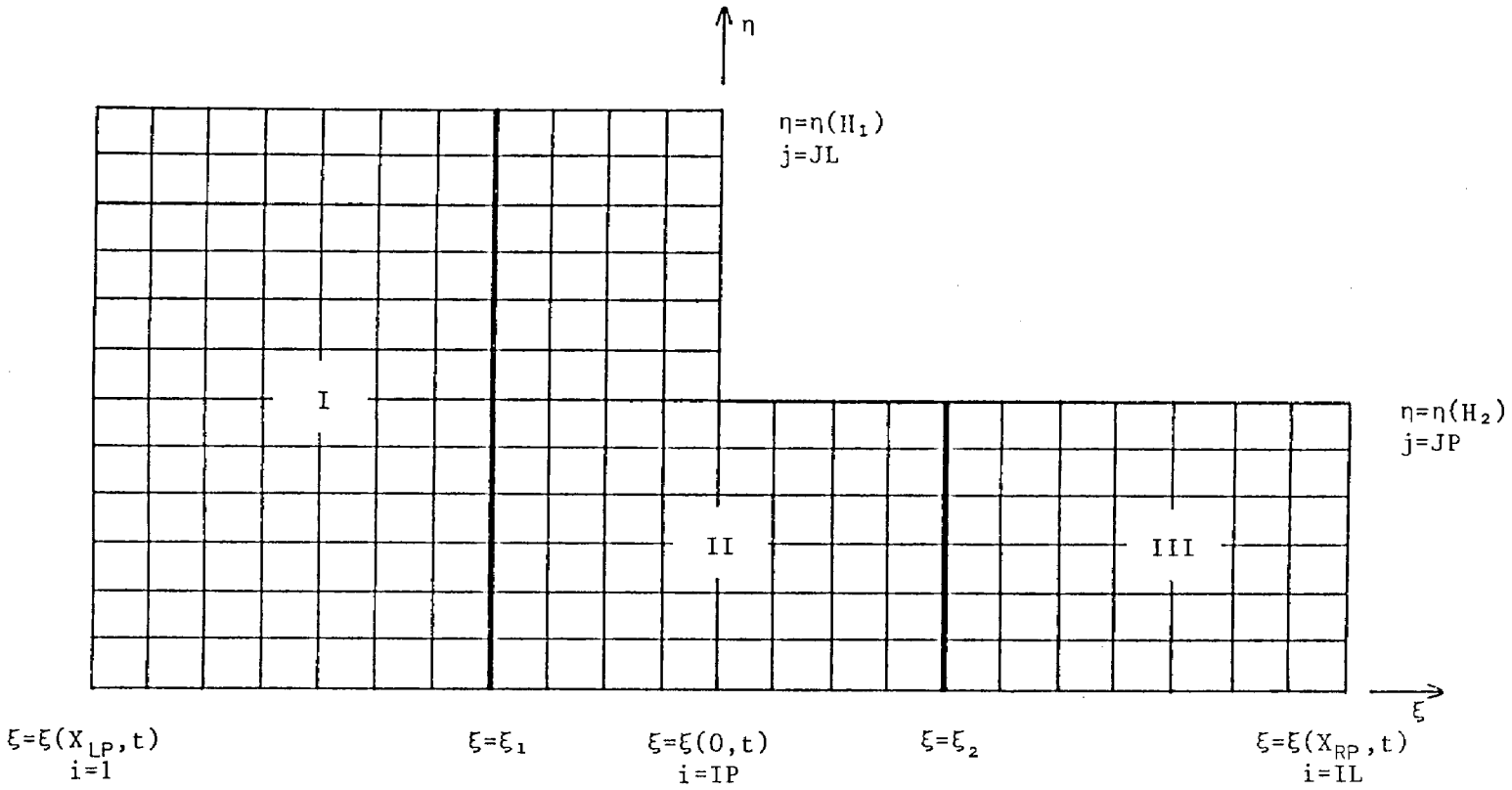

Figure 4-2. Grid system in the transformed domain. In the transformed domain, the grid points are uniformly distributed and stationary regardless of the motion of the two pistons.

based on the piston position (x_{RP}) and the second is a stretching function. The shearing transformation results in an intermediate variable ξ' given by

$$\xi' = \frac{x-x_2}{x_{RP}-x_2} \qquad x_2 < x < x_{RP} \qquad (4.1\text{-}4)$$

The stretching function used is from a family of general stretching functions proposed by Roberts [39,41] and has the form

$$\xi = \xi_2 + \left(1 - \frac{\ln[(\beta+1-\xi')/(\beta-1+\xi')]}{\ln[(\beta+1)/(\beta-1)]}\right)(1-\xi) \qquad 0 < \xi' < 1 \qquad (4.1\text{-}5)$$

where β controls the distribution of grid points. As β approaches 1 the grid spacing near $x=x_2$ becomes smaller and the grid spacing near $x=x_{RP}$ becomes larger. For this study β was solved for iteratively to find a value such that the minimum grid spacing for region III will match the grid spacing for region II. This was done so that grid spacings would change smoothly when going from region II to region III.

As noted earlier, the transformations used for region I were similar to those used for region III and are given below

$$\xi' = 1 - \frac{x-x_{LP}}{x_1-x_{LP}} \qquad x_{LP} < x < x_1 \qquad (4.1\text{-}6)$$

$$\xi = \frac{\ln[(\beta+1-\xi')/(\beta-1+\xi')]}{\ln[(\beta+1)/(\beta-1)]} \qquad 0 < \xi' < 1 \qquad (4.1\text{-}7)$$

For convienence, each grid point is classified as either a boundary or an interior grid point. Boundary grid points are those grid points which lie on the boundaries (i.e. surfaces 1,2,3,4,5 and 6 in Fig. 2-1). Grid points that do not lie on boundaries are refered to as interior grid points.

The continuous time domain was replaced by a set of time levels. In this study the time levels were equally incremented so that the numerical solutions were found at t given by

$$t=n\Delta t \qquad n=0,1,2,3,\ldots \tag{4.1-8}$$

4.2 Finite Difference Equations at Interior Grid Points

Once the continuous domain of the problem has been replaced by a system of grid points and time levels, the governing PDE's can be replaced by a system of FDE's. In this section, the FDE's at the interior grid points are derived. Finite-difference equations at boundary grid points are derived in Section 4.3.

Finite-difference equations to be applied at the interior grid points are derived by using the time-split method of MacCormack [40,41]. The first step in applying the time-split method of MacCormack is to divide the two-dimensional governing equations (summarized in Table 3-3) into two one-dimensional governing equations as follows:

$$\frac{\partial}{\partial\tau}\underset{\sim}{U} + \xi_t \frac{\partial}{\partial\xi}\underset{\sim}{U} + \xi_x \frac{\partial}{\partial\xi}\underset{\sim}{F} = \xi_x \frac{\partial}{\partial\xi}\underset{\sim}{V}_1 + \xi_x \frac{\partial}{\partial\xi}\underset{\sim}{V}_2 \tag{4.2-1}$$

$$\frac{\partial}{\partial\tau}\underset{\sim}{U} + \eta_y \frac{\partial}{\partial\eta}\underset{\sim}{G} = \eta_y \frac{\partial}{\partial\eta}\underset{\sim}{W}_1 + \eta_y \frac{\partial}{\partial\eta}\underset{\sim}{W}_2 \tag{4.2-2}$$

Each of these one-dimensional governing equations was solved by using MacCormack's predictor-corrector method which prescribes how temporal and spatial derivatives are to be replaced by finite-difference formulas. MacCormack's predictor-corrector method is a two step method. In the first step (predictor step), the time derivative term is replaced by

$$\frac{\partial\underset{\sim}{U}}{\partial\tau} = \frac{\underset{\sim}{U}^{\overline{n+1}} - \underset{\sim}{U}^{n}}{\Delta\tau} \tag{4.2-3}$$

where $\underset{\sim}{U}^{n}$ is the solution at time level n and $\underset{\sim}{U}^{\overline{n+1}}$ is an intermediate solution. In the second step (corrector step), the time derivative term is replaced by

$$\frac{\partial \underset{\sim}{U}}{\Delta\tau} = \frac{\underset{\sim}{U}^{n+1} - \frac{1}{2}\left(\underset{\sim}{U}^{n} + \overline{\underset{\sim}{U}^{n+1}} \right)}{\Delta\tau/2} \tag{4.2-4}$$

where $\underset{\sim}{U}^{n+1}$ is the solution at time level n+1.

Finite difference formulas used for the spatial derivative terms are as follows. The first derivative terms were replaced by backward-differencing formulas for the predictor step and forward-differencing formulas for the corrector step. The second derivative terms, including the cross derivative terms, were replaced by central-differencing formulas for both the predictor and corrector steps.

Replacing derivative terms in Eqs. (4.2-1) and (4.2-2) in the manner described above yields a set of FDE's that are applied at each of the interior grid points. These FDE'S are summarized in Table 4-1.

To facilitate description of the solution procedure in Section 4.4, $L_{\xi}(\Delta t_{\xi})$ and $L_{\eta}(\Delta t_{\eta})$ are defined. The operator $L_{\xi}(\Delta t_{\xi})$ is defined so that

$$\underset{\sim}{U}^{n+1} = L_{\xi}(\Delta t_{\xi})\ \underset{\sim}{U}^{n} \tag{4.2-14}$$

is equivalent to the two-step formula given by Eqs. (4.2-5) and (4.2-6) when Δt_{ξ} is equal to Δt. The operator $L_{\eta}(\Delta t_{\eta})$ is defined so

$$\underset{\sim}{U}^{n+1} = L_{\eta}(\Delta t_{\eta})\ \underset{\sim}{U}^{n} \tag{4.2-15}$$

is equivalent to the two-step formula given by Eqs. (4.2-7) and (4.2-8) when Δt_{η} is equal to Δt.

4.3 Finite Difference Equations at Boundary Grid Points

Finite-difference equations at the boundary grid points are found by using the boundary conditions described in Section 3.4. In addition to the boundary conditions described in Section 3.4, a fourth numerical boundary condition is needed. The numerical boundary condition used is

Table 4-1. Finite difference equations at interior grid points

For Eq. (4.2-1)

Predictor:

$$\overline{\underset{\sim}{U}^{n+1}_{i,j}} = \underset{\sim}{U}^{n}_{i,j} - \xi_{+}\frac{\Delta\tau}{\Delta\xi}\left[\underset{\sim}{U}^{n}_{i,j} - \underset{\sim}{U}^{n}_{i-1,j}\right] - \xi_{x}\frac{\Delta\tau}{\Delta\xi}\left[\underset{\sim}{F}^{n}_{i,j} - \underset{\sim}{F}^{n}_{i-1,j}\right]$$
$$+ \xi_{x}\frac{\Delta\tau}{\Delta\xi}\left[(\underset{\sim}{V}_1)^{n}_{i+\frac{1}{2},j} - (\underset{\sim}{V}_1)^{n}_{i-\frac{1}{2},j}\right]$$
$$+ \xi_{x}\frac{\Delta\tau}{2\Delta\xi}\left[(\underset{\sim}{V}_2)^{n}_{i+1,j} - (\underset{\sim}{V}_2)^{n}_{i-1,j}\right] \qquad (4.2\text{-}5)$$

Corrector:

$$\underset{\sim}{U}^{n+1}_{i,j} = \frac{1}{2}\left[\underset{\sim}{U}^{n}_{i,j} + \overline{\underset{\sim}{U}^{n+1}_{i,j}} - \xi_{+}\frac{\Delta\tau}{\Delta\xi}\left[\overline{\underset{\sim}{U}^{n+1}_{i+1,j}} - \overline{\underset{\sim}{U}^{n+1}_{i,j}}\right]\right.$$
$$- \xi_{x}\frac{\Delta\tau}{\Delta\xi}\left[\overline{\underset{\sim}{F}^{n+1}_{i+1,j}} - \overline{\underset{\sim}{F}^{n+1}_{i,j}}\right]$$
$$+ \xi_{x}\frac{\Delta\tau}{\Delta\xi}\left[\overline{(\underset{\sim}{V}_1)^{n+1}_{i+\frac{1}{2},j}} - \overline{(\underset{\sim}{V}_1)^{n+1}_{i-\frac{1}{2},j}}\right]$$
$$\left. + \xi_{x}\frac{\Delta\tau}{2\Delta\xi}\left[\overline{(\underset{\sim}{V}_2)^{n+1}_{i+1,j}} - \overline{(\underset{\sim}{V}_2)^{n+1}_{i-1,j}}\right]\right] \qquad (4.2\text{-}6)$$

For Eq. (4.2-2)

Predictor:

$$\overline{\underset{\sim}{U}^{n+1}_{i,j}} = \underset{\sim}{U}^{n}_{i,j} - \eta_{y}\frac{\Delta\tau}{\Delta\eta}\left[\underset{\sim}{G}^{n}_{i,j} - \underset{\sim}{G}^{n}_{i-1,j}\right]$$
$$+ \eta_{y}\frac{\Delta\tau}{2\Delta\eta}\left[(\underset{\sim}{W}_1)^{n}_{i,j+1} - (\underset{\sim}{W}_1)^{n}_{i,j-1}\right]$$
$$+ \eta_{y}\frac{\Delta\tau}{\Delta\eta}\left[(\underset{\sim}{W}_2)^{n}_{i,j+\frac{1}{2}} - (\underset{\sim}{W}_2)^{n}_{i,j-\frac{1}{2}}\right] \qquad (4.2\text{-}7)$$

Table 4-1. Continued

Corrector:

$$\underset{\sim}{U}_{i,j}^{n+1} = \frac{1}{2}\left[\underset{\sim}{U}_{i,j}^{n} + \overline{\underset{\sim}{U}_{i,j}^{n+1}} - \eta_y \frac{\Delta\tau}{\Delta\eta}\left(\overline{\underset{\sim}{G}_{i,j+1}^{n+1}} - \overline{\underset{\sim}{G}_{i,j}^{n+1}} \right) + \eta_y \frac{\Delta\tau}{2\Delta\eta}\left(\overline{(\underset{\sim}{W}_1)_{i,j+1}^{n+1}} - \overline{(\underset{\sim}{W}_1)_{i,j-1}^{n+1}} \right) + \eta_y \frac{\Delta\tau}{\Delta\eta}\left(\overline{(\underset{\sim}{W}_2)_{i,j+\frac{1}{2}}^{n+1}} - \overline{(\underset{\sim}{W}_2)_{i,j-\frac{1}{2}}^{n+1}} \right) \right] \tag{4.2-8}$$

Where

$$(\underset{\sim}{V}_1)_{i,j} = \begin{bmatrix} 0 \\ \frac{4}{3}\mu\,\xi_{x_{i,j}} \dfrac{\left(\frac{m}{\rho}\right)_{i+\frac{1}{2},j} - \left(\frac{m}{\rho}\right)_{i-\frac{1}{2},j}}{\Delta\xi} \\ \mu\,\xi_{x_{i,j}} \dfrac{\left(\frac{n}{\rho}\right)_{i+\frac{1}{2},j} - \left(\frac{n}{\rho}\right)_{i-\frac{1}{2},j}}{\Delta\xi} \\ \frac{2}{3}\mu\,\xi_{x_{i,j}} \dfrac{\left(\frac{m}{\rho}\right)^2_{i+\frac{1}{2},j} - \left(\frac{m}{\rho}\right)^2_{i-\frac{1}{2},j}}{\Delta\xi} \\ + \frac{1}{2}\mu\,\xi_{x_{i,j}} \dfrac{\left(\frac{n}{\rho}\right)^2_{i+\frac{1}{2},j} - \left(\frac{n}{\rho}\right)^2_{i-\frac{1}{2},j}}{\Delta\xi} \\ + k\xi_{x_{i,j}} \dfrac{T_{i+\frac{1}{2},j} - T_{i-\frac{1}{2},j}}{\Delta\xi} \end{bmatrix} \tag{4.2-9}$$

Table 4-1. Continued

$$(\underset{\sim}{V}_2)_{i,j} = \begin{bmatrix} 0 \\ -\frac{2}{3}\mu\,\eta_{y_{i,j}} \dfrac{\left(\frac{n}{\rho}\right)_{i,j+1} - \left(\frac{n}{\rho}\right)_{i,j-1}}{2\Delta\eta} \\ \mu\,\eta_{y_{i,j}} \dfrac{\left(\frac{m}{\rho}\right)_{i,j+1} - \left(\frac{m}{\rho}\right)_{i,j-1}}{2\Delta\eta} \\ \mu\left(\frac{n}{\rho}\right)_{i,j}\eta_{y_{i,j}} \dfrac{\left(\frac{n}{\rho}\right)_{i,j+1} - \left(\frac{n}{\rho}\right)_{i,j-1}}{2\Delta\eta} \\ -\frac{2}{3}\mu\left(\frac{m}{\rho}\right)_{i,j}\eta_{y_{i,j}} \dfrac{\left(\frac{n}{\rho}\right)_{i,j+1} - \left(\frac{n}{\rho}\right)_{i,j-1}}{2\Delta\eta} \end{bmatrix} \tag{4.2-10}$$

$$(\underset{\sim}{W}_1)_{i,j} = \begin{bmatrix} 0 \\ \mu\,\xi_{x_{i,j}} \dfrac{\left(\frac{n}{\rho}\right)_{i+1,j} - \left(\frac{n}{\rho}\right)_{i-1,j}}{2\Delta\xi} \\ -\frac{2}{3}\mu\,\xi_{x_{i,j}} \dfrac{\left(\frac{m}{\rho}\right)_{i+1,j} - \left(\frac{m}{\rho}\right)_{i-1,j}}{2\Delta\xi} \\ \mu\left(\frac{m}{\rho}\right)_{i,j}\xi_{x_{i,j}} \dfrac{\left(\frac{n}{\rho}\right)_{i+1,j} - \left(\frac{n}{\rho}\right)_{i-1,j}}{2\Delta\xi} \\ -\frac{2}{3}\mu\left(\frac{n}{\rho}\right)_{i,j}\xi_{x_{i,j}} \dfrac{\left(\frac{m}{\rho}\right)_{i+1,j} - \left(\frac{m}{\rho}\right)_{i-1,j}}{2\Delta\xi} \end{bmatrix} \tag{4.2-11}$$

Table 4-1. Continued

$$(\underset{\sim}{W}_2)_{i,j} = \begin{bmatrix} 0 \\ \mu\, \eta_{y_{i,j}} \dfrac{\left(\frac{m}{\rho}\right)_{i,j+\frac{1}{2}} - \left(\frac{m}{\rho}\right)_{i,j-\frac{1}{2}}}{\Delta\eta} \\ \frac{2}{3}\,\mu\, \eta_{y_{i,j}} \dfrac{\left(\frac{n}{\rho}\right)_{i,j+\frac{1}{2}} - \left(\frac{n}{\rho}\right)_{i,j-\frac{1}{2}}}{\Delta\eta} \\ \frac{2}{3}\,\mu\, \eta_{y_{i,j}} \dfrac{\left(\frac{n}{\rho}\right)^2_{i,j+\frac{1}{2}} - \left(\frac{n}{\rho}\right)^2_{i,j-\frac{1}{2}}}{\Delta\eta} \\ + \frac{1}{2}\,\mu\, \eta_{y_{i,j}} \dfrac{\left(\frac{m}{\rho}\right)^2_{i,j+\frac{1}{2}} - \left(\frac{m}{\rho}\right)^2_{i,j-\frac{1}{2}}}{\Delta\eta} \\ + k\, \eta_{y_{i,j}} \dfrac{T_{i,j+\frac{1}{2}} - T_{i,j-\frac{1}{2}}}{\Delta\eta} \end{bmatrix} \qquad (4.2\text{-}12)$$

and $\underset{\sim}{U}$, $\underset{\sim}{F}$ and $\underset{\sim}{G}$ are given by Eqs. (3.1-12) to (3.1-14) in Table 3-2.

Note: The metric coefficients at locations mid-way between grid points (e.g., $\xi_{x_{i+\frac{1}{2},j}}$) are evaluated by averaging, i.e.,

$$\xi_{x_{i+\frac{1}{2},j}} = \frac{1}{2}\left(\xi_{x_{i+1,j}} + \xi_{x_{i,j}}\right) \qquad (4.2\text{-}13)$$

the first derivative of pressure in the direction normal to the wall equal to zero.

The zero first derivative boundary conditions for temperature and pressure were approximated by using one sided differencing formulas. For example, the pressure boundary condition on the left piston given as

$$\frac{\partial P}{\partial \xi} = 0 \tag{4.3-1}$$

was approximated by

$$\frac{P_{1,j} - P_{2,j}}{\Delta \xi} = 0 \tag{4.3-2}$$

which reduces to

$$P_{1,j} = P_{2,j} \tag{4.4-3}$$

By using approximations of this type for the derivative boundary conditions and by using the equation of state for an ideal gas

$$P = \rho RT \tag{4.3-4}$$

the FDE's at the boundary grid points were derived. These FDE's are summarized in Table 4-2.

The dependent variables at the boundary grid point located at the intersection of lines $\xi = \xi(0,t)$ and $\eta = \eta(H_2)$ (see Fig. 4-2) are double valued. At this point, the FDE's were given by

$$\begin{aligned} \rho_{IP,JP} &= \rho_{IP-1,JP} & m_{IP,JP} &= 0 \\ e_{IP,JP} &= e_{IP-1,JP} & n_{IP,JP} &= 0 \end{aligned} \tag{4.3-14}$$

when used in conjunction with Eq. (4.2-14) and by

$$\begin{aligned} \rho_{IP,JP} &= \rho_{IP,JP-1} & m_{IP,JP} &= 0 \\ e_{IP,JP} &= e_{IP,JP-1} & n_{IP,JP} &= 0 \end{aligned} \tag{4.3-15}$$

when used in conjunction with Eq. (4.2-15).

Table 4-2. Finite difference equations at boundary grid points

For i = 1; j = 1 to JL-1 (see Fig. 4-2)

$$\rho_{1,j} = \frac{P_{2,J}}{R * T_{LP}}$$

$$m_{1,j} = \rho_{i,j} * V_{LP}$$

$$n_{1,j} = 0$$

$$e_{1,j} = \frac{\rho_{1,j} * R * T_{LP}}{(\gamma - 1)} \qquad (4.3\text{-}5)$$

For i = 2 to IP-1; j = JL

$$\rho_{i,JL} = \rho_{i,JL-1}$$

$$m_{i,JL} = 0$$

$$n_{i,JL} = 0$$

$$e_{i,JL} = \frac{P_{i,JL-1}}{(\gamma - 1)} \qquad (4.3\text{-}6)$$

For i = IP; j = JP+1 to JL-1

$$\rho_{IP,j} = \rho_{IP-1,j}$$

$$m_{IP,j} = 0$$

$$n_{IP,j} = 0$$

$$e_{IP,j} = \frac{P_{IP-1,j}}{(\gamma - 1)} \qquad (4.3\text{-}7)$$

Table 4-2. Continued

For i = IP+1 to IL; j = JP

$$\rho_{i,JP} = \rho_{i,JP-1}$$

$$m_{i,JP} = 0$$

$$n_{i,JP} = 0$$

$$e_{i,JP} = \frac{P_{i,JP-1}}{(\gamma - 1)} \qquad (4.3\text{-}8)$$

For i = IL; j = 1 to JP-1

$$\rho_{IL,j} = \frac{P_{IL-1,j}}{R * T_{RP}}$$

$$m_{IL,j} = \rho_{IL,j} * V_{RP}$$

$$n_{IL,j} = 0$$

$$e_{IL,j} = \frac{\rho_{IL,j} * R * T_{RP}}{(\gamma - 1)} \qquad (4.3\text{-}9)$$

For i = 2 to IL-1; j = 1

$$\rho_{i,1} = \rho_{i,2}$$

$$m_{i,1} = m_{i,2}$$

$$n_{i,1} = 0$$

$$e_{i,1} = e_{i,2} \qquad (4.3\text{-}10)$$

Table 4-2. Continued

For i = 1; j = JL

$$\rho_{1,JL} = \rho_{2,JL-1}$$

$$m_{1,JL} = 0$$

$$n_{1,JL} = 0$$

$$e_{1,JL} = \frac{P_{2,JL-1}}{(\gamma - 1)} \qquad (4.3\text{-}11)$$

For i = IP; j = JL

$$\rho_{IP,JL} = \rho_{IP-1,JL-1}$$

$$m_{IP,JL} = 0$$

$$n_{IP,JL} = 0$$

$$e_{IP,JL} = \frac{P_{IP-1,JL-1}}{(\gamma - 1)} \qquad (4.3\text{-}12)$$

For i = IL; j = JP

$$\rho_{IL,JP} = \rho_{IL-1,JP-1}$$

$$m_{IL,JP} = 0$$

$$n_{IL,JP} = 0$$

$$e_{IL,JP} = \frac{P_{IL-1,JP-1}}{(\gamma - 1)} \qquad (4.3\text{-}13)$$

4.4 Solution Procedure

This section describes how numerical solutions at the grid points and time levels can be obtained by using the FDE's derived in Sections 4.2 and 4.3.

The method for obtaining numerical solutions is prescribed by the time-split method of MacCormack as follows:

$$U^{n+1} = [\, L_\eta(\Delta t_\eta)\,]^{d/2}\, L_\xi(\Delta t_\xi)\, [\, L_\eta(\Delta t_\eta)\,]^{d/2}\, U^n \qquad (4.4\text{-}1)$$

where the operators $L_\eta(\Delta t_\eta)$ and $L\xi(\Delta t_\xi)$ are defined by Eqs. (4.2-14) and (4.2-15), respectively. The parameter d in the above equation is defined by

$$d = \frac{\Delta t_\eta}{\Delta t_\xi} \qquad (4.4\text{-}2)$$

where Δt_η and Δt_ξ are the maximum time step sizes that can be used to obtain stable solutions to Eqs. (4.2-14) and (4.2-15), respectively. If d given by Eq (4.4-2) is not an even integer, then the value for d is rounded to the next higher even integer.

When using Eq. (4.4-1) to obtain solutions it is assumed that the solutions at time level n (i.e. U^n) is known and the solution at time level n+1 (i.e. U^{n+1}) is sought. When n=0, U^n is given by the initial condition (Eq. (3.2-12)).

To demonstrate how Eq. (4.4-1) is used to obtain solutions, let d=2. With d=2, Eq. (4.4-1) becomes

$$U^{n+1} = [\, L_\eta(\Delta t_\eta)\,]\, L_\xi(\Delta t_\xi)\, [\, L_\eta(\Delta t_\eta)\,]\, U^n \qquad (4.4\text{-}3)$$

The above equation can be split as follows:

$$U^* = L_\eta(\Delta t_\eta) U^n \qquad (4.4\text{-}4)$$

$$U^{**} = L_\xi(\Delta t_\xi) U^* \qquad (4.4\text{-}5)$$

$$\underset{\sim}{U}^{n+1} = L_{\eta}(\Delta t_{\eta})\underset{\sim}{U}^{**} \qquad (4.4\text{-}6)$$

One can verify that Eqs. (4.4-4) to (4.4-6) are equivalent to Eq. (4.4-3) by substituting Eq. (4.4-4) into Eq. (4.4-5) and then substituting the resulting equation into Eq. (4.4-6).

To obtain solutions, Eq. (4.4-4) was first applied at every interior grid point to yield an intermediate solution $\underset{\sim}{U}^{*}$. $\underset{\sim}{U}^{*}$ at the boundary grid points were obtained by using Eqs. (4.3-5) to (4.3-15). Once $\underset{\sim}{U}^{*}$ at every grid point had been determined, Eq. (4.4-5) was used to obtain another intermediate solution $\underset{\sim}{U}^{**}$ at the interior grid points. $\underset{\sim}{U}^{**}$ at the boundary grid points were again determined by Eqs. (4.3-5) to (4.3-15). Once $\underset{\sim}{U}^{**}$ at every grid point had been determined , Eq. (4.4-6) was used to obtain $\underset{\sim}{U}^{n+1}$ at every interior grid point. With $\underset{\sim}{U}^{n+1}$ at interior grid points known, Eqs. (4.3-5) to (4.3-15) were used to determine $\underset{\sim}{U}^{n+1}$ at the boundary grid points. Repeating this procedure yields $\underset{\sim}{U}$ at successively higher time levels. This completes the solution procedure.

4.5 Vectorization of Computer Program

The solution procedure described in the previous sections was coded into a FORTRAN program so that a computer could be used to find the solutions. In this study, the computer used was the CRAY XMP located at NASA-Lewis Research Center.

The CRAY XMP is a supercomputer based on the pipeline architecture. In order to fully utilize computers with such an architecture, it is necessary to write the computer program so that it can be vectorized [42,43]. The details of the programming techniques employed to allow the computer program to vectorize are given in reference 44 and will not be repeated here.

Here, it is noted that the considerable efforts spent in making the computer program vectorizable increased the speed of the calculations by a factor of 10.

CHAPTER V

RESULTS

In order to assess the usefulness of the computer program developed, numerical solutions were generated for the step problem described in Chapter II. Three types of the step problem were analyzed and they are as follows (see Table 5-1):

1. Steady flows past a step (cases 1 and 2 in Table 5-1)
2. Oscillating flows past a step: pistons oscillating in phase (cases 3 and 4)
3. Oscillating flows past a step: pistons oscillating out of phase (cases 5 and 6)

The parameters which were the same for all cases analyzed are summarized in Table 5-2.

For each of the six cases analyzed, density, x- and y-components of the velocity, total energy, temperature and pressure were calculated at 3,111 grid points (i.e., IL=61 and JL=51) and 20,000 time levels. Here, only results for the velocity are presented to show flow patterns.

In the following three sections (Sections 5.1 to 5.3), the results of the three types of the step problem analyzed are described.

5.1 Steady Flows Past a Step

The first type of the step problem analyzed by the computer program involves steady flows (cases 1 and 2 in Table 5-1). Figure 5-1 shows the steady-state flow pattern for case 1 in which the gas flows from the

Table 5-1. Summary of cases studied

Case	Frequency of Piston Oscillation (Hz)	Phase Shift of Large Piston α_1 (rad)	Amplitude of Piston Oscillation		Maximum Velocity of Small Piston (m/s)
			Large Piston A_1 (m)	Small Piston A_2 (m)	
1	------				26
2	------				22
3	1250		$\frac{0.01}{\pi}$	$\frac{0.02}{\pi}$	50
4	1250		$\frac{0.015}{\pi}$	$\frac{0.03}{\pi}$	75
5	1250	$\frac{\pi}{2}$	$\frac{0.01}{\pi}$	$\frac{0.02}{\pi}$	50
6	1250	$-\frac{\pi}{2}$	$\frac{0.01}{\pi}$	$\frac{0.02}{\pi}$	50

Table 5-2. Parameters which remain constant for all cases

$\Delta t = 2 \times 10^{-7}$ (sec)
$\omega = 1250$ Hz
$L_1 = 0.02$ (m)
$L_3 = 0.03$ (m)
$\alpha_2 = 0.0$
$H_1 = 0.005$ (m)
$H_2 = 0.0025$ (m)
$\mu = 0.00185$ (kg/m sec)
$k = 2.61$ (W/m K)
$\gamma = 1.4$
$R = 287.0$ (J/(kg K))
$T_0 = 300.0$ (K)
$P_0 = 101000.0$ (N/m)

right toward the left. In this figure, a recirculating flow pattern can be seen just downstream of the step. This recirculating flow pattern has been observed experimentally (see e.g., ref. 45).

Figure 5-2 shows the steady-state flow pattern for case 2 in which the gas flows from the left toward the right. In this figure, no recirculating flows are observed. For this case, recirculating flows are not expected near the intersection of surfaces 3 and 4 (see Fig. 2-1) because the Reynolds number is very low.

The fact that the computer program generated the expected flow patterns for cases 1 and 2 lends some confidence to the usefulness of the computer program.

5.2 Oscillating Flows Past a Step: Pistons Oscillating in Phase

The second type of the step problem investigated involves oscillating flows past a step with the pistons oscillating in phase with each other (cases 3 and 4 in Table 5-1). For these cases, the two pistons always move in the same direction but the small piston moves farther than the large piston in order to keep the volume between the pistons constant.

For these cases, the flow patterns are presented after four complete oscillations of the pistons. This is because after four oscillations of the pistons, the numerical solutions generated by the computer program become periodic and independent of the initial conditions.

Figures 5-3 to 5-23 show the flow patterns for case 3 during the fifth oscillation of the pistons. Figure 5-3 shows a large clockwise (CW) recirculating flow that was formed during the previous oscillation. As the pistons accelerate to the right, a separation bubble begins to

form on surface 4 (see Figs 2-1 and 5-4). In Figs. 5-5 to 5-8 this separation bubble can be seen to persist until the large CW recirculating flow formed during the previous oscillation moves toward the plane of symmetry and begins to dissipate in Fig. 5-8. Figures 5-9 to 5-13 show the flow patterns as the pistons slow down and come to rest at their rightmost position. Note that at this time, the large CW recirculating flow seen at the beginning of the fifth oscillation has completely dissipated.

As the pistons begin to move to the left, the inertia of the gas in the region outside the boundary layer continues to carry the gas in that region to the right. Since the inertia of the gas inside the boundary layer is less than the inertia of the gas outside the boundary layer, the motion of the gas inside the boundary layer is more easily affected by the motion of the pistons. This can be seen in Fig. 5-14 where the gas in the boundary layer has begun to move to the left while the gas outside the boundary layer continues to move to the right.

Later, as the pistons moved to the left, a large CW recirculating flow pattern began to form on the downstream side of the step (see Figs. 5-15 to 5-23). This CW recirculating flow persisted throughout the remainder of the fifth oscillation.

In Figs. 5-21 and 5-22 the gas in the boundary layer can be seen to change direction before the gas outside the boundary layer changes direction. As noted earlier, this is due to differences in the inertia of the gas.

Figures 5-24 to 5-44 show the flow patterns for case 4. Case 4 was calculated by using the same geometry as case 3 except the amplitude of piston oscillations was 1.5 times greater. This resulted in higher piston velocities, and therefore, higher gas velocities.

Figure 5-24 shows the flow pattern at the beginning of the fifth oscillation for case 4. Due to the higher piston velocities, there are two recirculating flows remaining from the previous oscillation. As seen in Figs. 5-24 to 5-29, the counterclockwise (CCW) recirculating flow causes the gas to enter the smaller side of the region more nearly parallel to the x-axis so that the flow does not separate on surface 4. In Figure 5-30 the CCW recirculating flow is seen to have dissipated as the pistons reach their maximum velocity and begin to slow down.

Figures 5-31 to 5-34 show the gas moving to the right as the pistons continue to slow down and come to a stop. In Figs. 5-35 and 5-36, it can be seen that as the pistons begin to move to the left, the gas in the boundary layer changes direction before the gas outside the boundary layer. This is due to differences in the inertia of the gas inside and outside of the boundary layer. Note that at this time the large CW recirculating flow seen at the beginning of the fifth oscillation has completely dissipated.

As the flow accelerates to the left (see Figs. 5-37 to 5-39), a CW recirculating flow begins to develop downstream of the step. As can be seen in Fig. 5-40, the flow continues to the left and pushes the CW recirculating flow to the left, causing a CCW recirculating flow to develop in the upper corner near the intersections of surfaces 2 and 3 (see Figs. 2-1 and 5-41). In Figs. 5-42 to 5-44, these two recirculating flows can be seen to grow in size and strength as the flow begins to change direction.

5.3 Oscillating Flows Past a Step: Pistons Oscillating Out of Phase

The third type of the step problem investigated involves oscillating flows past a step in which the pistons are oscillating out

of phase (cases 5 and 6 in Table 5-1). In these cases the pistons move according to Eqs. (2-1) and (2-2) with the value of α_1 being $\pi/2$ for case 5 and $-\pi/2$ for case 6. Similar to cases 3 and 4 the small piston traverses a greater distance than the large piston. Cases 5 and 6 differ from cases 3 and 4 in that the volume between the pistons is no longer constant since the pistons are oscillating out of phase. For both case 5 and case 6 the peak velocity of the small piston is 50 m/s. The flow patterns for these cases are again presented for the fifth complete oscillation of the pistons to allow the effects of the initial condition to be eliminated and a periodic solution to prevail.

For case 5 the value of α_1 in Eq. (2-1) is $\pi/2$ and the value of α_2 in Eq. (2-2) is zero. Since α_1 does not equal α_2 (i.e. the pistons are oscillating out of phase), there is periodic compression and expansion of the gas in the region between the pistons. The flow patterns for case 5 are shown in Figs. 5-45 to 5-65.

In Fig. 5-45, the large piston can be seen moving to the right while the small piston is stationary resulting in compression of the gas between the pistons. Figures 5-45 to 5-48 show the gas moving to the right and a separation bubble forming on surface 4 (see Fig. 2-1). Figures 5-45 to 5-47 show the small piston accelerating to the right while the large piston is slowing down. In Fig. 5-48 the velocity of the small piston is seen to become greater than twice that of the large piston, allowing the gas in the region between the pistons to expand. The expanding gas continues to move to the right as seen in in Figs. 5-48 through 5-53 even though the large piston begins to move to the left in Fig. 5-50. At this point, both of the recirculating flow patterns present at the beginning of the fifth oscillation have

dissipated. Figures 5-54 and 5-55 show the fluid beginning to change directions with the lower inertia gas in the boundary layer changing directions before the gas outside the boundary layer.

In Figs. 5-56 through 5-61 the gas can be seen moving to the left and the CW recirculating flow pattern seen at the beginning of the fifth oscillation is forming. In Fig. 5-58, it can be seen that the velocity of the small piston is no longer greater than twice that of the large piston causing the fluid to be compressed. Figure 5-62 shows the flow beginning to change direction with the gas in the boundary layer changing direction before the gas outside the boundary layer. In Figs. 5-63 to 5-65 the flow is seen moving to the right and the separation bubble on surface 4 (see Fig. 2-1) is beginning to form.

For case 6 the value of α_1 in Eq. (2-1) is $-\pi/2$ and the value of in Eq. (2-2) is zero. Since α_1 does not equal α_2 there is a periodic compression and expansion of the gas in the region between the pistons. The flow patterns for case 6 are shown in Figs. 5-66 to 5-86.

In Fig. 5-66, the large piston is seen moving to the left while the small piston is stationary, resulting in the expansion of the gas in the region between the pistons. In this figure the flow is beginning to change directions. Figures 5-67 through 5-72 show the flow moving to the right and a seperation bubble forming on surface 4 (see Fig. 2-1). In Fig. 5-73, the seperation bubble is seen to dissipate as the large clockwise recirculating flow moves toward the plane of symmetry. In Fig. 5-74, it is seen that twice the velocity of the large piston becomes greater than the velocity of the small piston and the fluid starts being compressed. At this time it is noted that the large CW recirculating flow present at the beginning of the fifth oscillation has completely dissipated.

Figures 5-75 to 5-78 show the gas continuing to move to the right as the volume of region between the pistons decreases. In Figs. 5-79 and 5-80 the flow is seen to begin to changing direction. Figures 5-81 to 5-84 show the flow continuing to the left and a large clockwise recirculating flow developing on the downstream side of the step. In Fig. 5-84 the velocity of the small piston is seen to become greater than twice that of the large piston allowing the fluid to expand. Figures 5-85 and 5-86 show the fluid beginning to change direction, again in the boundary layer first.

Comparisons of the results obtained for cases 5 and 6 with previously calculated numerical or analytical solutions are not made. This is because other solutions to this problem do not exist.

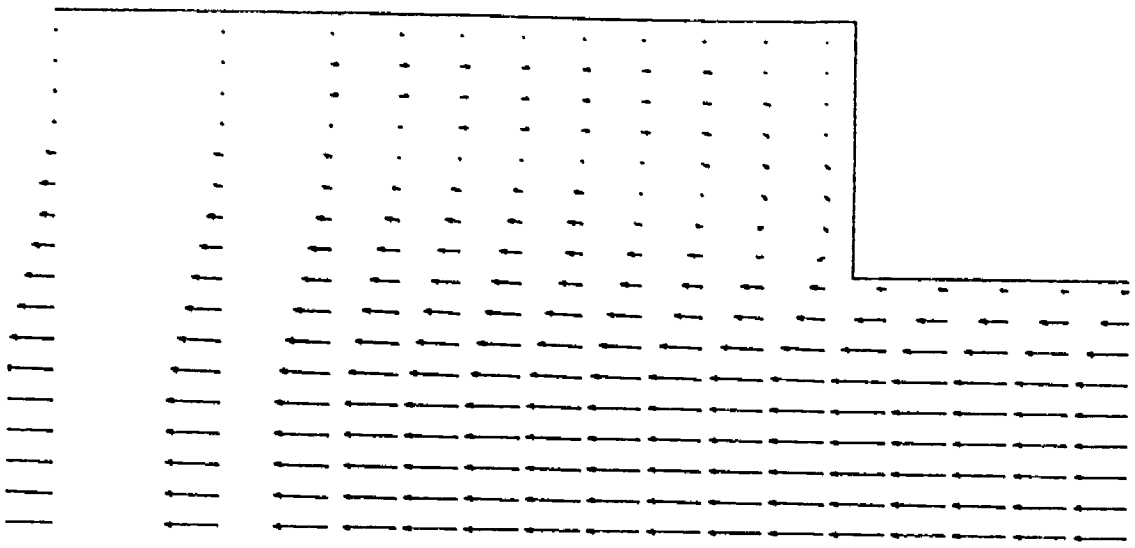

Figure 5-1. Flowfield for steady flow case
The peak velocity of the fluid in the smaller side of the region is about 25 meters/second

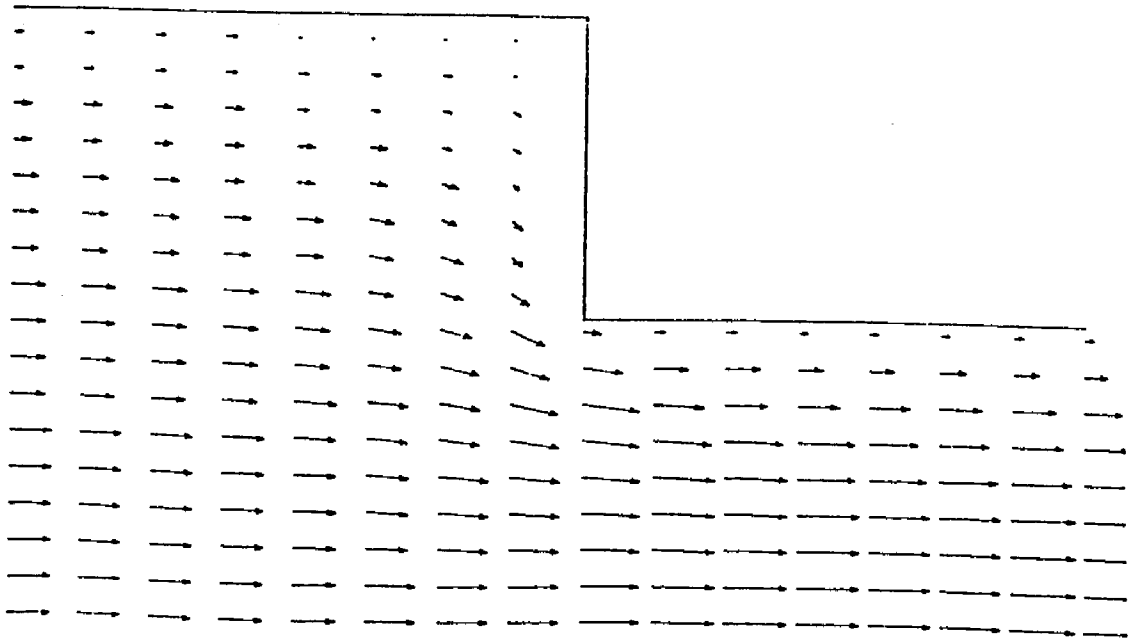

Figure 5-2. Flowfield for steady flow case
The peak velocity of the fluid in the smaller side of the region is about 22 meters/second

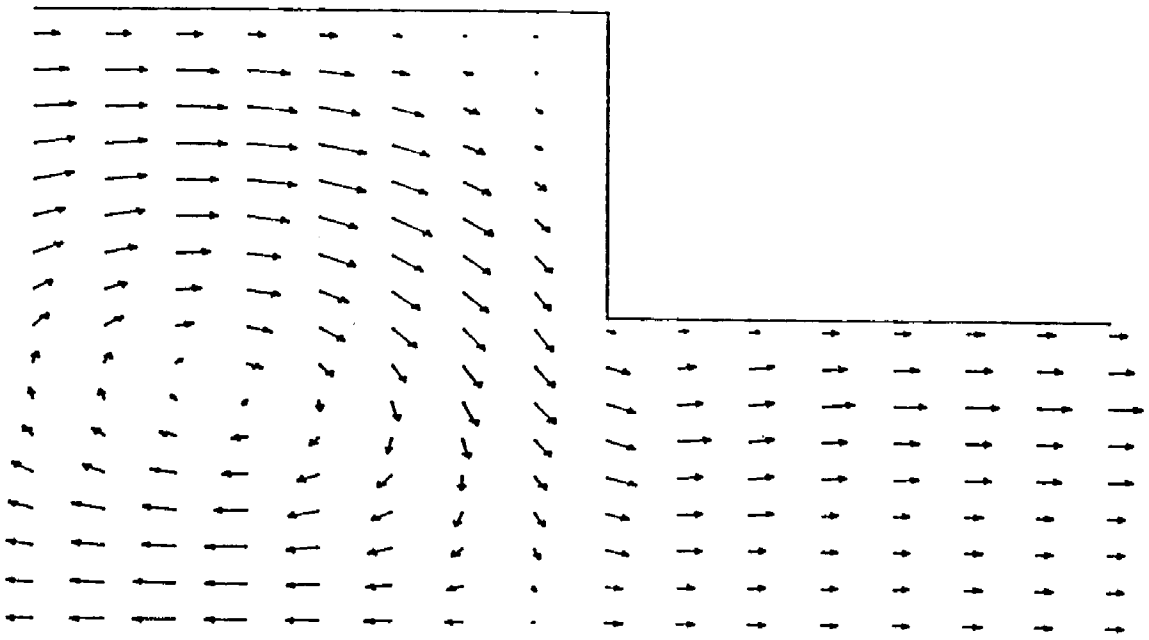

Figure 5-3. Flowfield for t = 0.0032 seconds
This is 0.0 radians after the end of the previous cycle
The velocity of the large piston is 0.0 meters/second
The velocity of the small piston is 0.0 meters/second

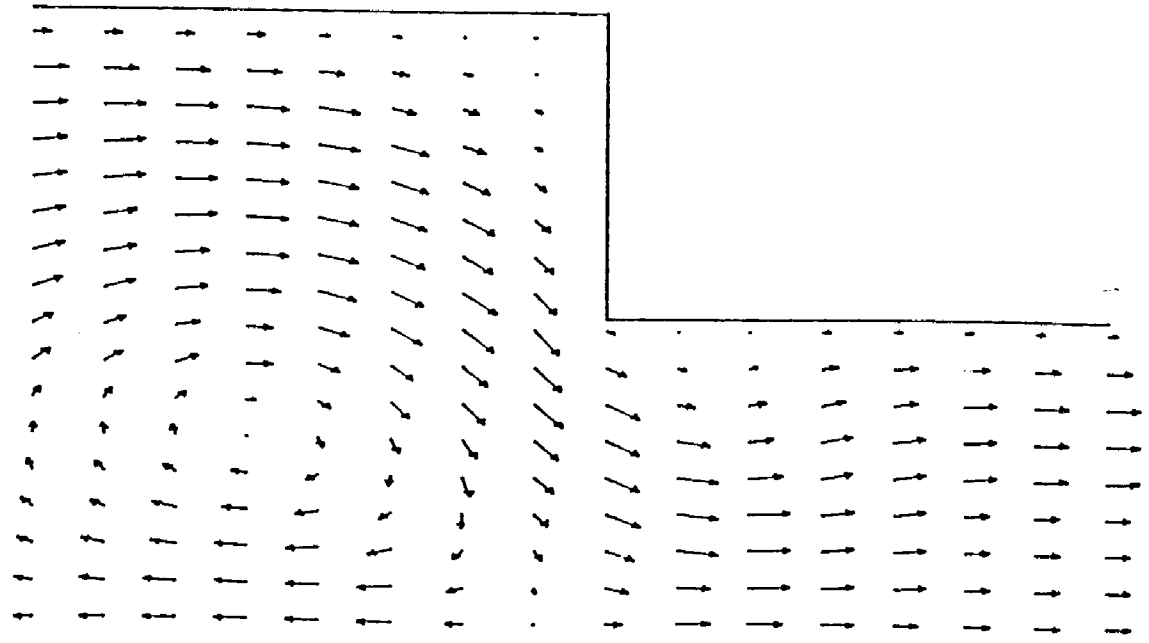

Figure 5-4. Flowfield for t = 0.00324 seconds
This is pi/10 radians after the end of the previous cycle
The velocity of the large piston is 7.72 meters/second
The velocity of the small piston is 15.45 meters/second

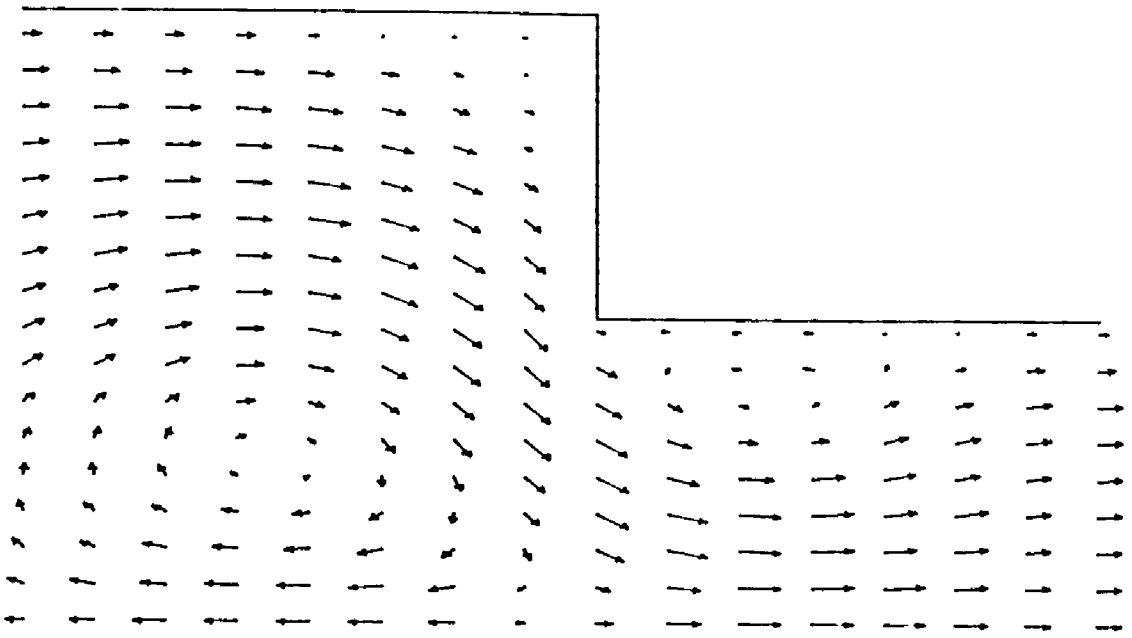

Figure 5-5. Flowfield for t = 0.00328 seconds
This is 2pi/10 radians after the end of the previous cycle
The velocity of the large piston is 14.69 meters/second
The velocity of the small piston is 29.39 meters/second

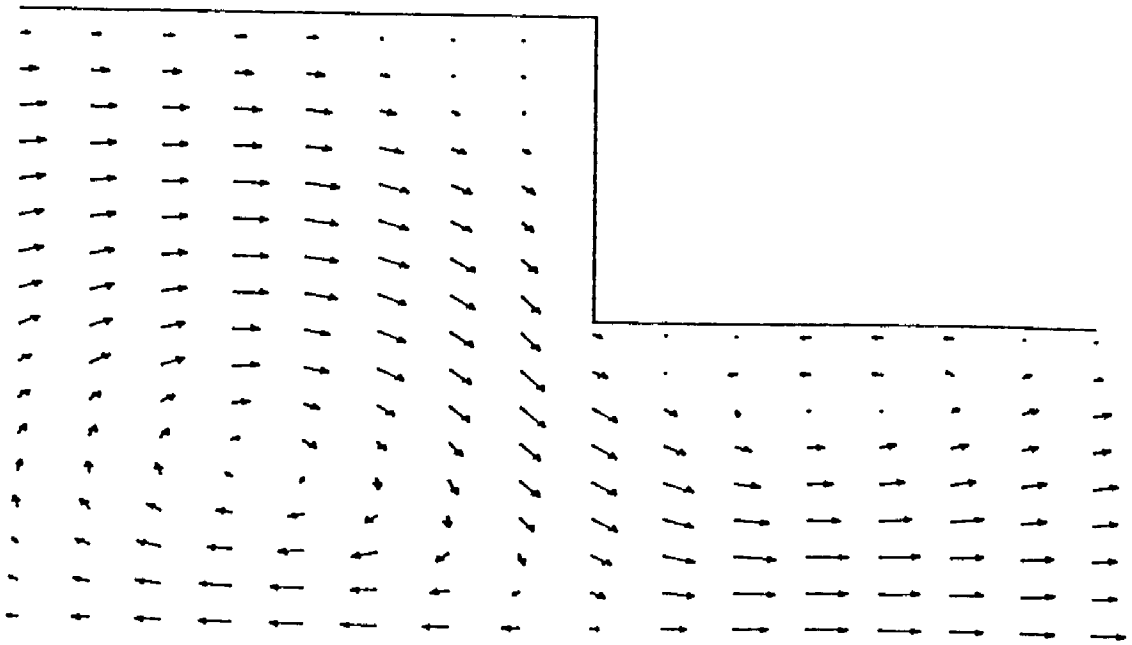

Figure 5-6. Flowfield for t = 0.00332 seconds
This is 3pi/10 radians after the end of the previous cycle
The velocity of the large piston is 20.23 meters/second
The velocity of the small piston is 40.45 meters/second

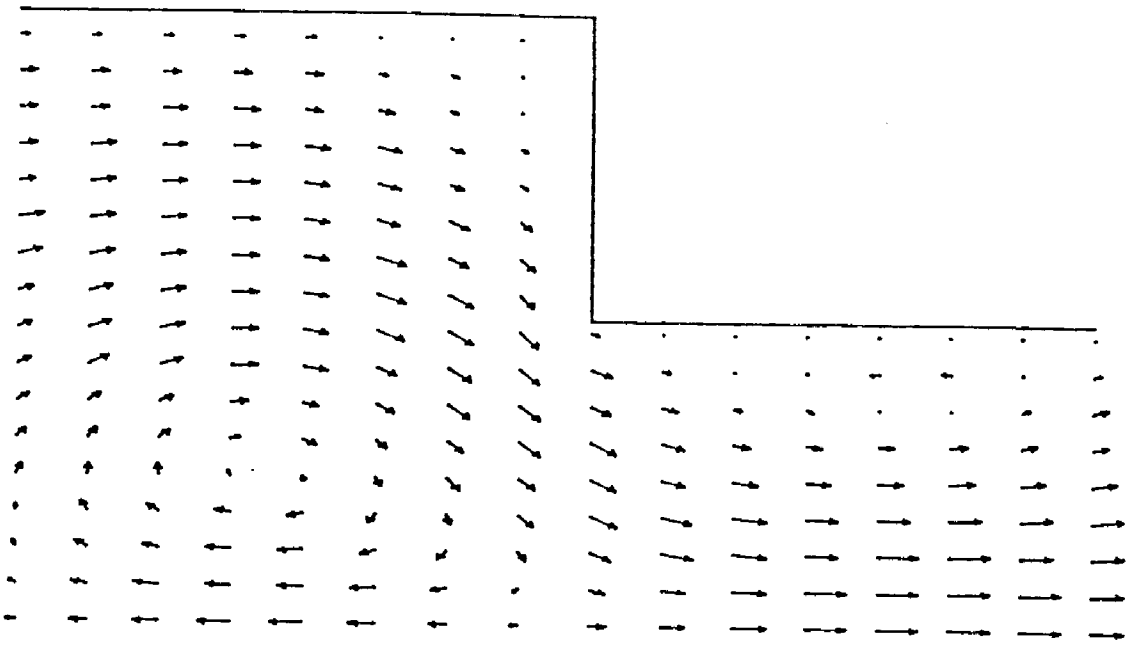

Figure 5-7. Flowfield for t = 0.00336 seconds
This is 4pi/10 radians after the end of the previous cycle
The velocity of the large piston is 23.78 meters/second
The velocity of the small piston is 47.55 meters/second

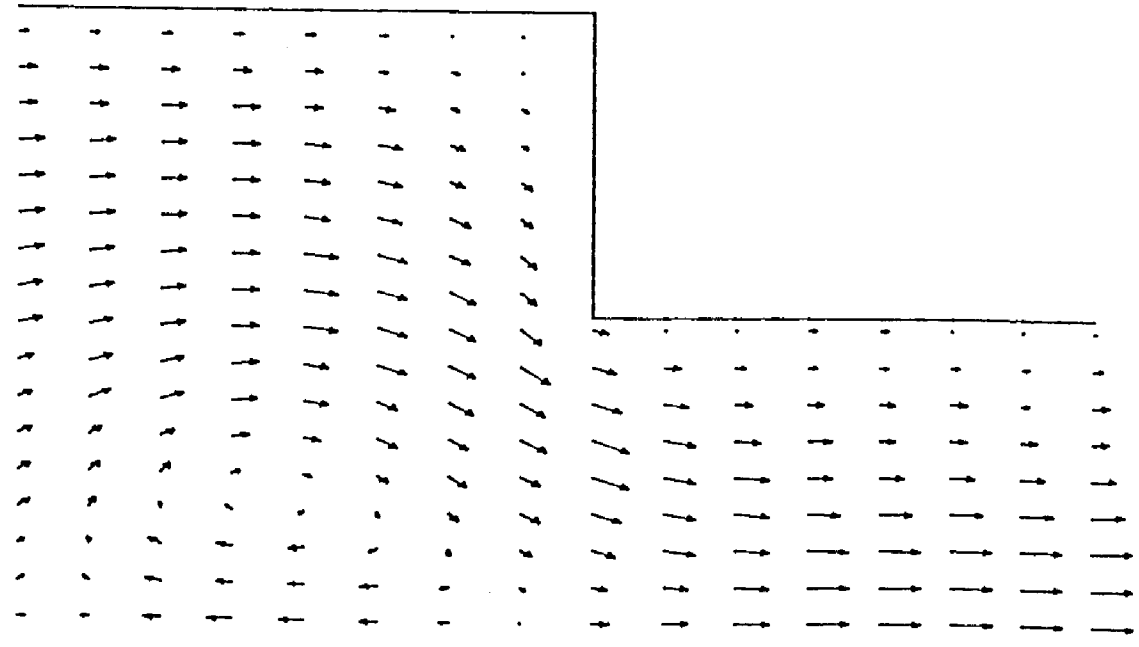

Figure 5-8. Flowfield for t = 0.00340 seconds
This is 5pi/10 radians after the end of the previous cycle
The velocity of the large piston is 25.00 meters/second
The velocity of the small piston is 50.00 meters/second

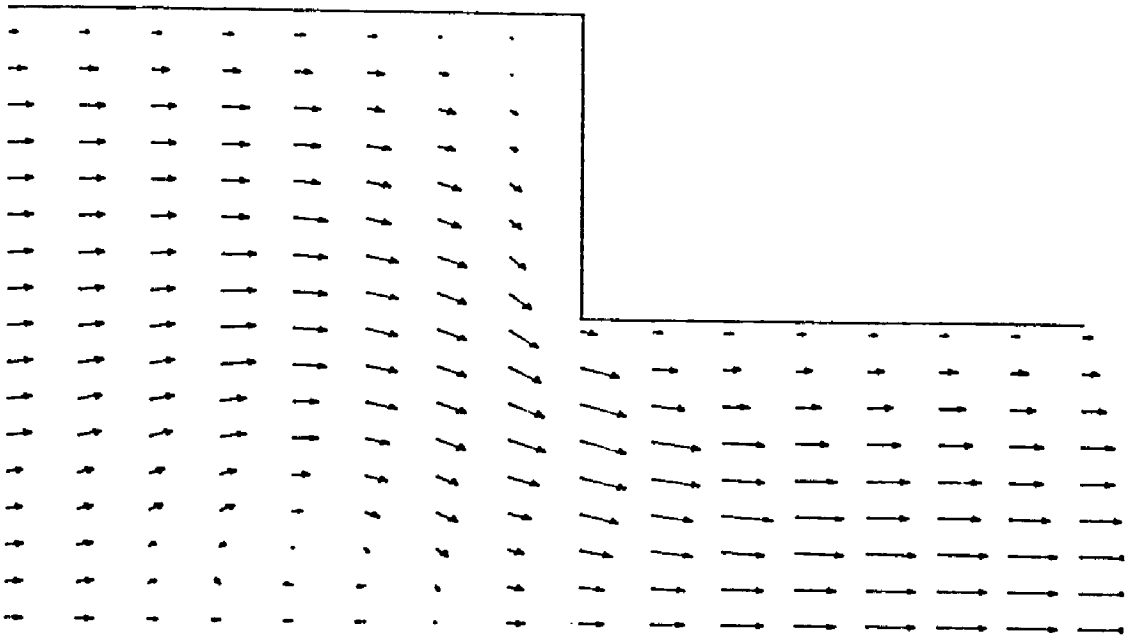

Figure 5-9. Flowfield for t = 0.00344 seconds
This is 6pi/10 radians after the end of the previous cycle
The velocity of the large piston is 23.78 meters/second
The velocity of the small piston is 47.55 meters/second

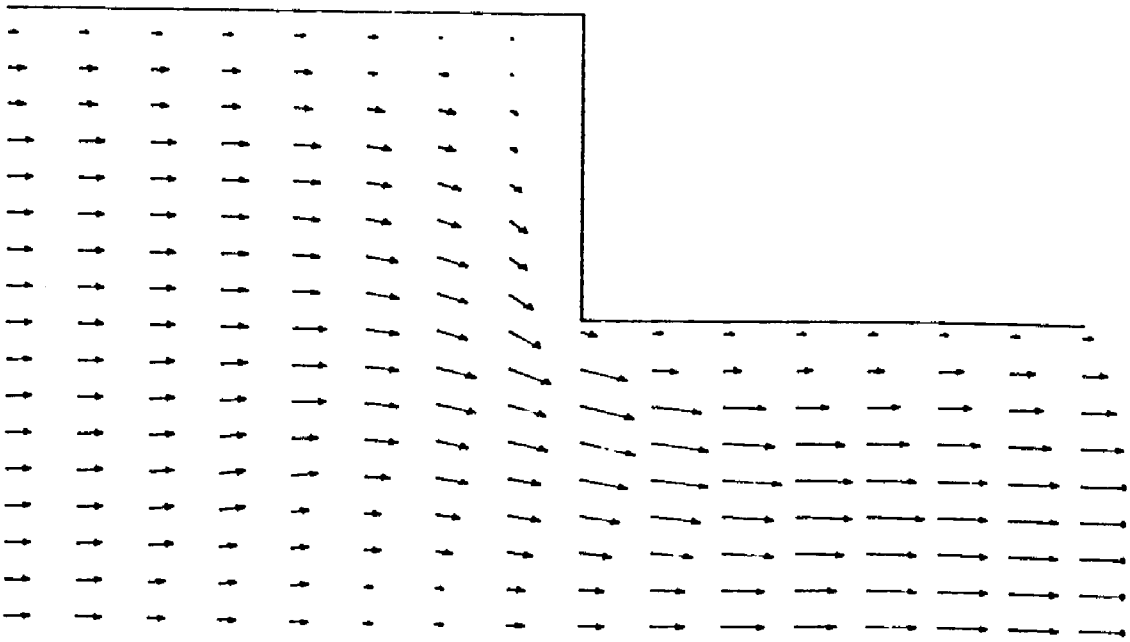

Figure 5-10. Flowfield for t = 0.00348 seconds
This is 7pi/10 radians after the end of the previous cycle
The velocity of the large piston is 20.23 meters/second
The velocity of the small piston is 40.45 meters/second

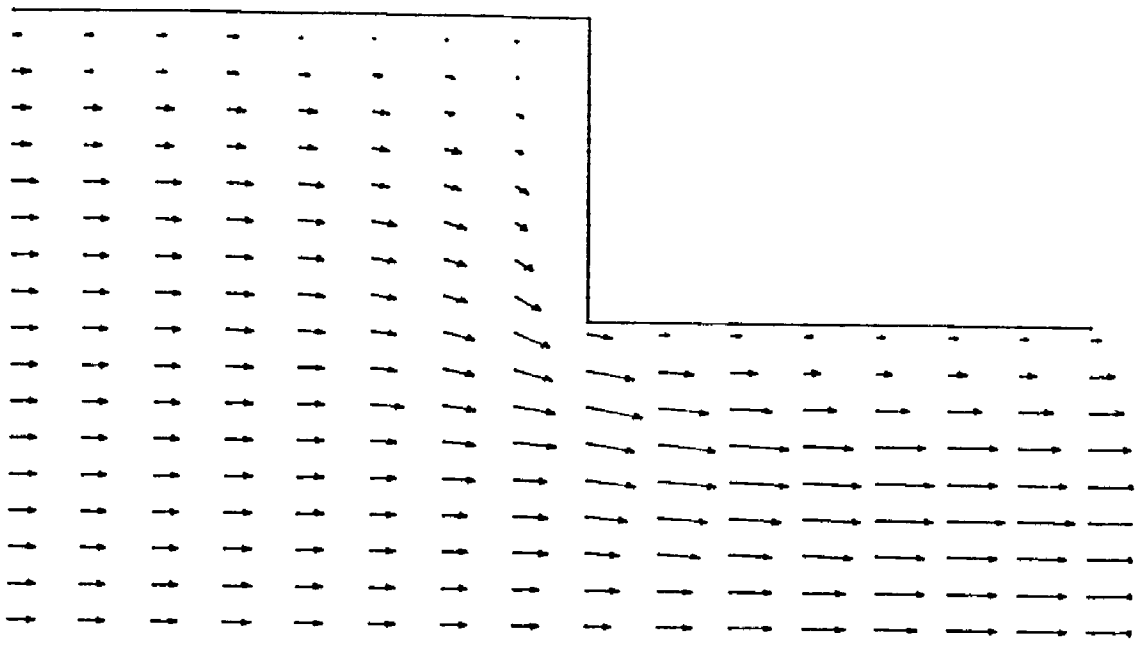

Figure 5-11. Flowfield for t = 0.00352 seconds
This is 8pi/10 radians after the end of the previous cycle
The velocity of the large piston is 14.69 meters/second
The velocity of the small piston is 29.39 meters/second

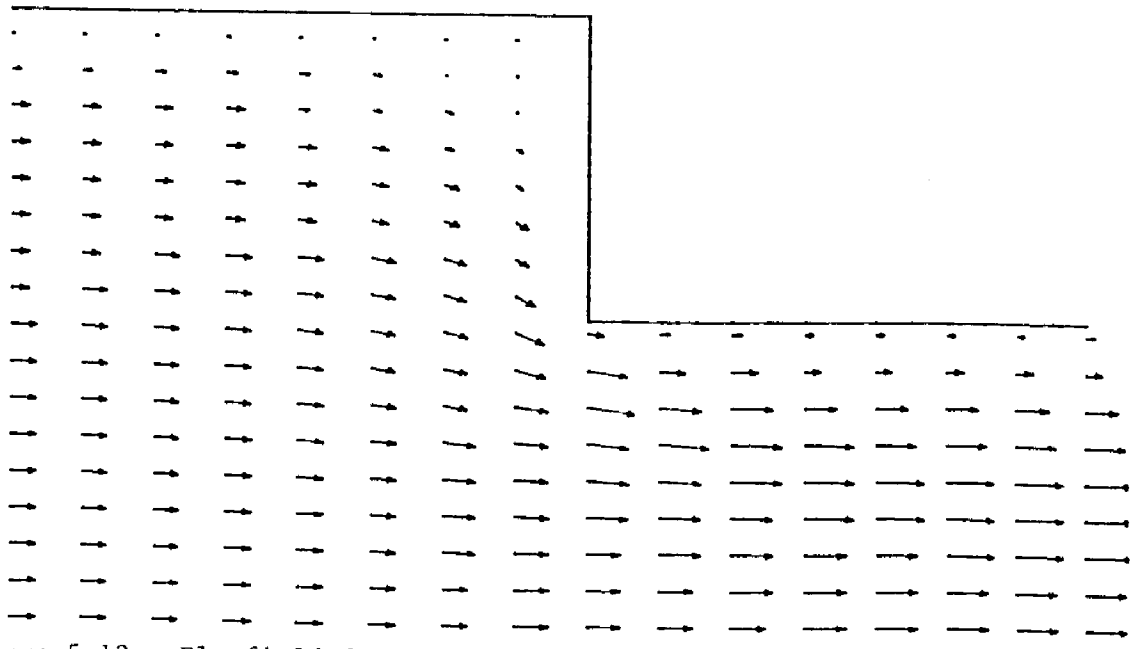

Figure 5-12. Flowfield for t = 0.00356 seconds
This is 9pi/10 radians after the end of the previous cycle
The velocity of the large piston is 7.72 meters/second
The velocity of the small piston is 15.45 meters/second

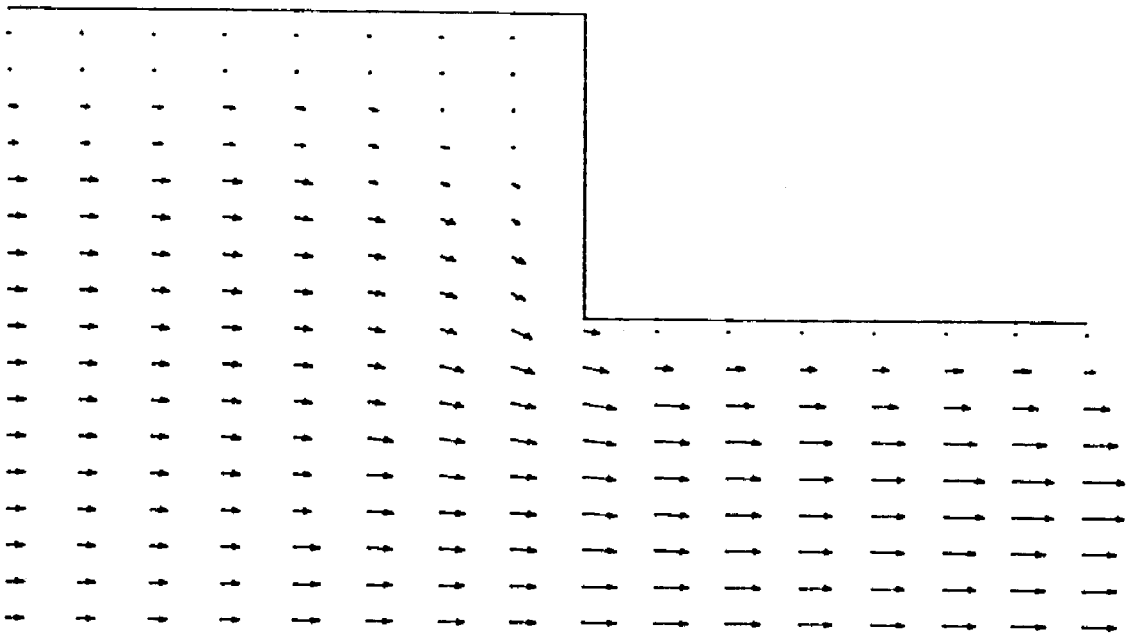

Figure 5-13. Flowfield for t = 0.00360 seconds
This is 10pi/10 radians after the end of the previous cycle
The velocity of the large piston is 0.0 meters/second
The velocity of the small piston is 0.0 meters/second

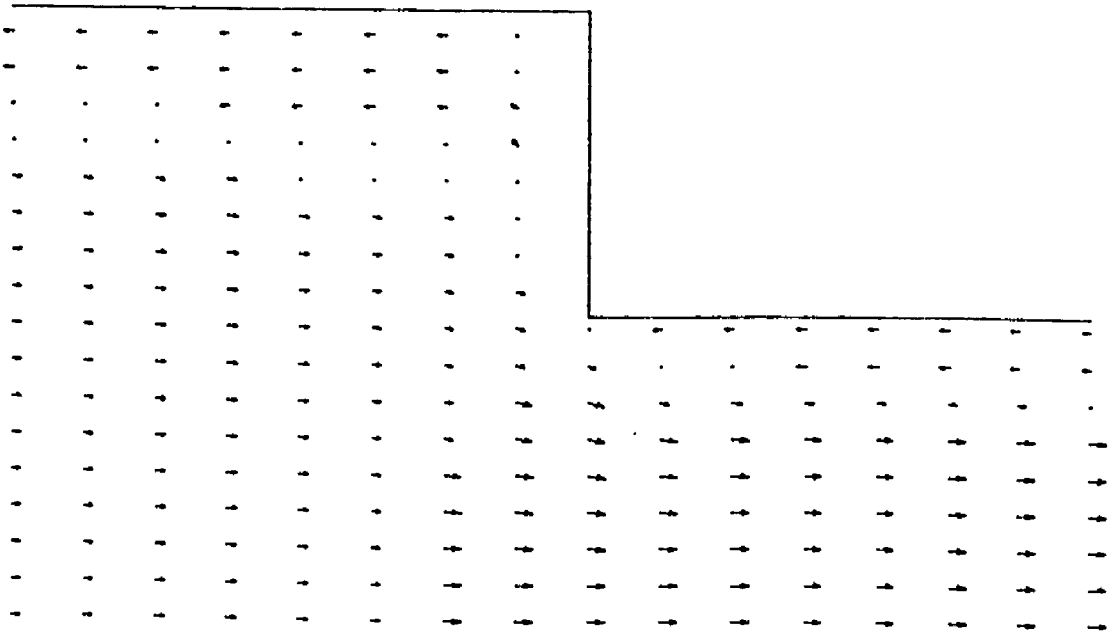

Figure 5-14. Flowfield for t = 0.00364 seconds
This is 11pi/10 radians after the end of the previous cycle
The velocity of the large piston is -7.72 meters/second
The velocity of the small piston is -15.45 meters/second

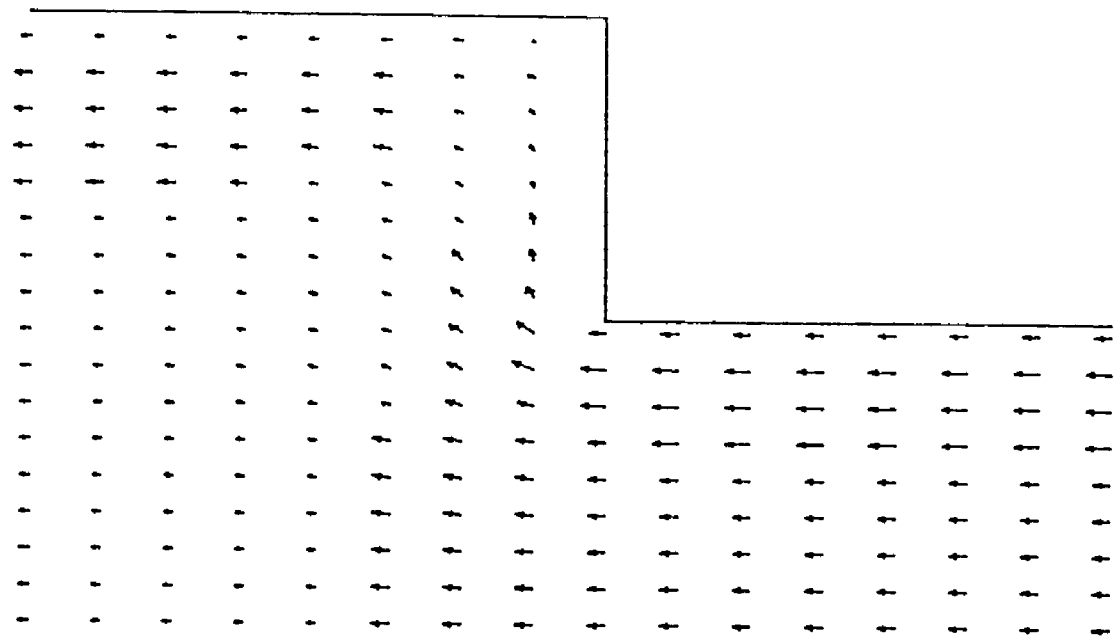

Figure 5-15. Flowfield for t = 0.00368 seconds
This is 12pi/10 radians after the end of the previous cycle
The velocity of the large piston is -14.69 meters/second
The velocity of the small piston is -29.39 meters/second

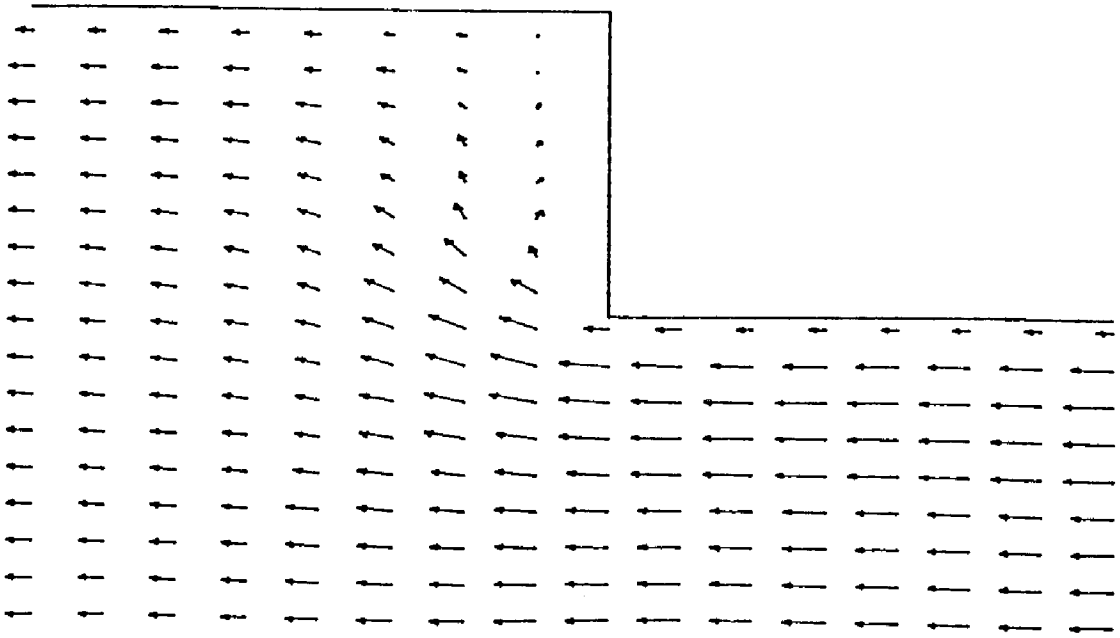

Figure 5-16. Flowfield for t = 0.00372 seconds
This is 13pi/10 radians after the end of the previous cycle
The velocity of the large piston is -20.23 meters/second
The velocity of the small piston is -40.45 meters/second

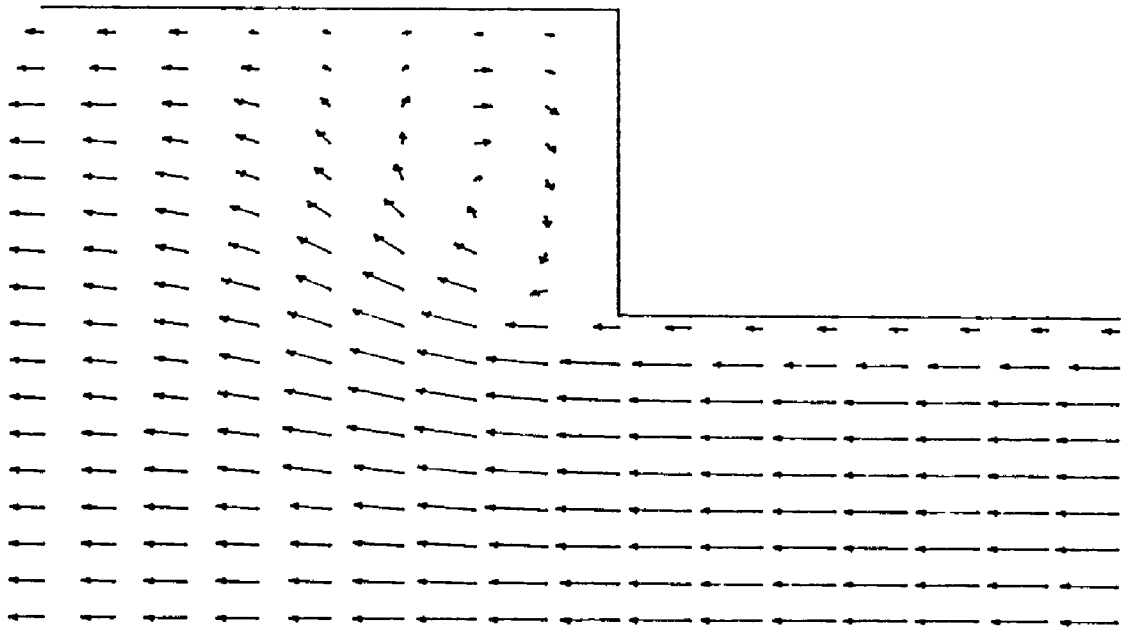

Figure 5-17. Flowfield for t = 0.00376 seconds
This is 14pi/10 radians after the end of the previous cycle
The velocity of the large piston is -23.78 meters/second
The velocity of the small piston is -47.55 meters/second

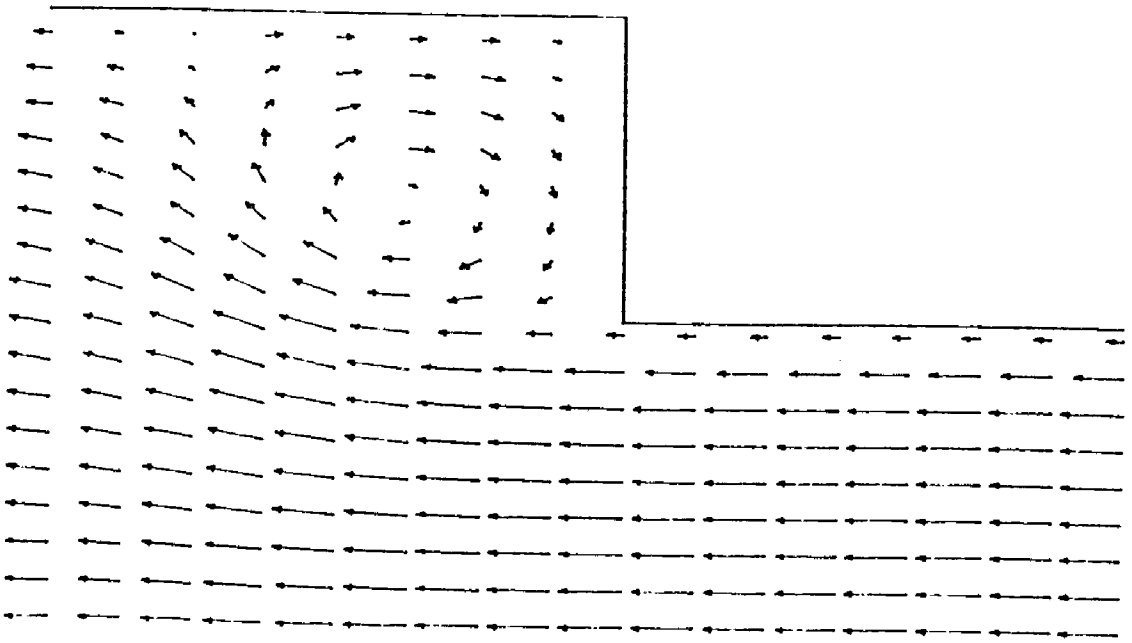

Figure 5-18. Flowfield for t = 0.00380 seconds
This is 15pi/10 radians after the end of the previous cycle
The velocity of the large piston is -25.00 meters/second
The velocity of the small piston is -50.00 meters/second

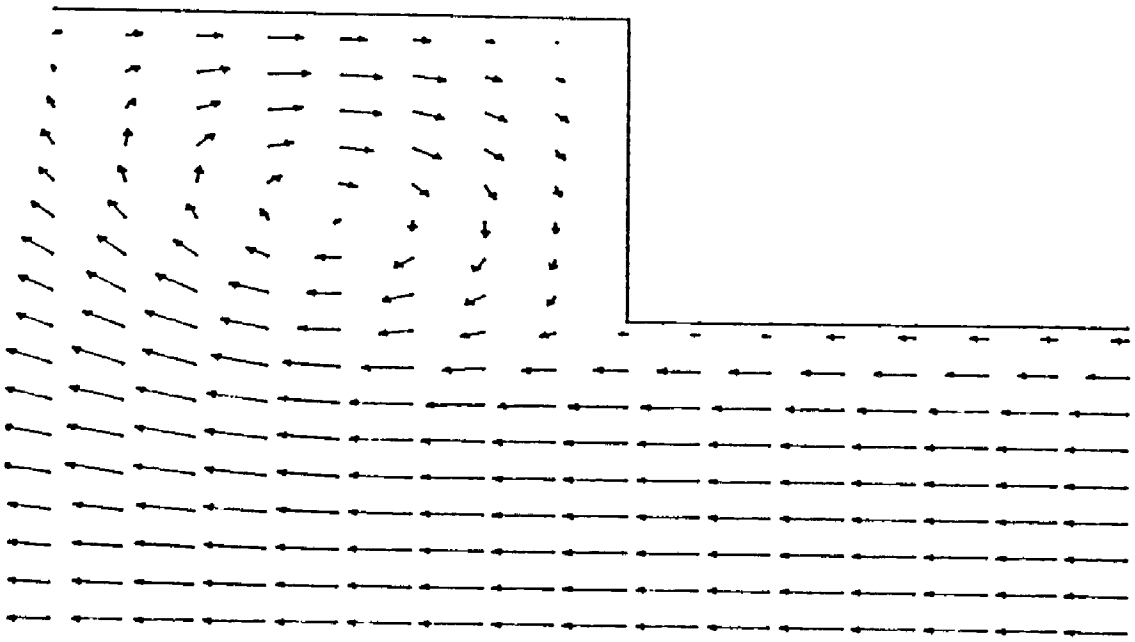

Figure 5-19. Flowfield for t = 0.00384 seconds
This is 16pi/10 radians after the end of the previous cycle
The velocity of the large piston is -23.78 meters/second
The velocity of the small piston is -47.55 meters/second

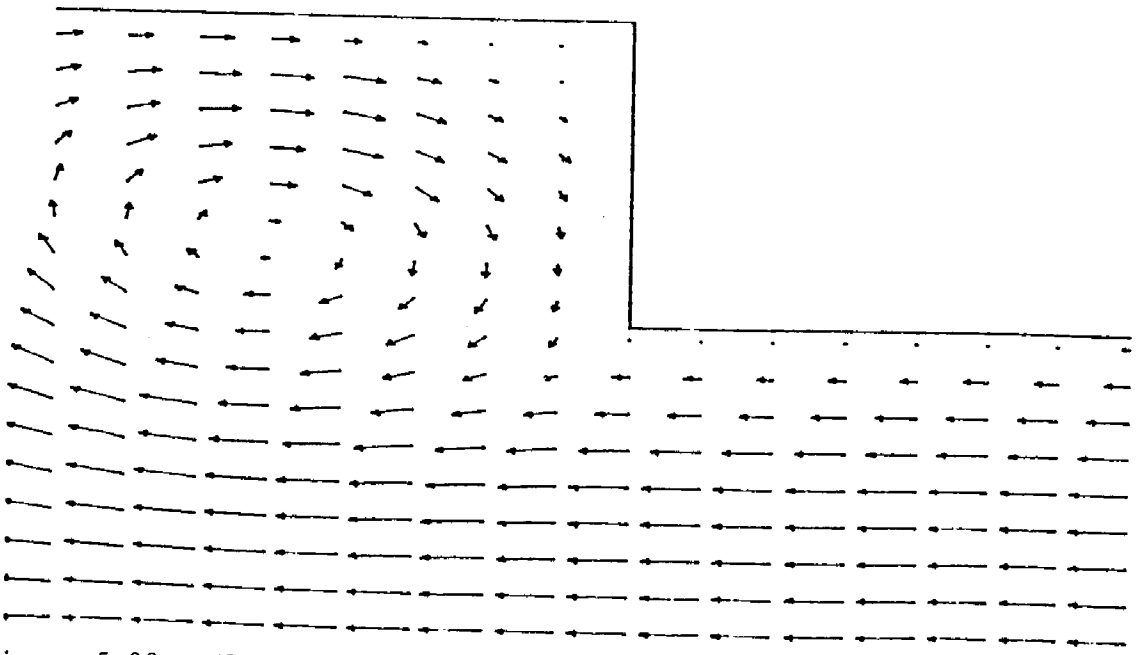

Figure 5-20. Flowfield for t = 0.00388 seconds
This is 17pi/10 radians after the end of the previous cycle
The velocity of the large piston is -20.23 meters/second
The velocity of the small piston is -40.45 meters/second

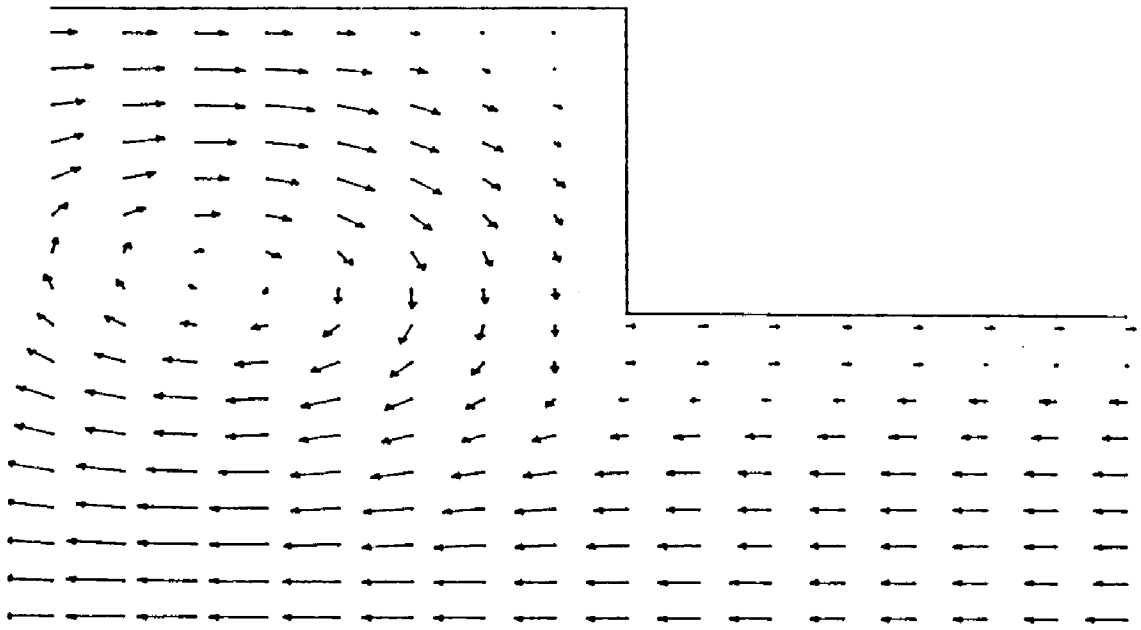

Figure 5-21. Flowfield for t = 0.00392 seconds
This is 18pi/10 radians after the end of the previous cycle
The velocity of the large piston is -14.69 meters/second
The velocity of the small piston is -29.39 meters/second

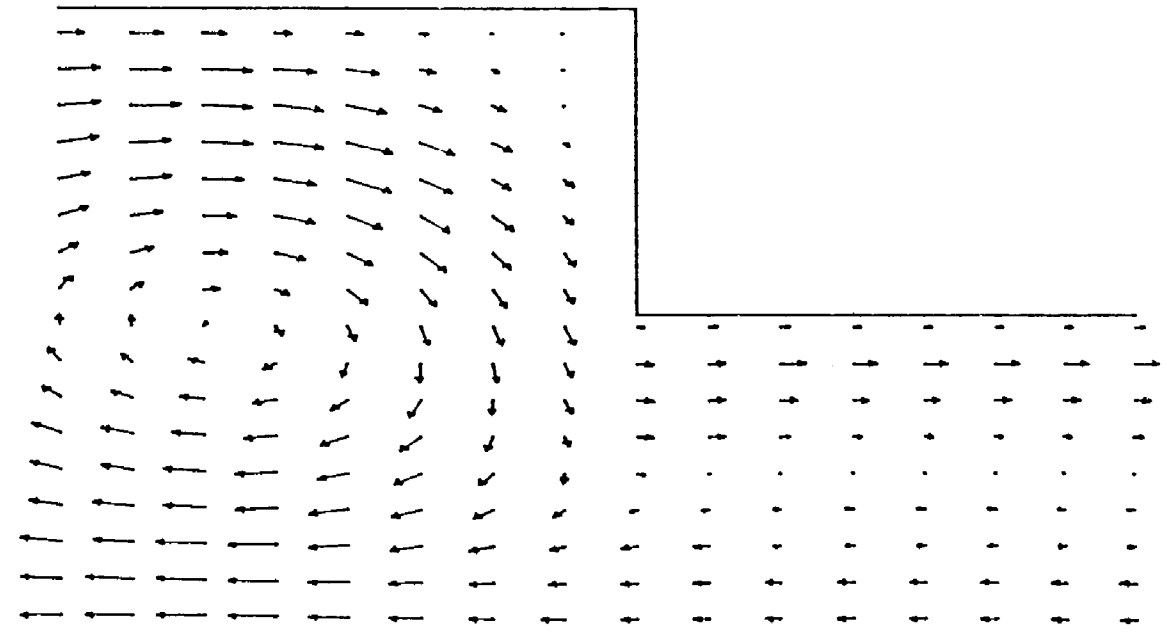

Figure 5-22. Flowfield for t = 0.00396 seconds
This is 19pi/10 radians after the end of the previous cycle
The velocity of the large piston is -7.73 meters/second
The velocity of the small piston is -15.45 meters/second

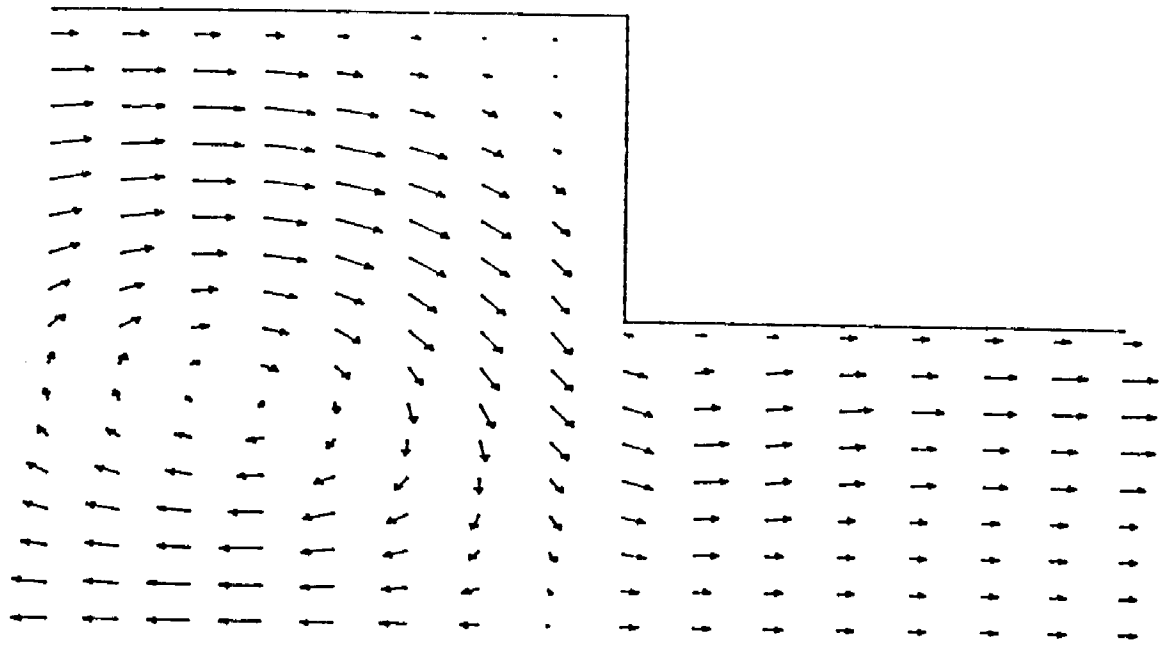

Figure 5-23. Flowfield for t = 0.00400 seconds
This is 20pi/10 radians after the end of the previous cycle
The velocity of the large piston is 0.0 meters/second
The velocity of the small piston is 0.0 meters/second

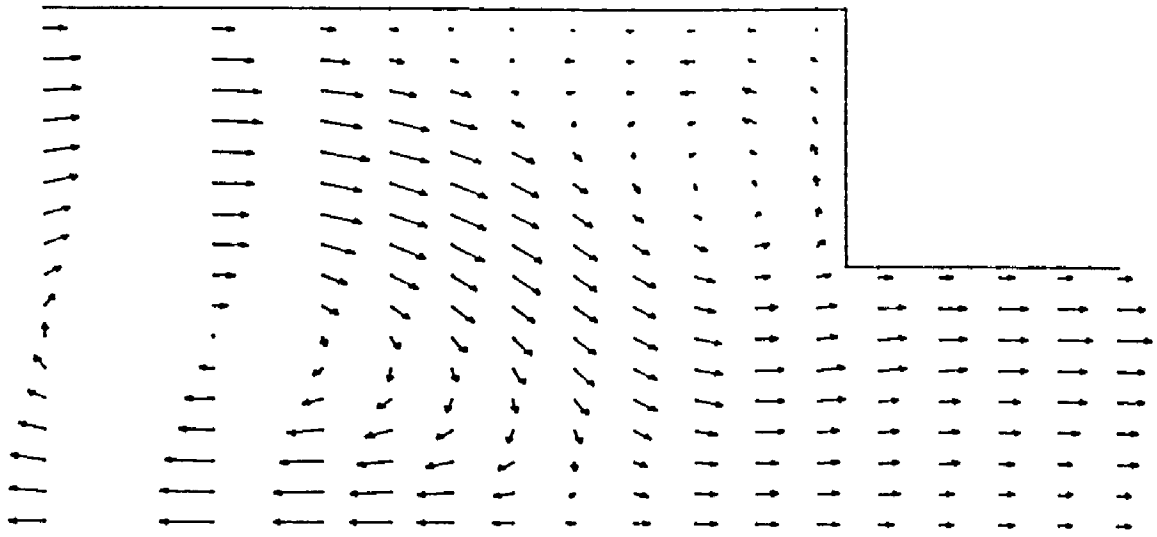

Figure 5-24. Flowfield for t = 0.00320 seconds
This is 0.0 radians after the end of the previous cycle
The velocity of the large piston is 0.0 meters/second
The velocity of the small piston is 0.0 meters/second

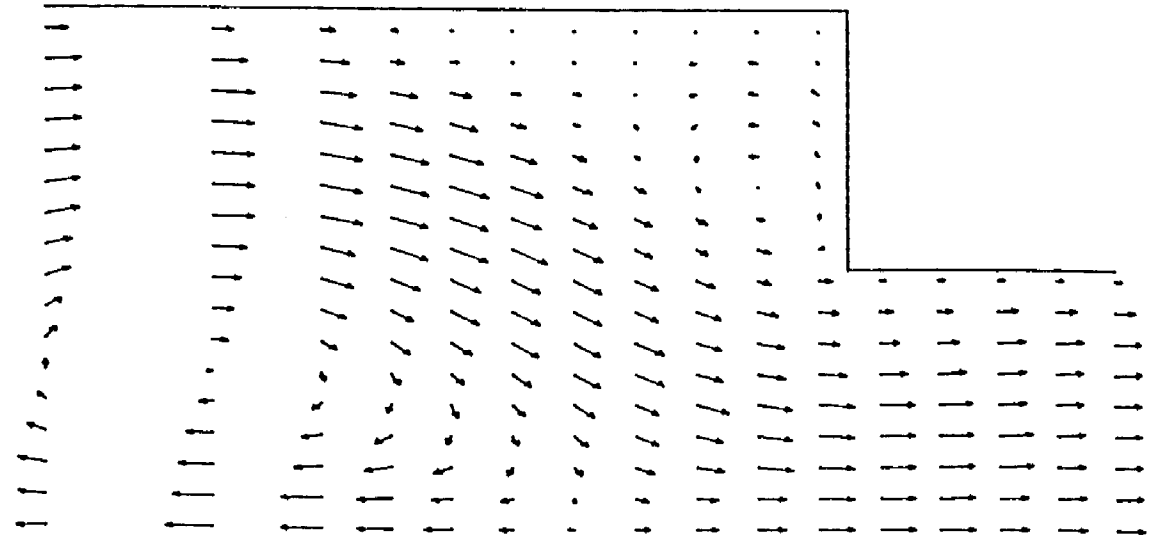

Figure 5-25. Flowfield for t = 0.00324 seconds
This is pi/10 radians after the end of the previous cycle
The velocity of the large piston is 11.58 meters/second
The velocity of the small piston is 23.18 meters/second

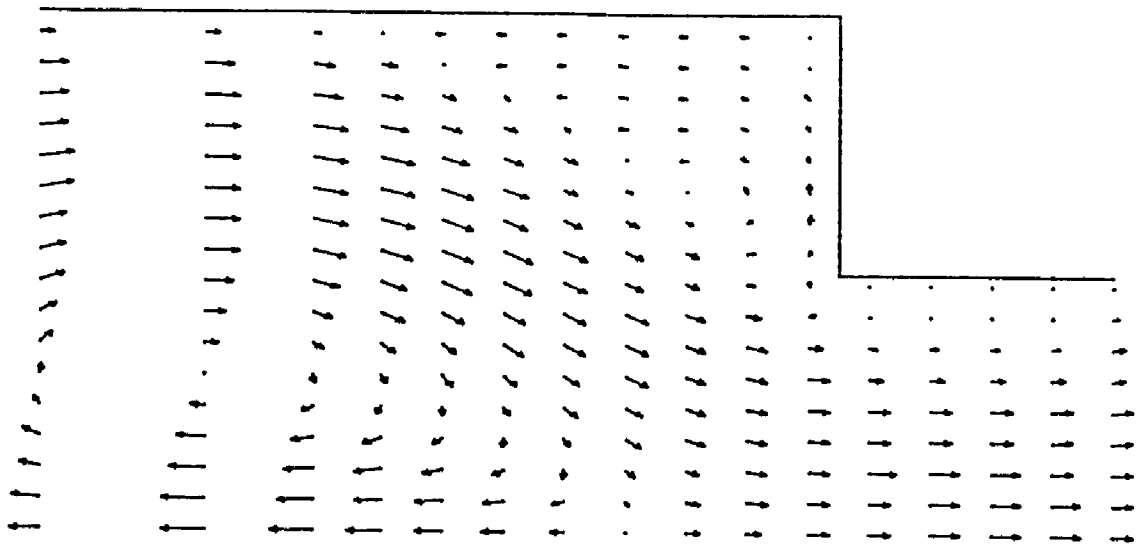

Figure 5-26. Flowfield for t = 0.00328 seconds
This is 2pi/10 radians after the end of the previous cycle
The velocity of the large piston is 22.04 meters/second
The velocity of the small piston is 44.09 meters/second

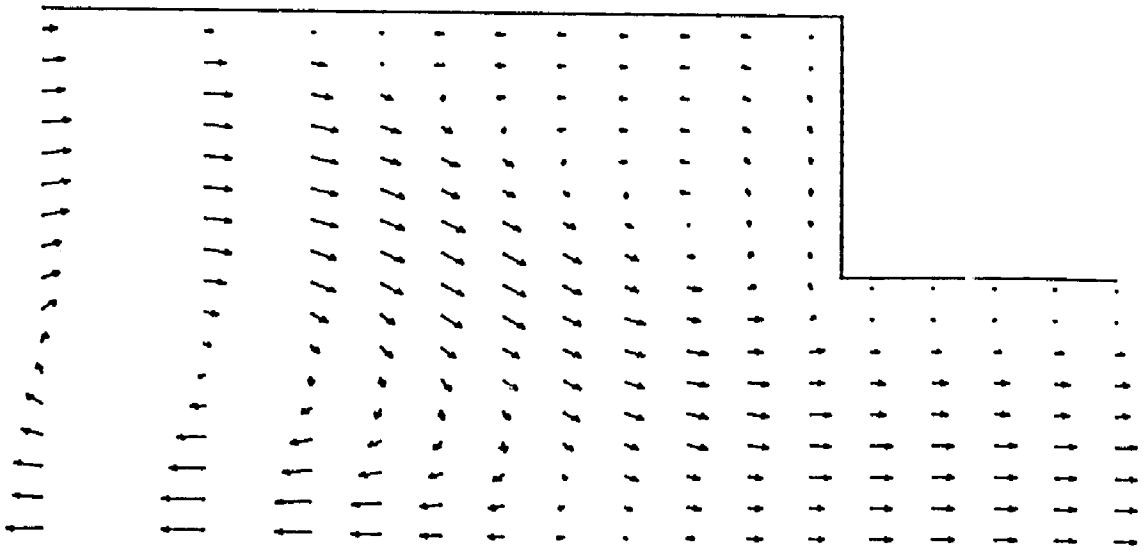

Figure 5-27. Flowfield for t = 0.00332 seconds
This is 3pi/10 radians after the end of the previous cycle
The velocity of the large piston is 30.35 meters/second
The velocity of the small piston is 60.68 meters/second

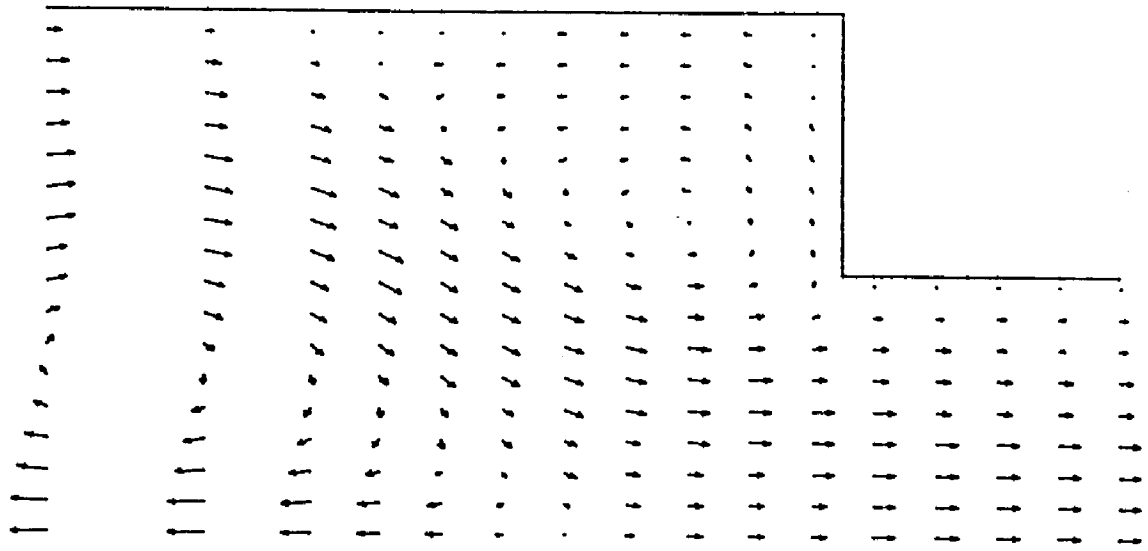

Figure 5-28. Flowfield for t = 0.00336 seconds
This is 4pi/10 radians after the end of the previous cycle
The velocity of the large piston is 35.67 meters/second
The velocity of the small piston is 71.33 meters/second

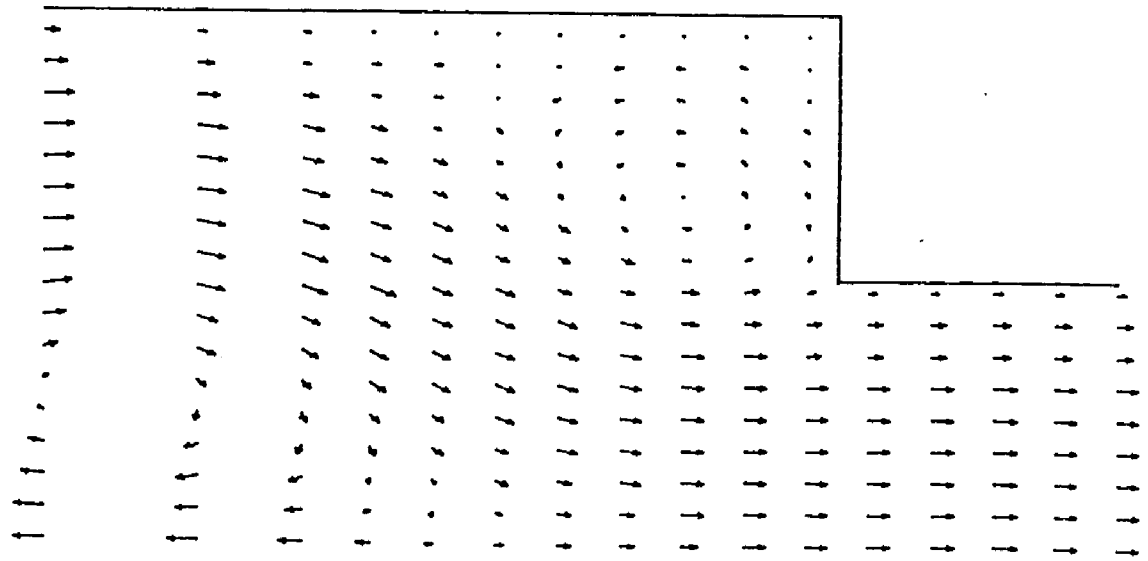

Figure 5-29. Flowfield for t = 0.00340 seconds
This is 5pi/10 radians after the end of the previous cycle
The velocity of the large piston is 37.50 meters/second
The velocity of the small piston is 75.00 meters/second

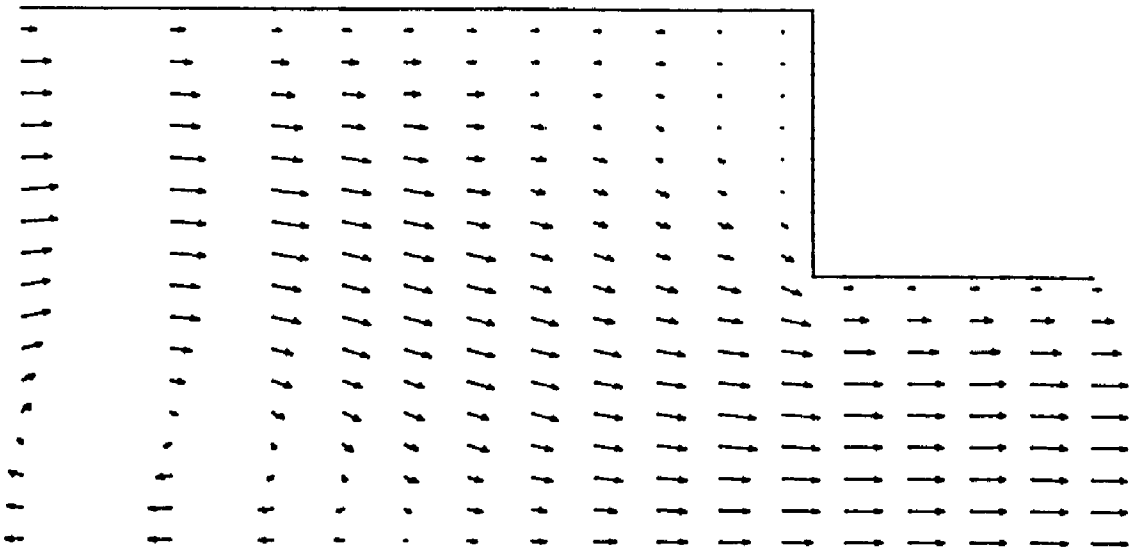

Figure 5-30. Flowfield for t = 0.00344 seconds
This is 6pi/10 radians after the end of the previous cycle
The velocity of the large piston is 35.67 meters/second
The velocity of the small piston is 71.33 meters/second

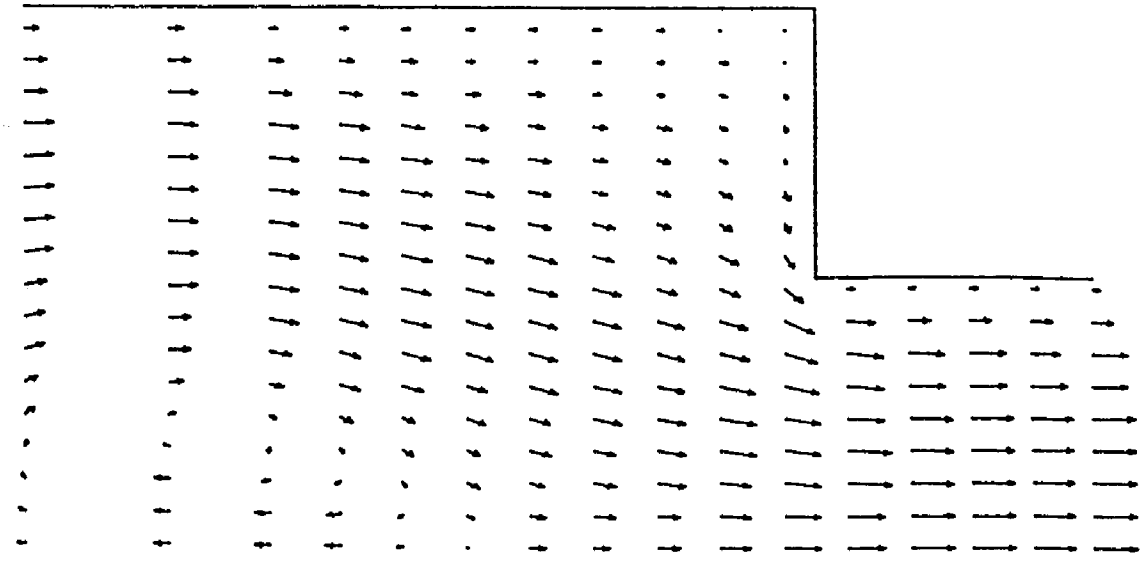

Figure 5-31. Flowfield for t = 0.00348 seconds
This is 7pi/10 radians after the end of the previous cycle
The velocity of the large piston is 30.35 meters/second
The velocity of the small piston is 60.68 meters/second

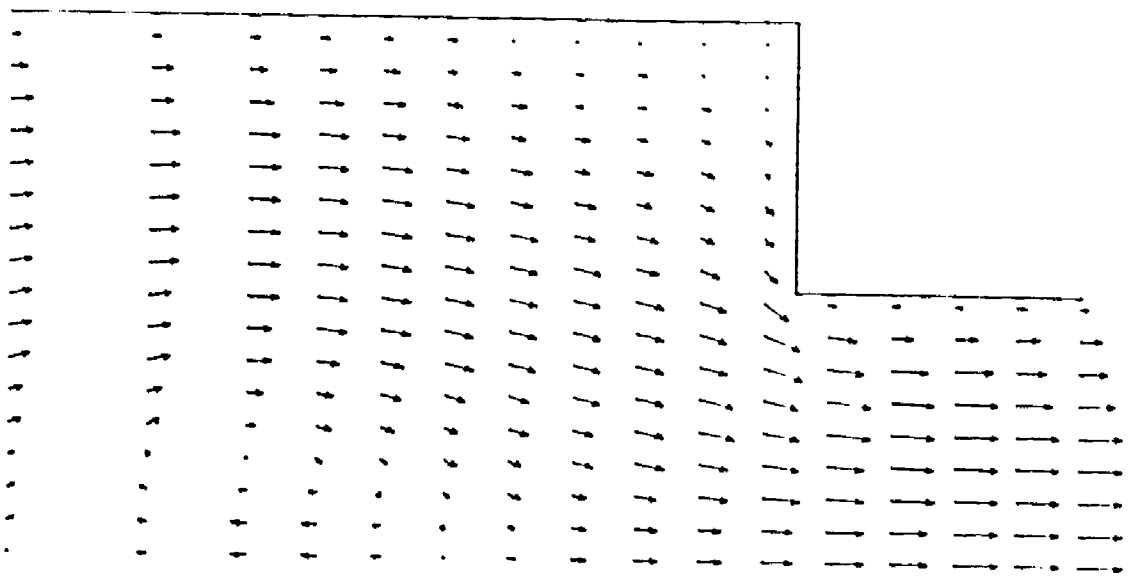

Figure 5-32. Flowfield for t = 0.00352 seconds
This is 8pi/10 radians after the end of the previous cycle
The velocity of the large piston is 22.04 meters/second
The velocity of the small piston is 44.09 meters/second

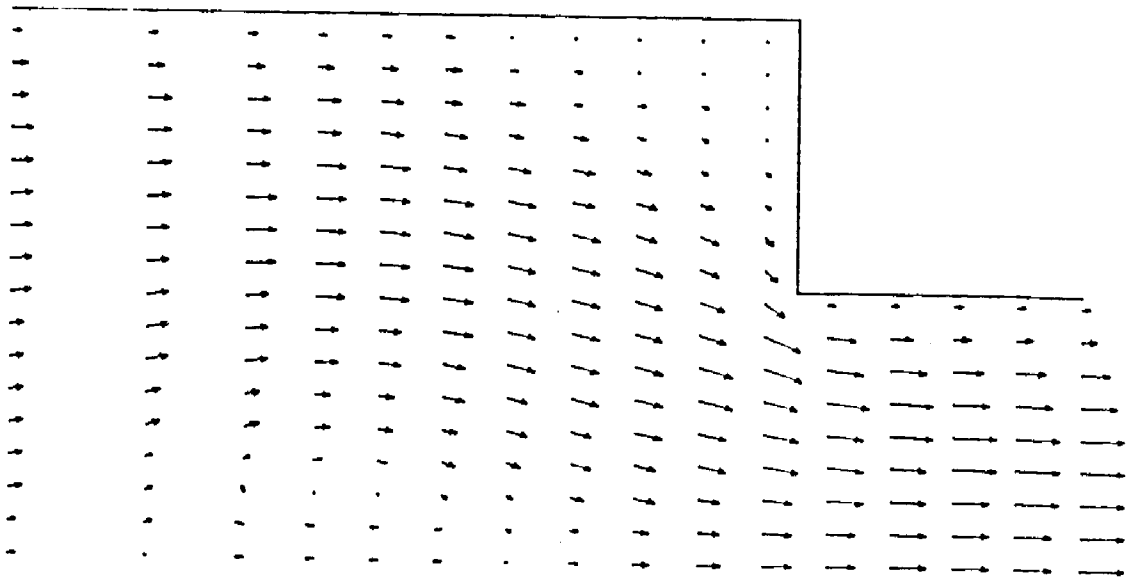

Figure 5-33. Flowfield for t = 0.00356 seconds
This is 9pi/10 radians after the end of the previous cycle
The velocity of the large piston is 11.58 meters/second
The velocity of the small piston is 23.18 meters/second

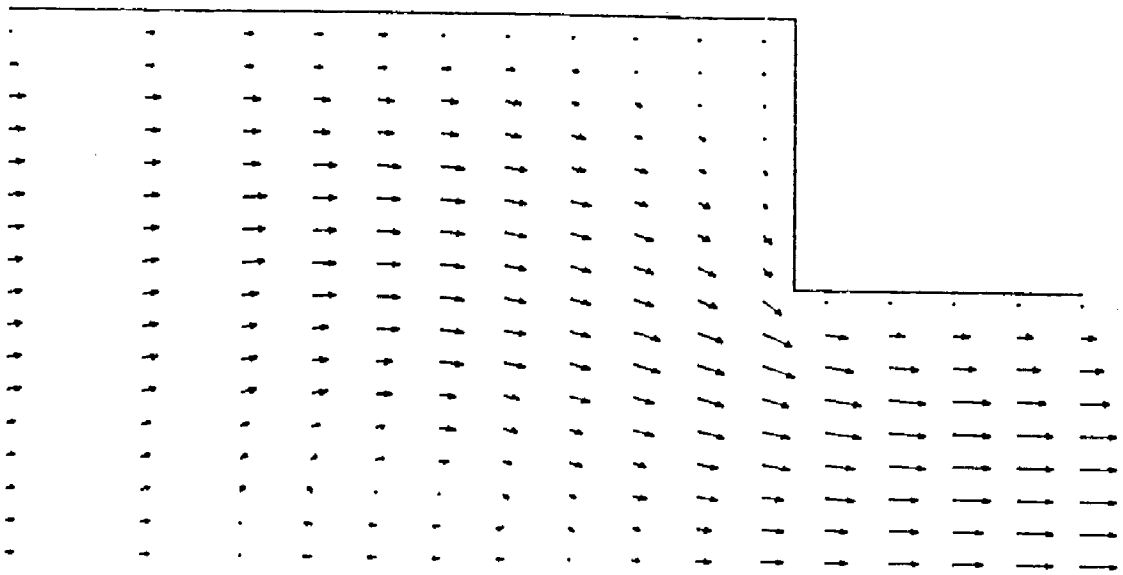

Figure 5-34. Flowfield for t = 0.00360 seconds
This is 10pi/10 radians after the end of the previous cycle
The velocity of the large piston is 0.0 meters/second
The velocity of the small piston is 0.0 meters/second

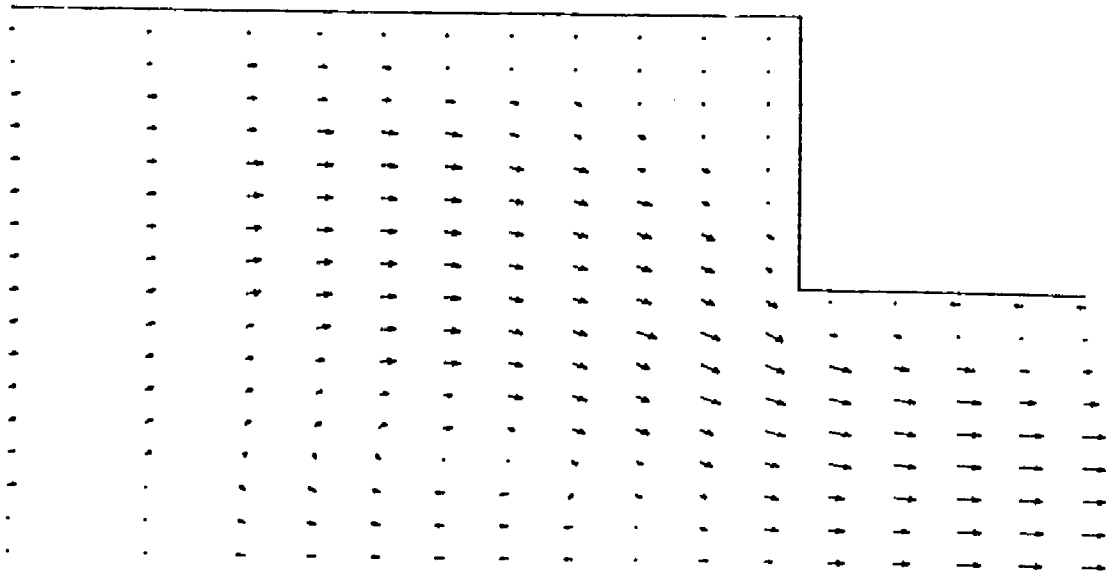

Figure 5-35. Flowfield for t = 0.00364 seconds
This is 11pi/10 radians after the end of the previous cycle
The velocity of the large piston is -11.58 meters/second
The velocity of the small piston is -23.18 meters/second

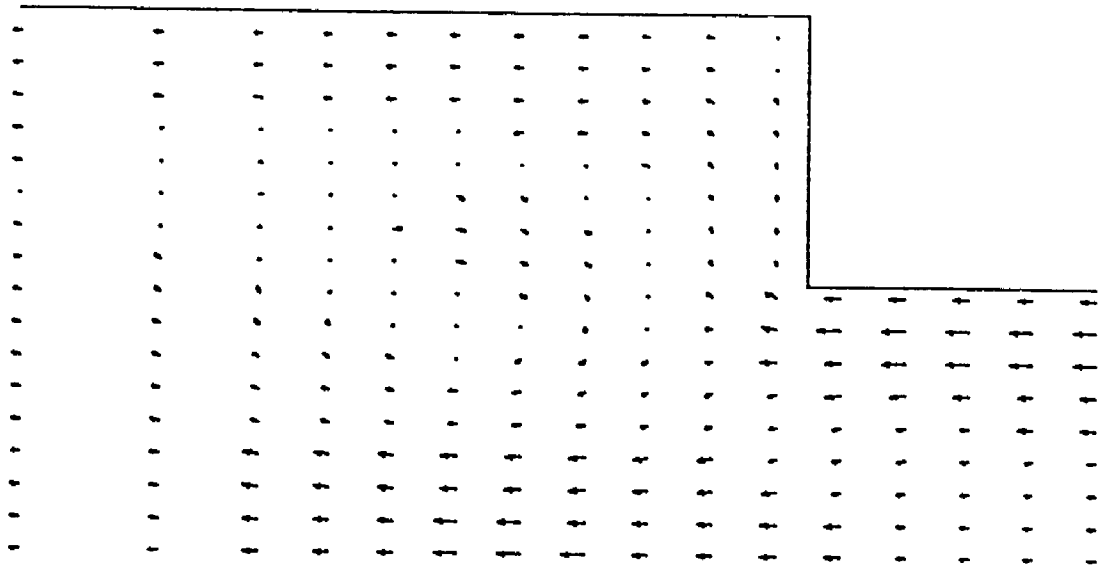

Figure 5-36. Flowfield for t = 0.00368 seconds
This is 12pi/10 radians after the end of the previous cycle
The velocity of the large piston is -22.04 meters/second
The velocity of the small piston is -44.09 meters/second

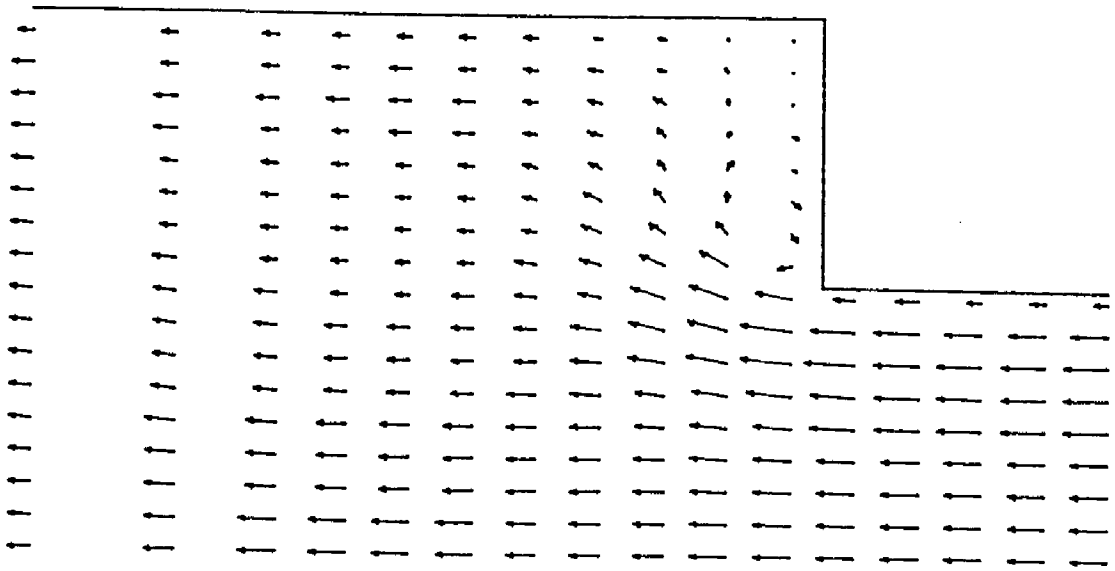

Figure 5-37. Flowfield for t = 0.00372 seconds
This is 13pi/10 radians after the end of the previous cycle
The velocity of the large piston is -30.35 meters/second
The velocity of the small piston is -60.68 meters/second

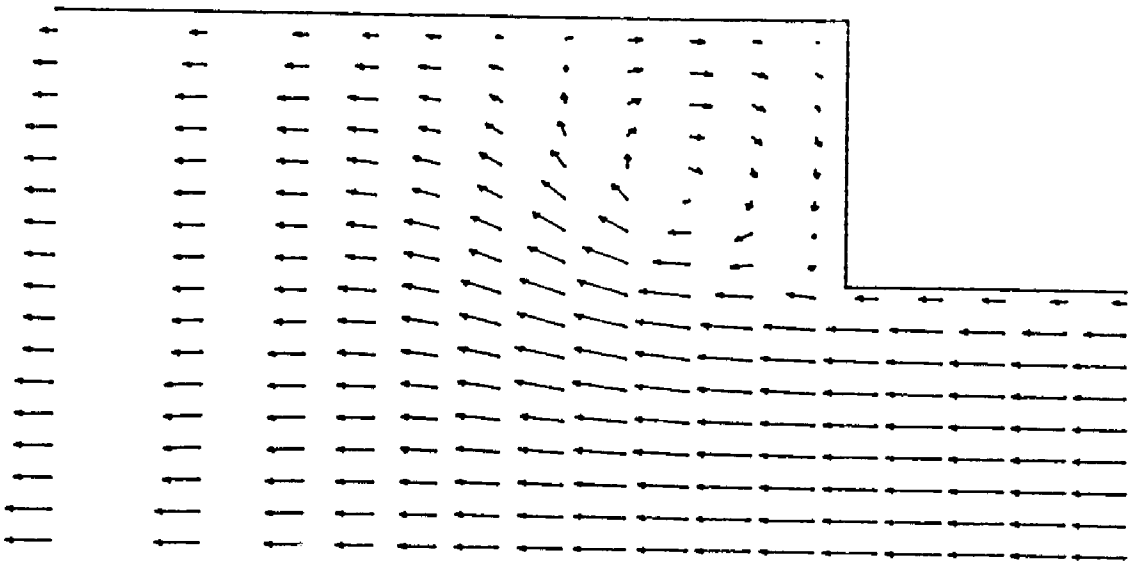

Figure 5-38. Flowfield for t = 0.00376 seconds
This is 14pi/10 radians after the end of the previous cycle
The velocity of the large piston is -35.67 meters/second
The velocity of the small piston is -71.33 meters/second

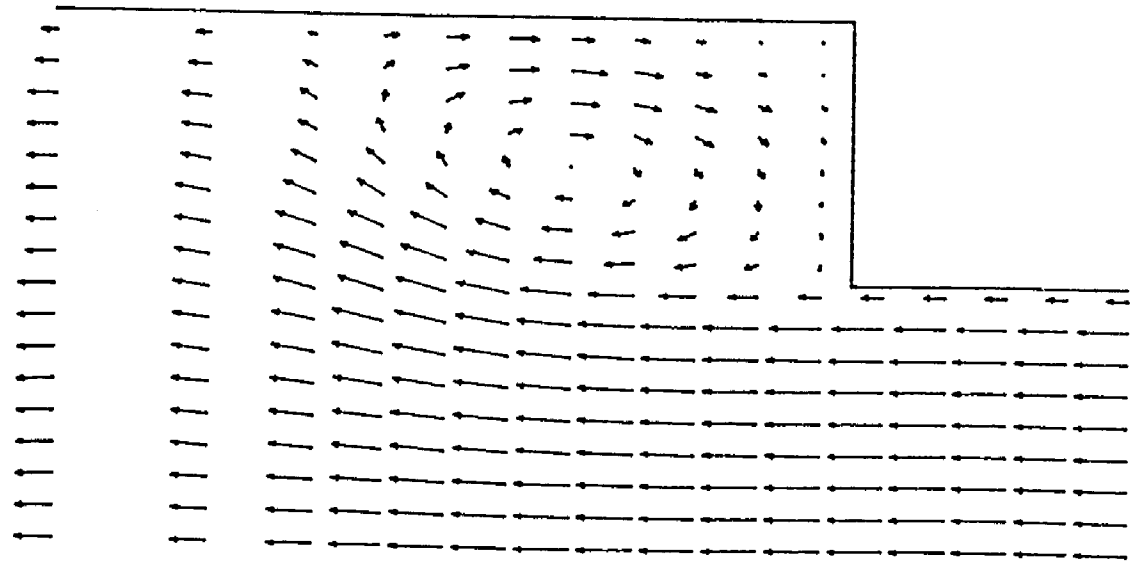

Figure 5-39. Flowfield for t = 0.00380 seconds
This is 15pi/10 radians after the end of the previous cycle
The velocity of the large piston is -37.50 meters/second
The velocity of the small piston is -75.00 meters/second

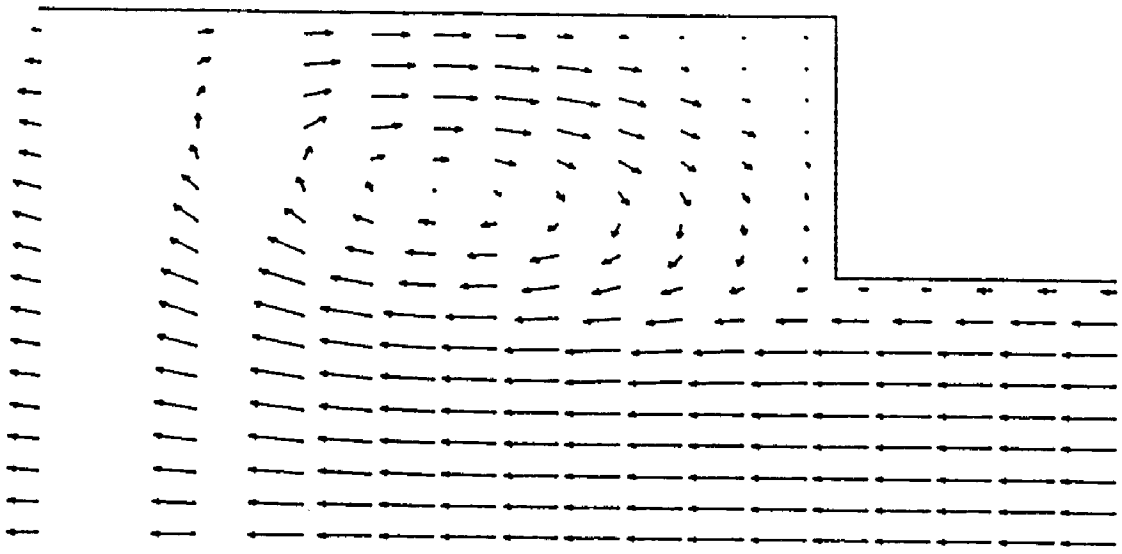

Figure 5-40. Flowfield for t = 0.00384 seconds
This is 16pi/10 radians after the end of the previous cycle
The velocity of the large piston is -35.67 meters/second
The velocity of the small piston is -71.33 meters/second

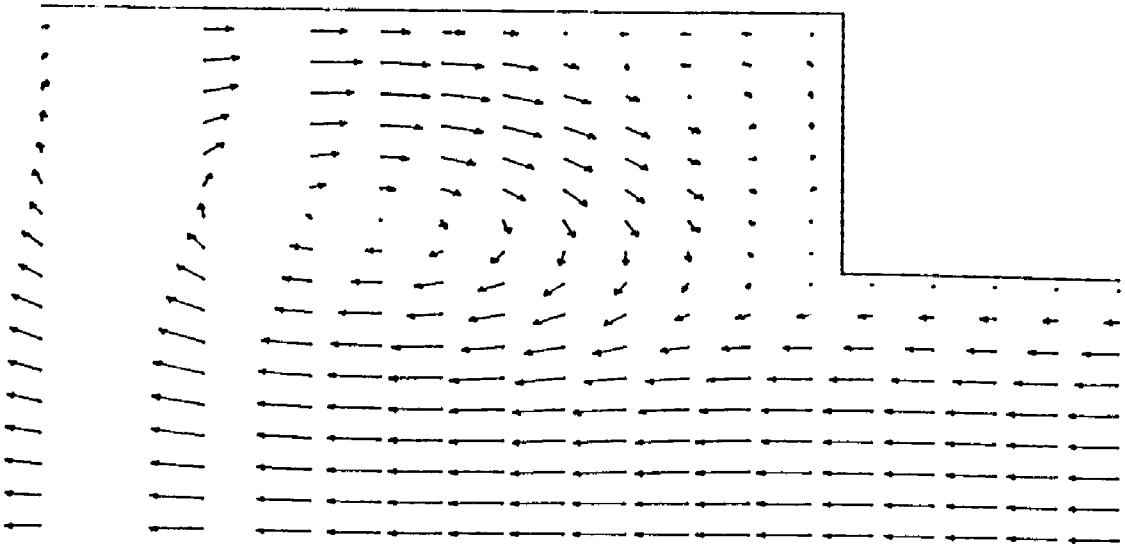

Figure 5-41. Flowfield for t = 0.00388 seconds
This is 17pi/10 radians after the end of the previous cycle
The velocity of the large piston is -30.35 meters/second
The velocity of the small piston is -60.68 meters/second

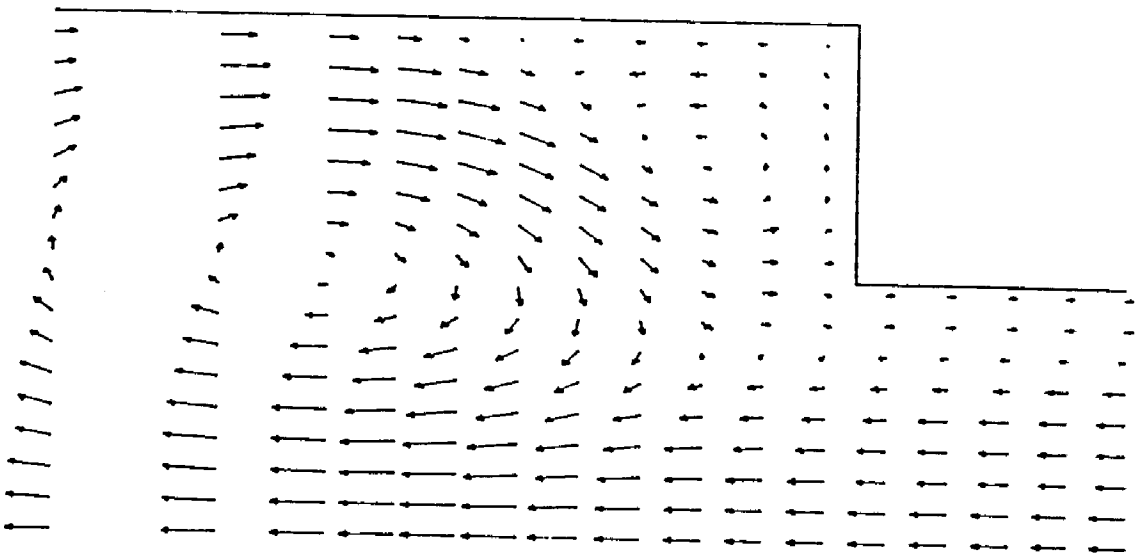

Figure 5-42. Flowfield for t = 0.00392 seconds
This is 18pi/10 radians after the end of the previous cycle
The velocity of the large piston is -22.04 meters/second
The velocity of the small piston is -44.09 meters/second

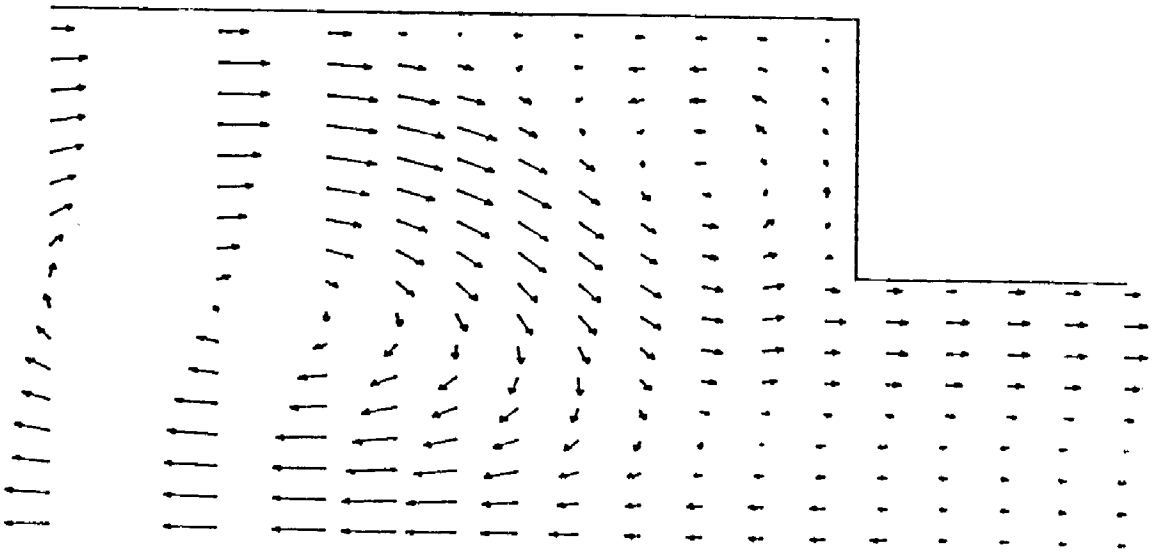

Figure 5-43. Flowfield for t = 0.00396 seconds
This is 19pi/10 radians after the end of the previous cycle
The velocity of the large piston is -11.60 meters/second
The velocity of the small piston is -23.10 meters/second

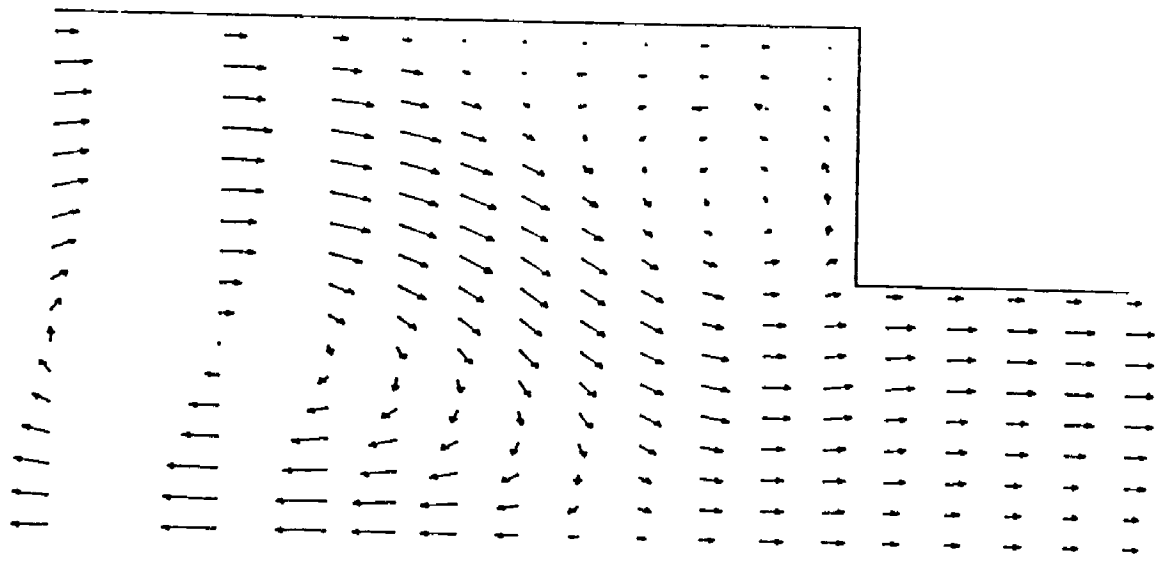

Figure 5-44. Flowfield for t = 0.00400 seconds
This is 20pi/10 radians after the end of the previous cycle
The velocity of the large piston is 0.0 meters/second
The velocity of the small piston is 0.0 meters/second

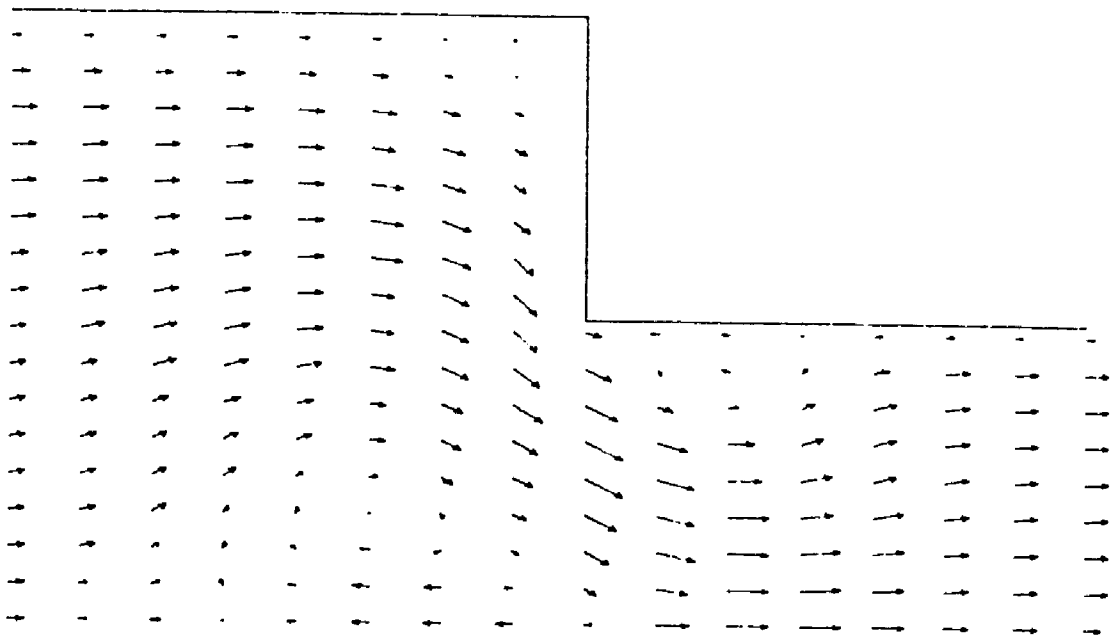

Figure 5-45. Flowfield for t = 0.00320 seconds
This is 0.0 radians after the end of the previous cycle
The velocity of the large piston is 25.0 meters/second
The velocity of the small piston is 0.0 meters/second

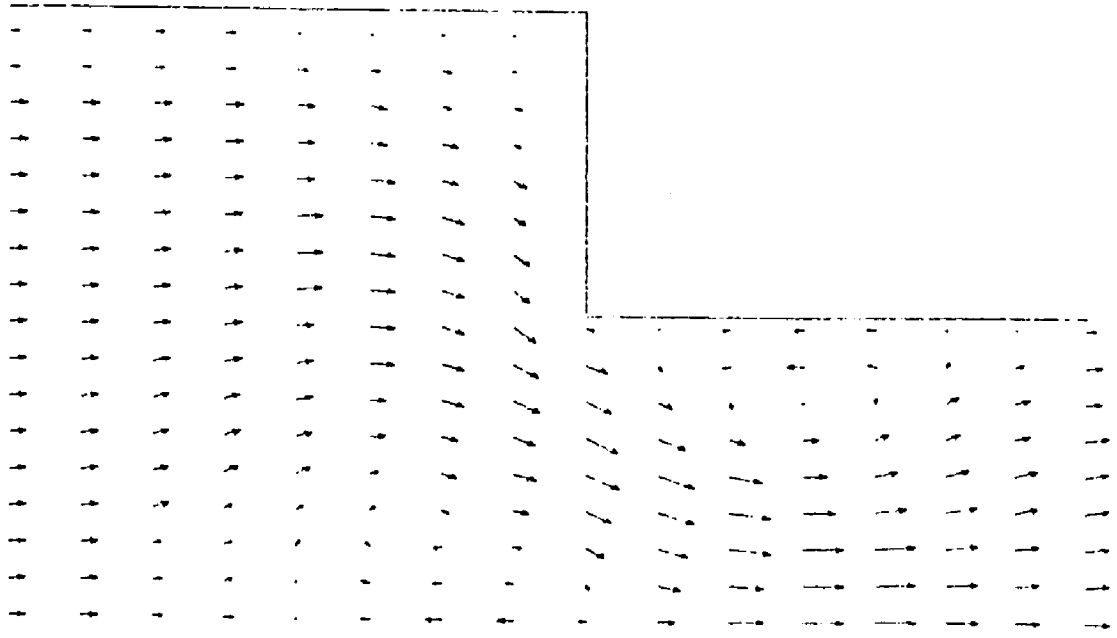

Figure 5-46. Flowfield for t = 0.00324 seconds
This is pi/10 radians after the end of the previous cycle
The velocity of the large piston is 23.78 meters/second
The velocity of the small piston is 15.45 meters/second

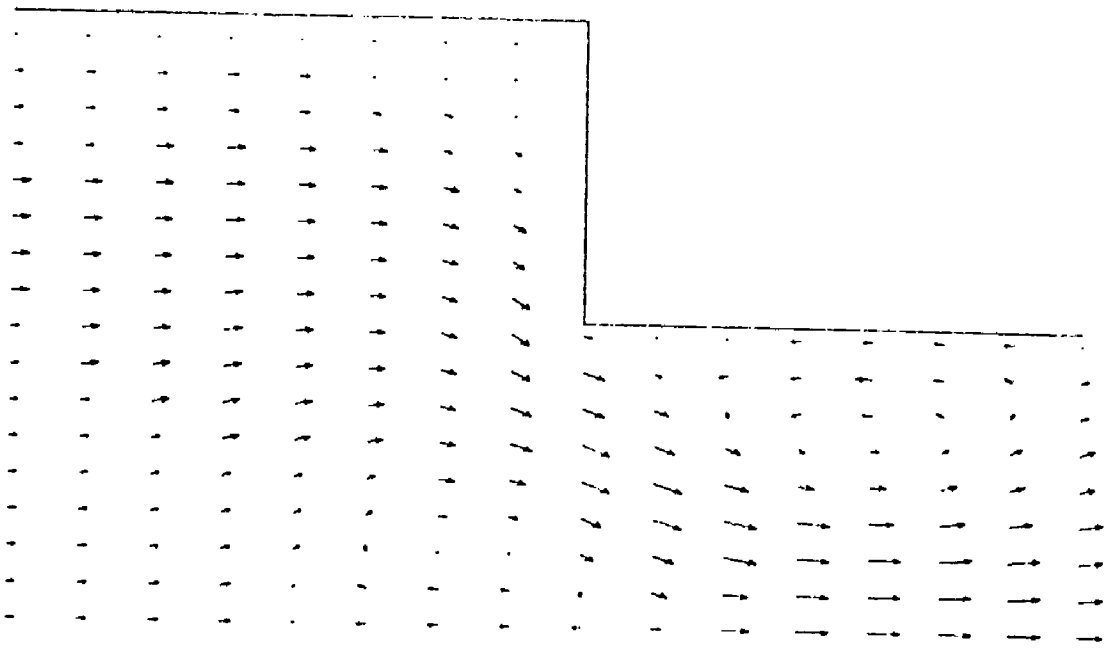

Figure 5-47. Flowfield for t = 0.00328 seconds
This is 2pi/10 radians after the end of the previous cycle
The velocity of the large piston is 20.23 meters/second
The velocity of the small piston is 29.39 meters/second

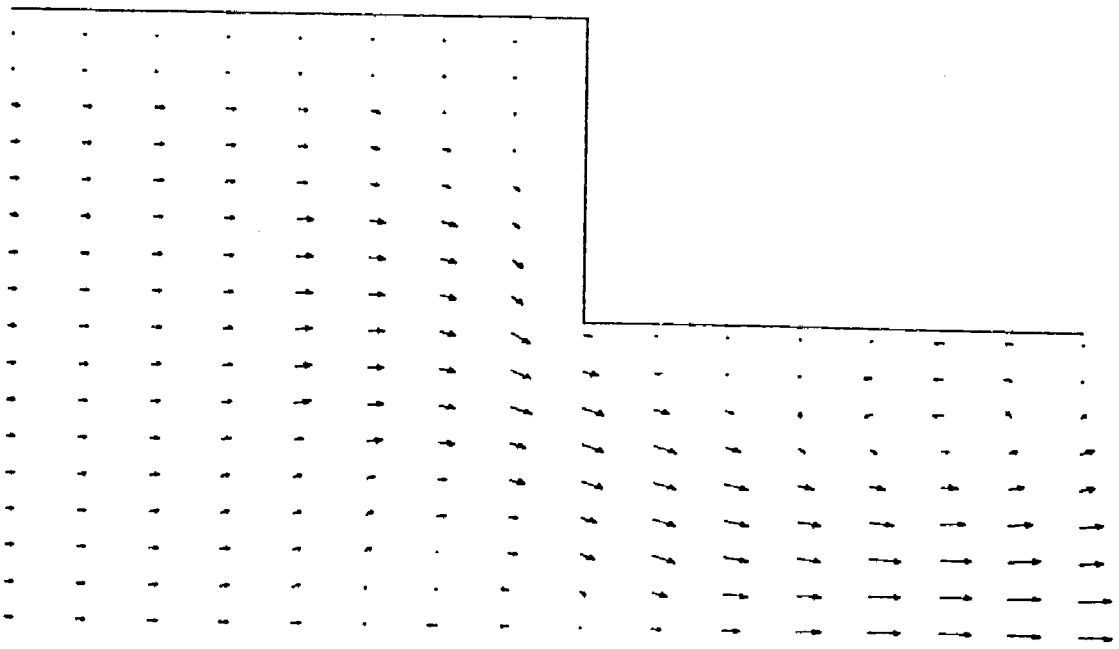

Figure 5-48. Flowfield for t = 0.00332 seconds
This is 3pi/10 radians after the end of the previous cycle
The velocity of the large piston is 14.70 meters/second
The velocity of the small piston is 40.45 meters/second

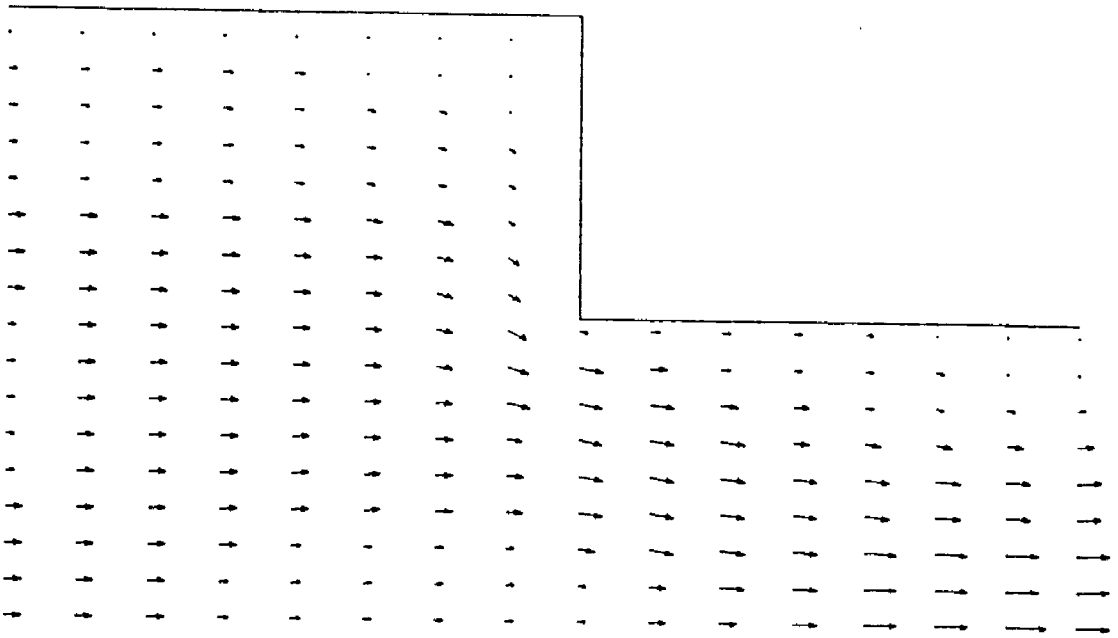

Figure 5-49. Flowfield for t = 0.00336 seconds
This is 4pi/10 radians after the end of the previous cycle
The velocity of the large piston is 7.73 meters/second
The velocity of the small piston is 47.55 meters/second

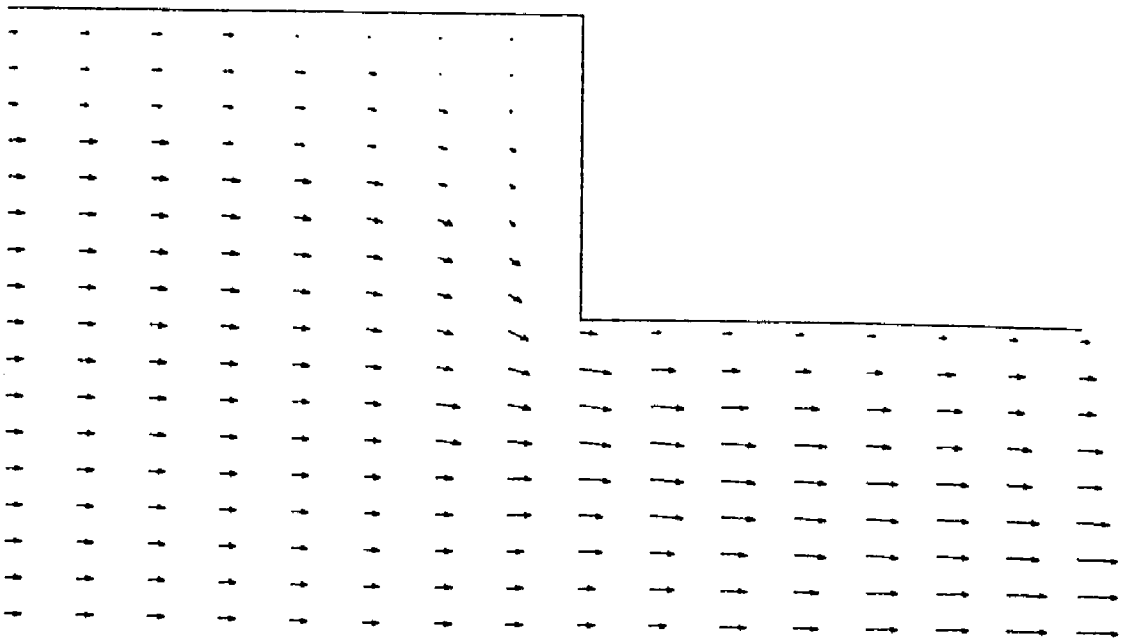

Figure 5-50. Flowfield for t = 0.00340 seconds
This is 5pi/10 radians after the end of the previous cycle
The velocity of the large piston is 0.00 meters/second
The velocity of the small piston is 50.00 meters/second

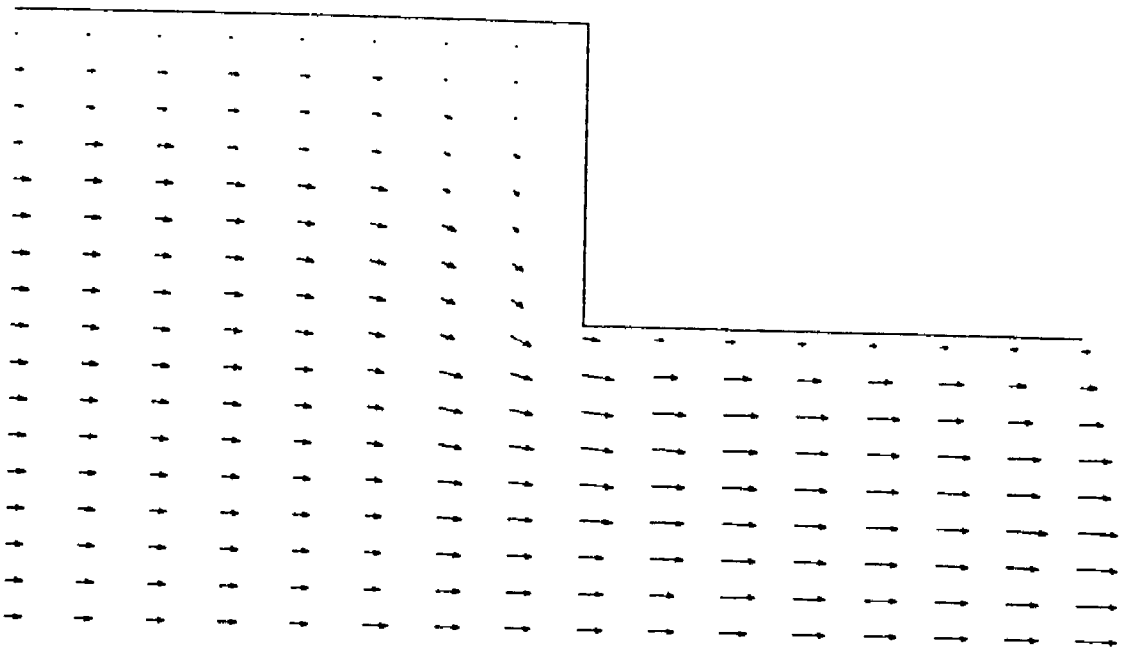

Figure 5-51. Flowfield for t = 0.00344 seconds
This is 6pi/10 radians after the end of the previous cycle
The velocity of the large piston is -7.73 meters/second
The velocity of the small piston is 47.55 meters/second

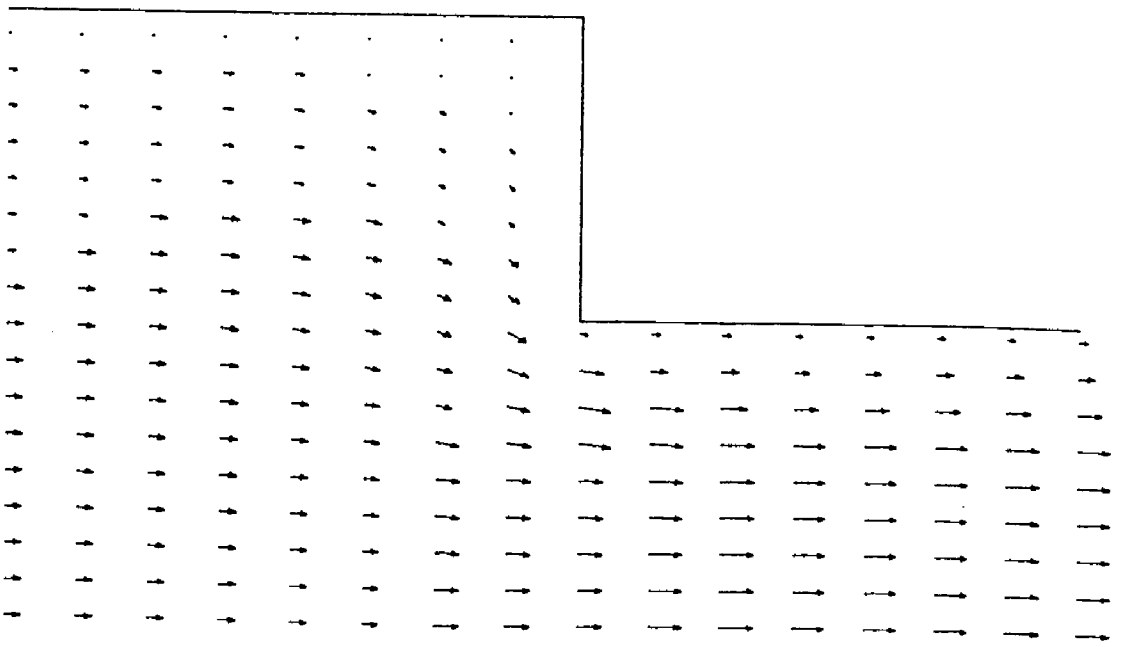

Figure 5-52. Flowfield for t = 0.00348 seconds
This is 7pi/10 radians after the end of the previous cycle
The velocity of the large piston is -14.69 meters/second
The velocity of the small piston is 40.45 meters/second

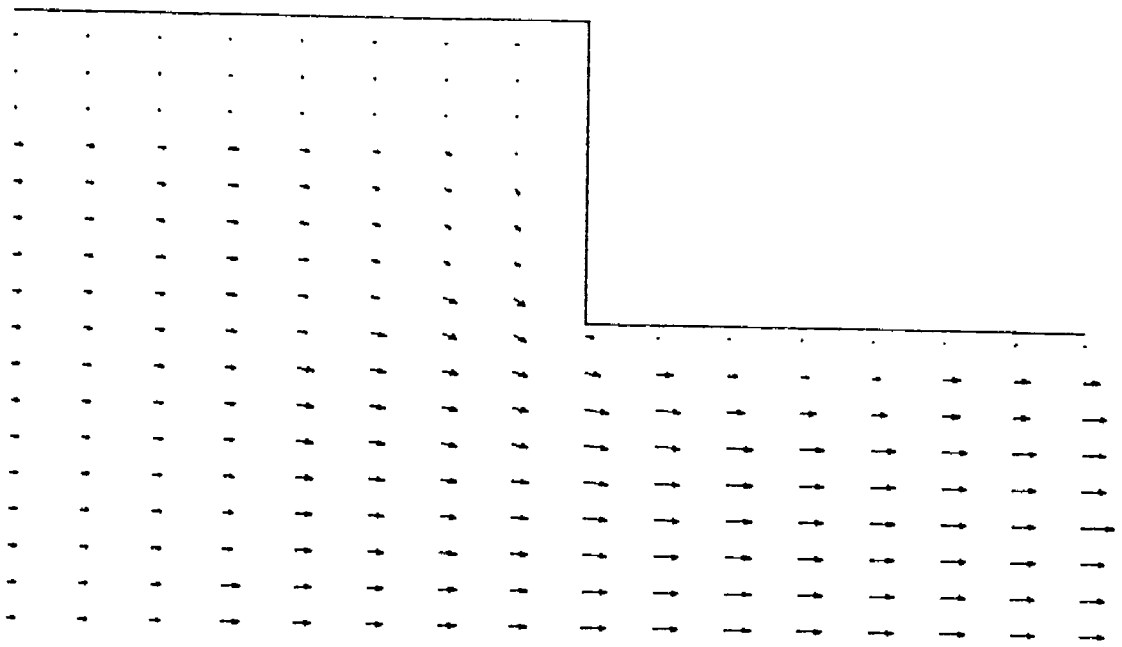

Figure 5-53. Flowfield for t = 0.00352 seconds
This is 8pi/10 radians after the end of the previous cycle
The velocity of the large piston is -20.23 meters/second
The velocity of the small piston is 29.39 meters/second

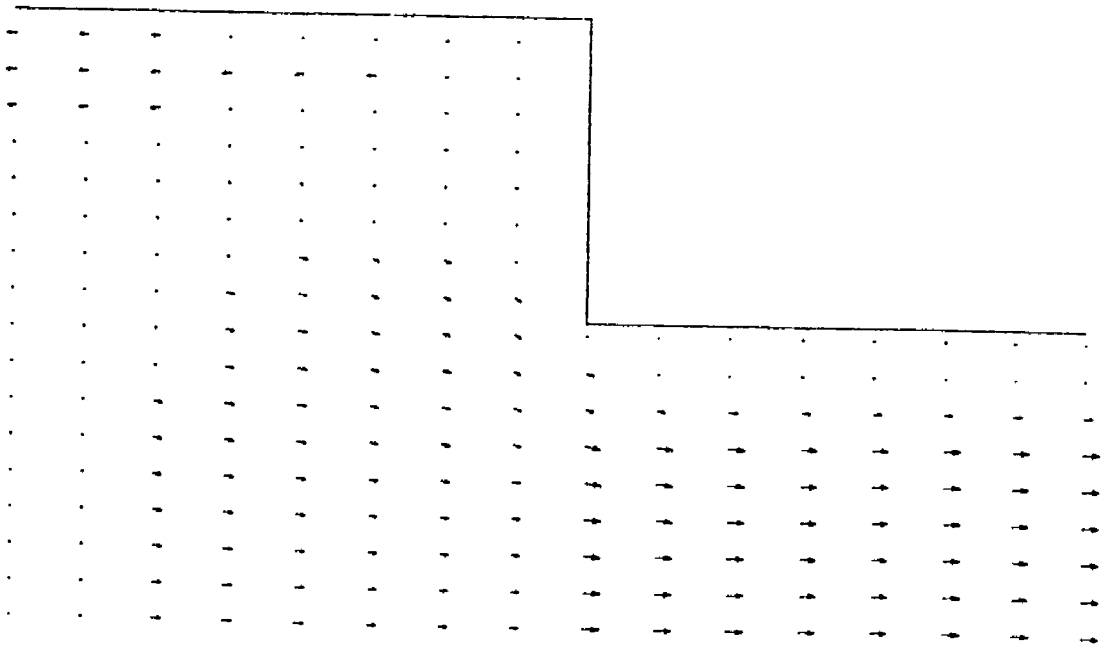

Figure 5-54. Flowfield for t = 0.00356 seconds
This is 9pi/10 radians after the end of the previous cycle
The velocity of the large piston is -23.78 meters/second
The velocity of the small piston is 15.45 meters/second

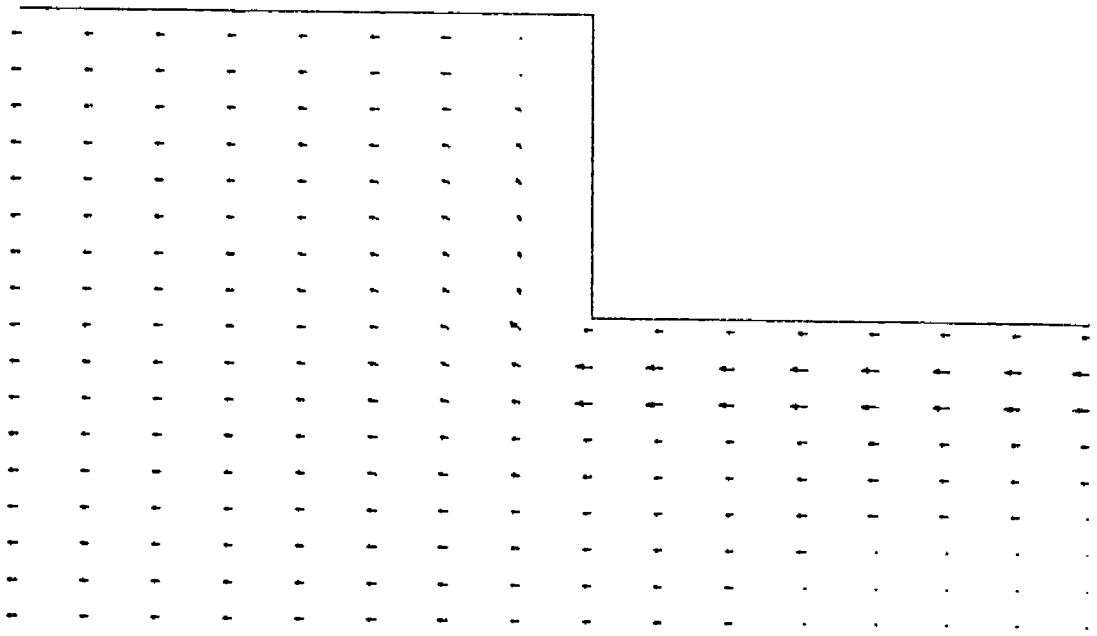

Figure 5-55. Flowfield for t = 0.00360 seconds
This is 10pi/10 radians after the end of the previous cycle
The velocity of the large piston is -25.0 meters/second
The velocity of the small piston is 0.0 meters/second

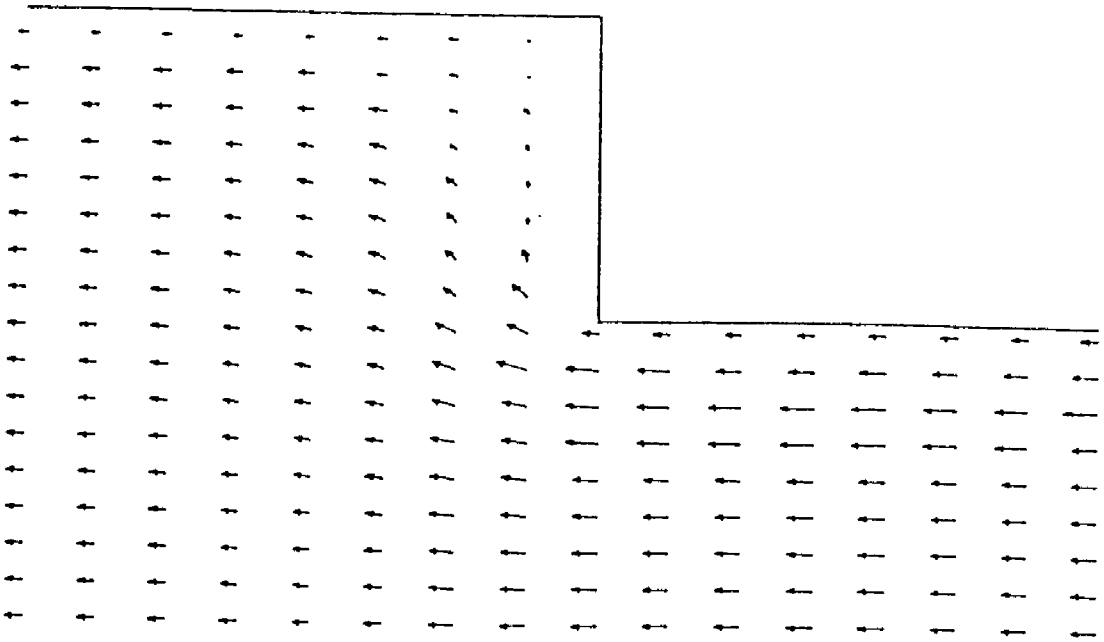

Figure 5-56. Flowfield for t = 0.00364 seconds
This is 11pi/10 radians after the end of the previous cycle
The velocity of the large piston is -23.78 meters/second
The velocity of the small piston is -15.45 meters/second

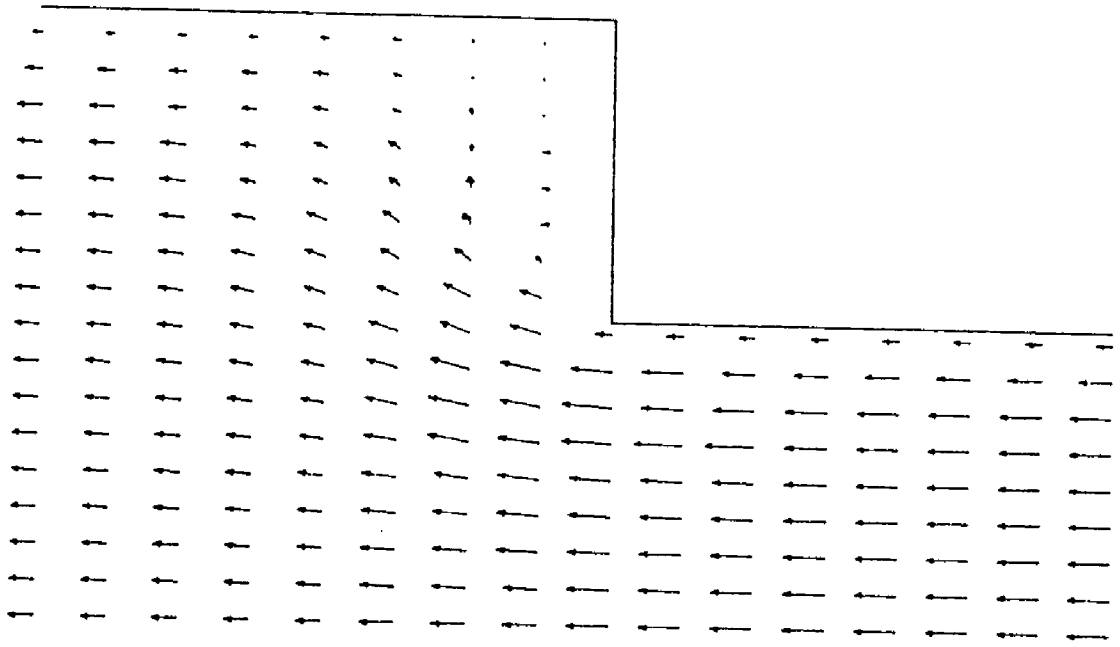

Figure 5-57. Flowfield for t = 0.00368 seconds
This is 12pi/10 radians after the end of the previous cycle
The velocity of the large piston is -20.23 meters/second
The velocity of the small piston is -29.39 meters/second

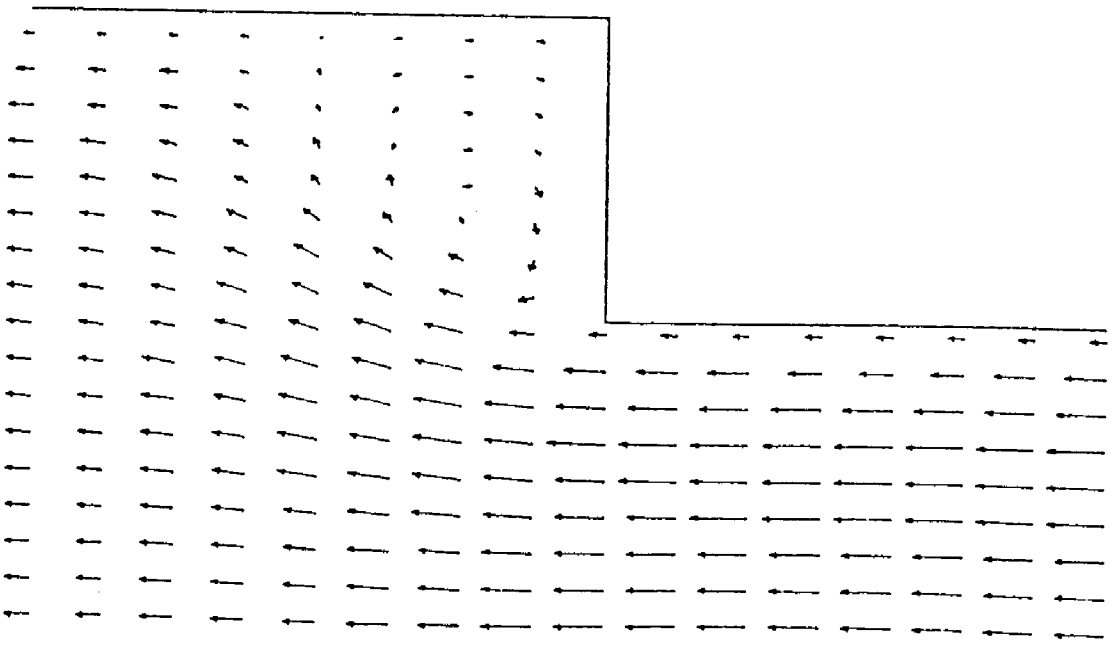

Figure 5-58. Flowfield for t = 0.00372 seconds
This is 13pi/10 radians after the end of the previous cycle
The velocity of the large piston is -14.69 meters/second
The velocity of the small piston is -40.45 meters/second

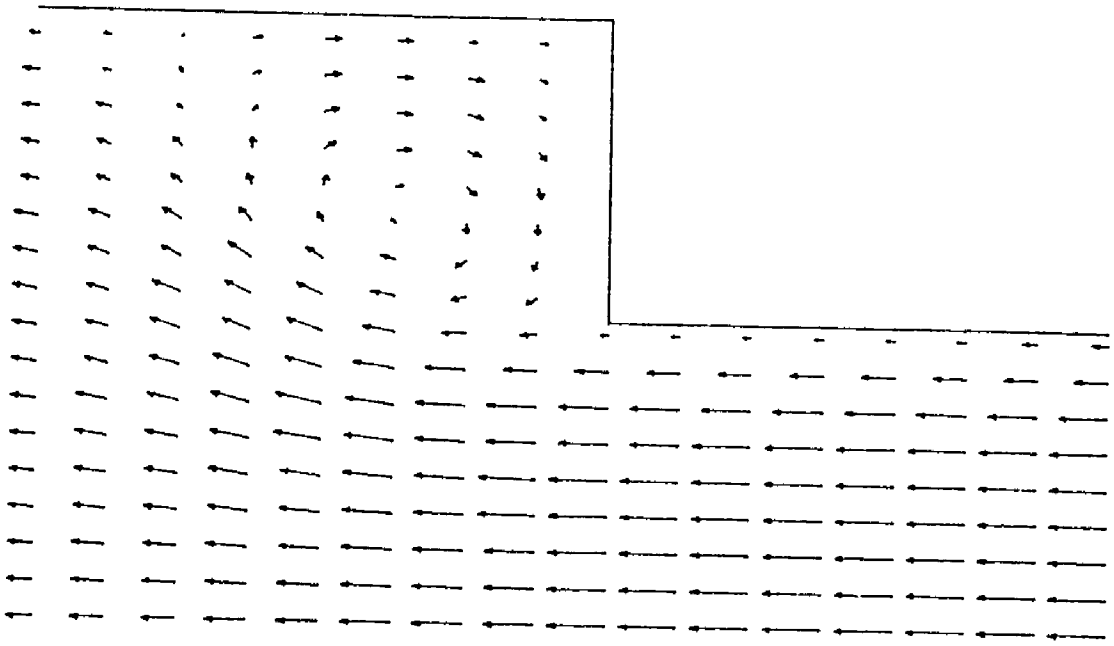

Figure 5-59. Flowfield for t = 0.00376 seconds
This is 14pi/10 radians after the end of the previous cycle
The velocity of the large piston is -7.73 meters/second
The velocity of the small piston is -47.55 meters/second

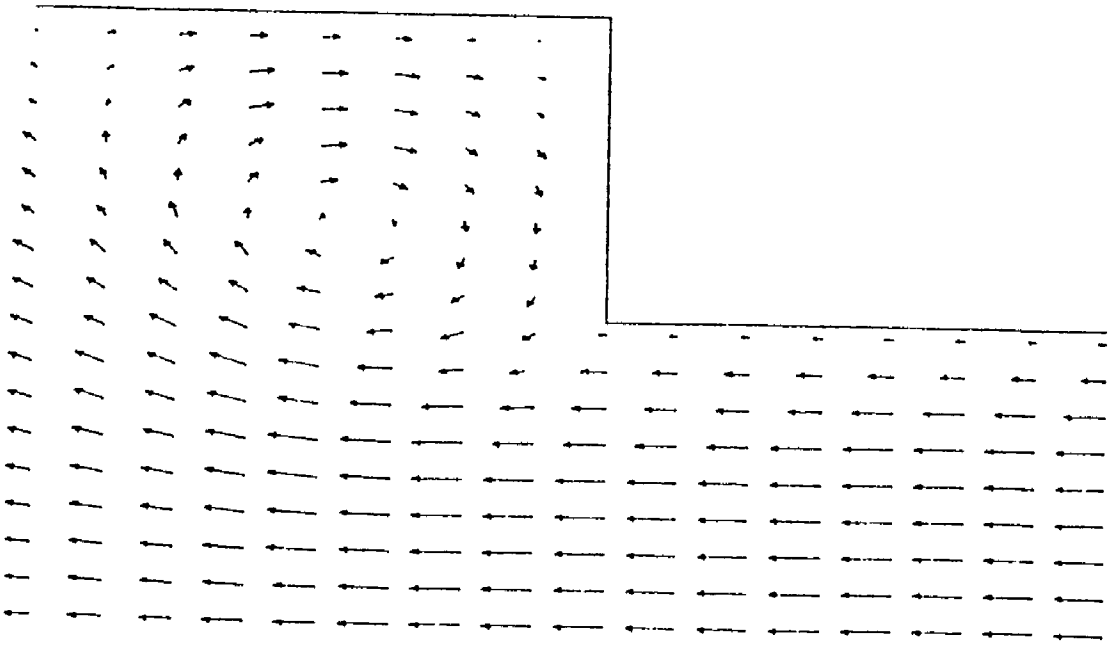

Figure 5-60. Flowfield for t = 0.00380 seconds
This is 15pi/10 radians after the end of the previous cycle
The velocity of the large piston is 0.00 meters/second
The velocity of the small piston is -75.00 meters/second

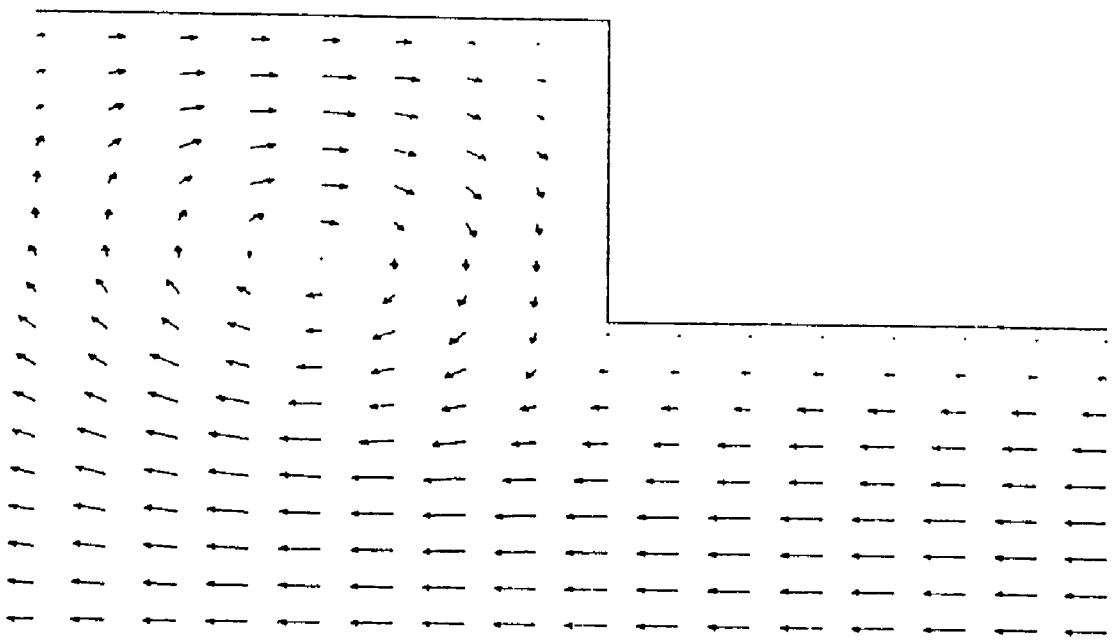

Figure 5-61. Flowfield for t = 0.00384 seconds
This is 16pi/10 radians after the end of the previous cycle
The velocity of the large piston is 7.73 meters/second
The velocity of the small piston is -47.55 meters/second

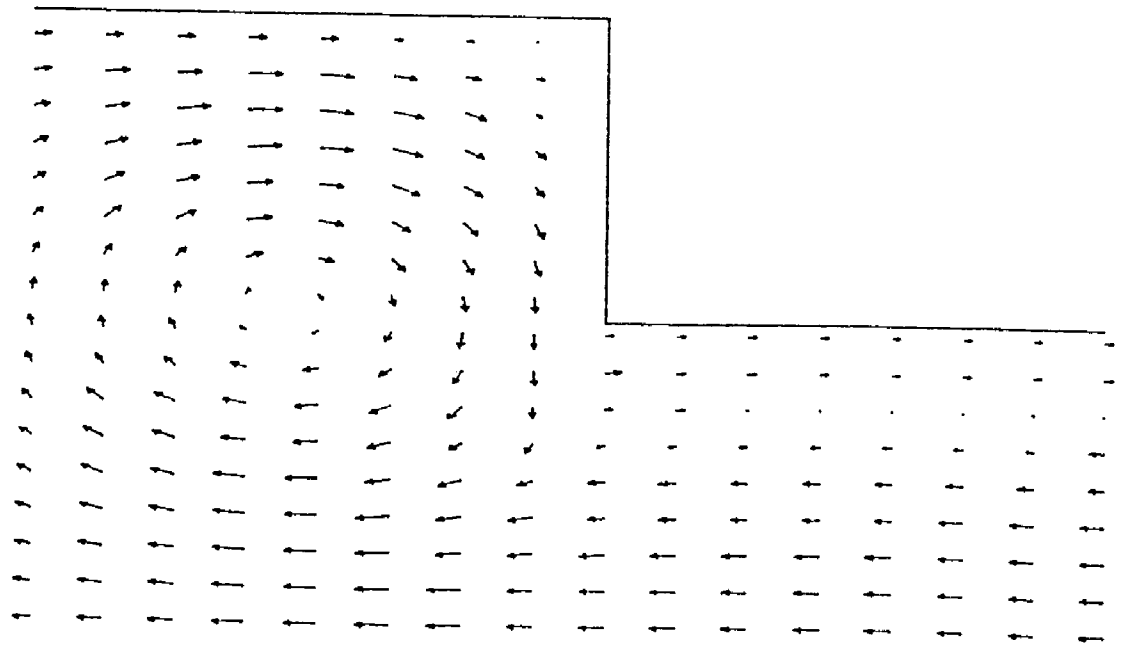

Figure 5-62. Flowfield for t = 0.00388 seconds
This is 17pi/10 radians after the end of the previous cycle
The velocity of the large piston is 14.69 meters/second
The velocity of the small piston is -40.45 meters/second

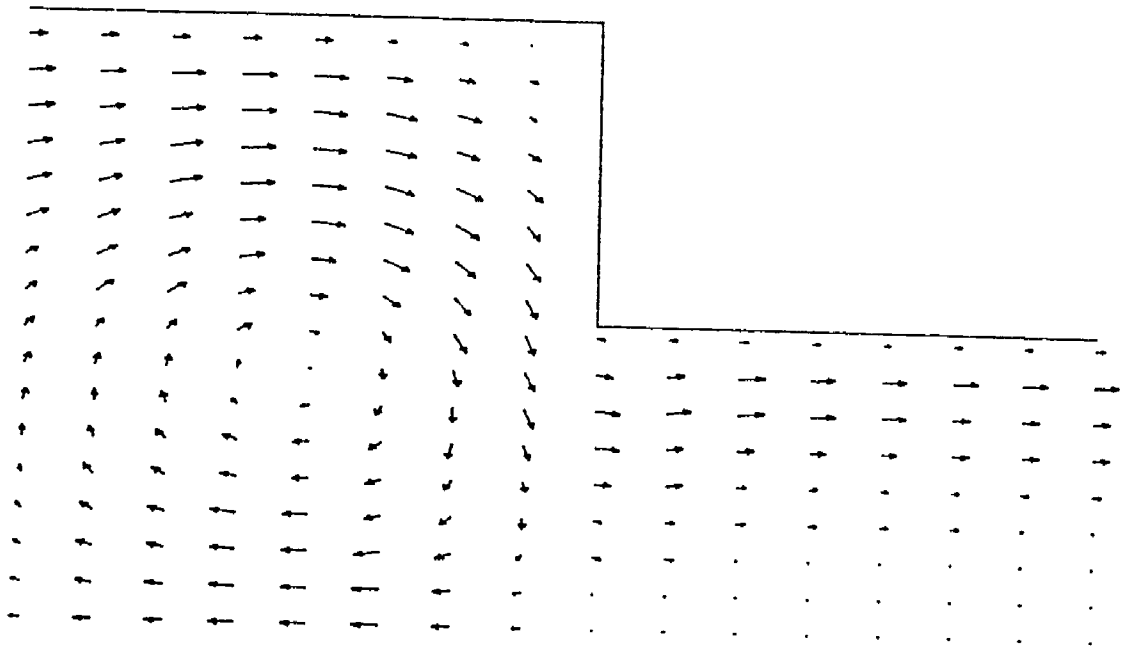

Figure 5-63. Flowfield for t = 0.00392 seconds
This is 18pi/10 radians after the end of the previous cycle
The velocity of the large piston is 20.23 meters/second
The velocity of the small piston is -29.39 meters/second

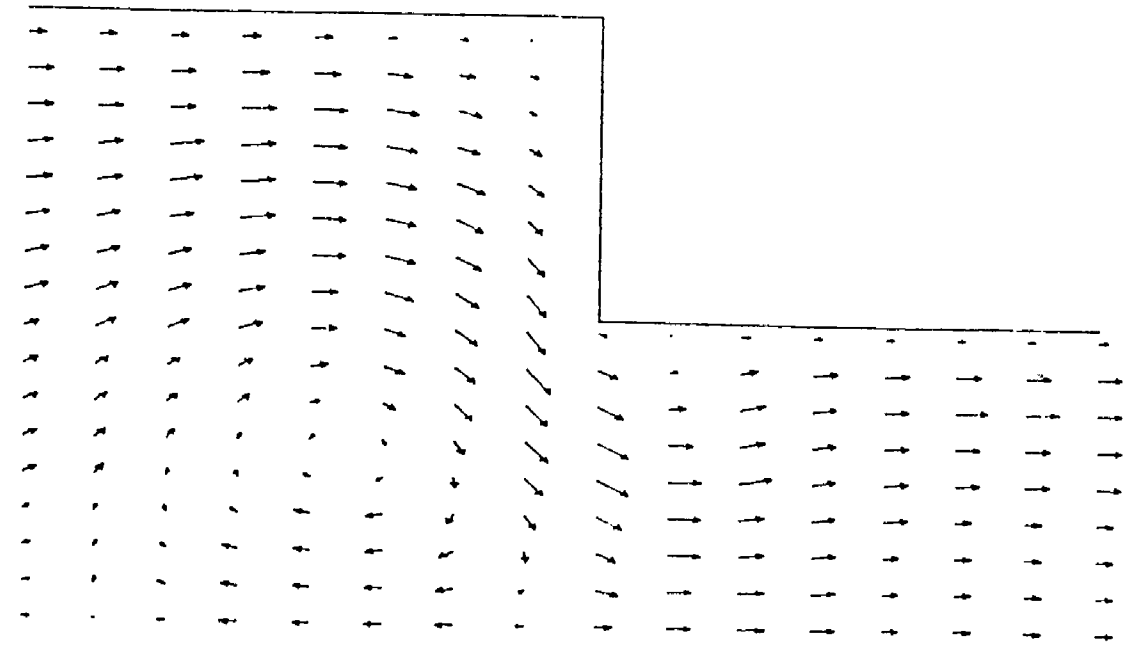

Figure 5-64. Flowfield for t = 0.00396 seconds
This is 19pi/10 radians after the end of the previous cycle
The velocity of the large piston is 23.78 meters/second
The velocity of the small piston is -15.45 meters/second

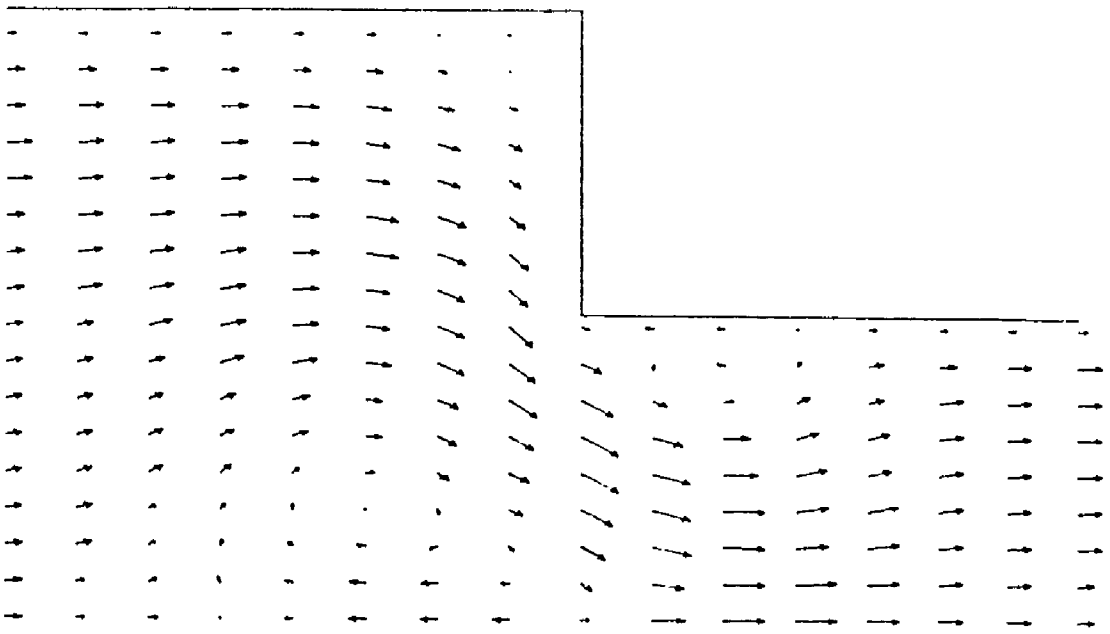

Figure 5-65. Flowfield for t = 0.00400 seconds
This is 20pi/10 radians after the end of the previous cycle
The velocity of the large piston is 25.0 meters/second
The velocity of the small piston is 0.0 meters/second

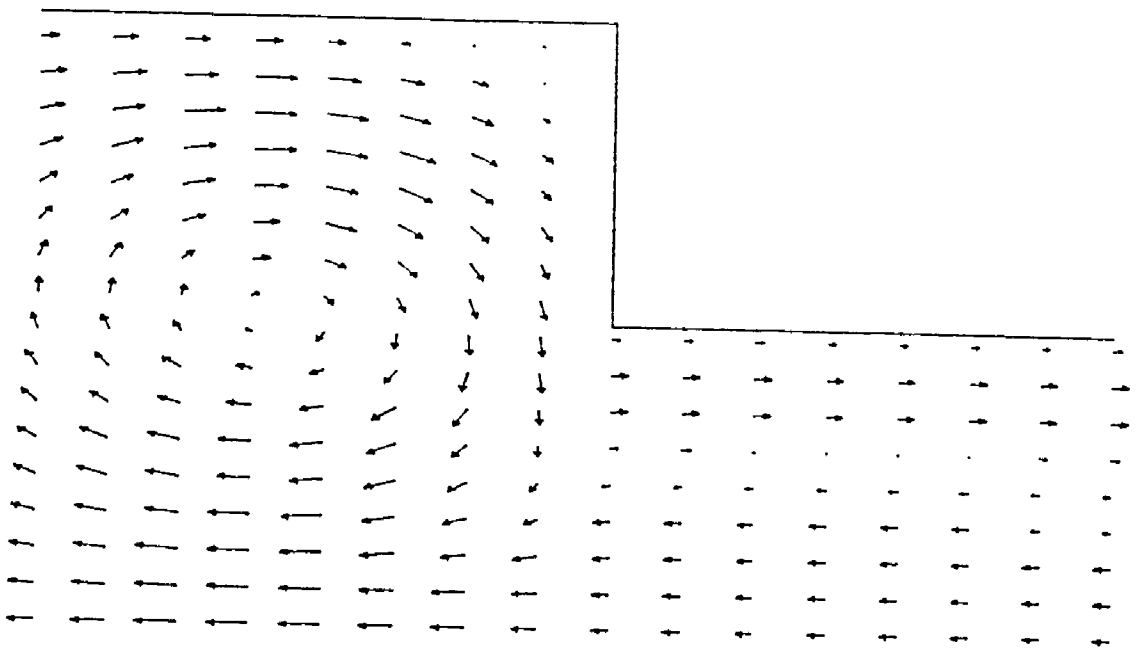

Figure 5-66. Flowfield for t = 0.00320 seconds
This is 0.0 radians after the end of the previous cycle
The velocity of the large piston is -25.0 meters/second
The velocity of the small piston is 0.0 meters/second

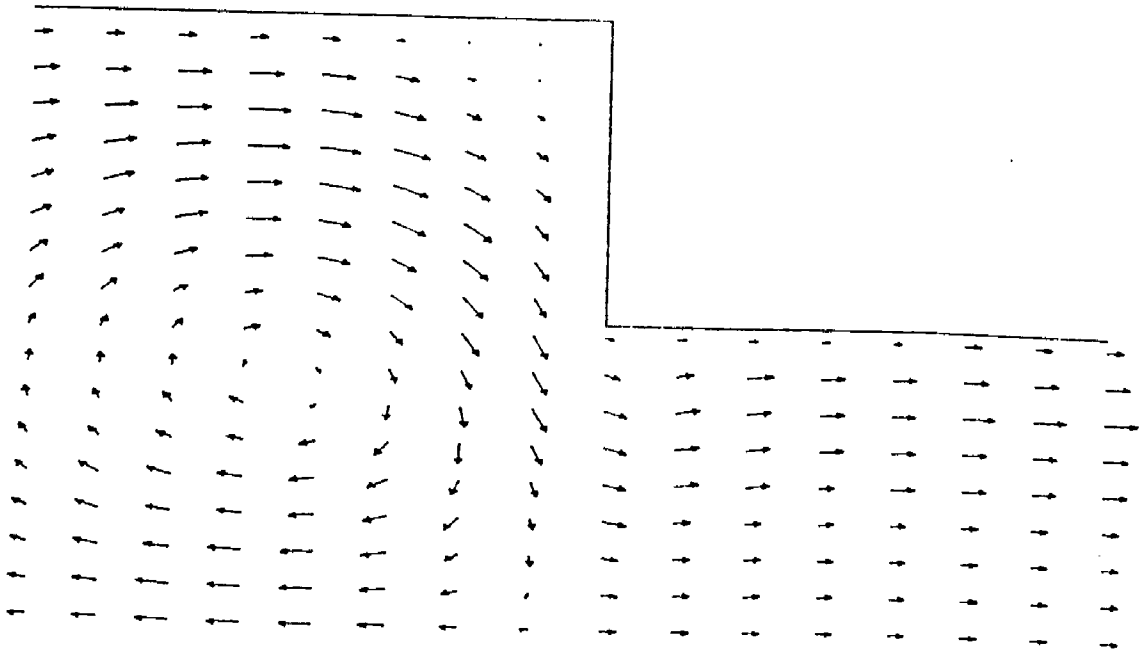

Figure 5-67. Flowfield for t = 0.00324 seconds
This is pi/10 radians after the end of the previous cycle
The velocity of the large piston is -23.78 meters/second
The velocity of the small piston is 15.45 meters/second

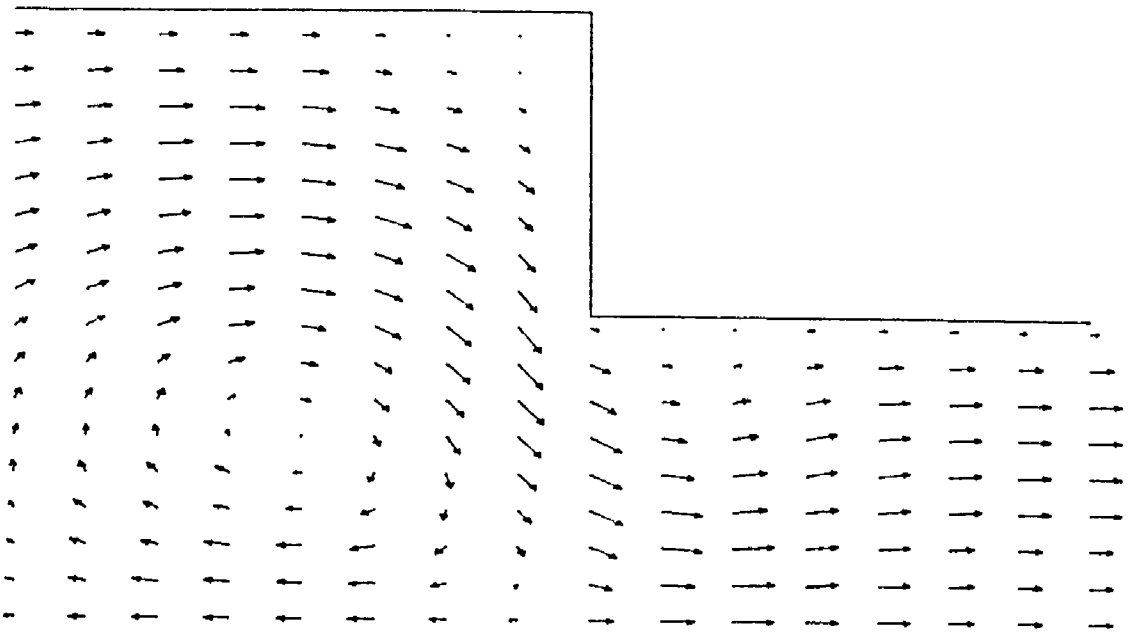

Figure 5-68. Flowfield for t = 0.00328 seconds
This is 2pi/10 radians after the end of the previous cycle
The velocity of the large piston is -20.23 meters/second
The velocity of the small piston is 29.39 meters/second

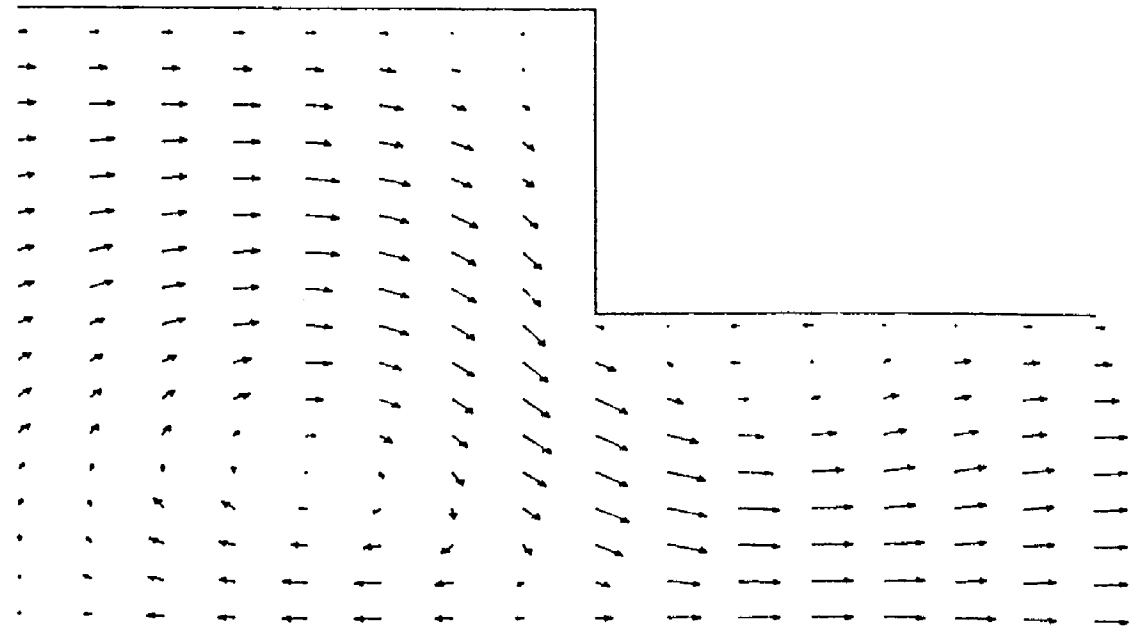

Figure 5-69. Flowfield for t = 0.00332 seconds
This is 3pi/10 radians after the end of the previous cycle
The velocity of the large piston is -14.69 meters/second
The velocity of the small piston is 40.45 meters/second

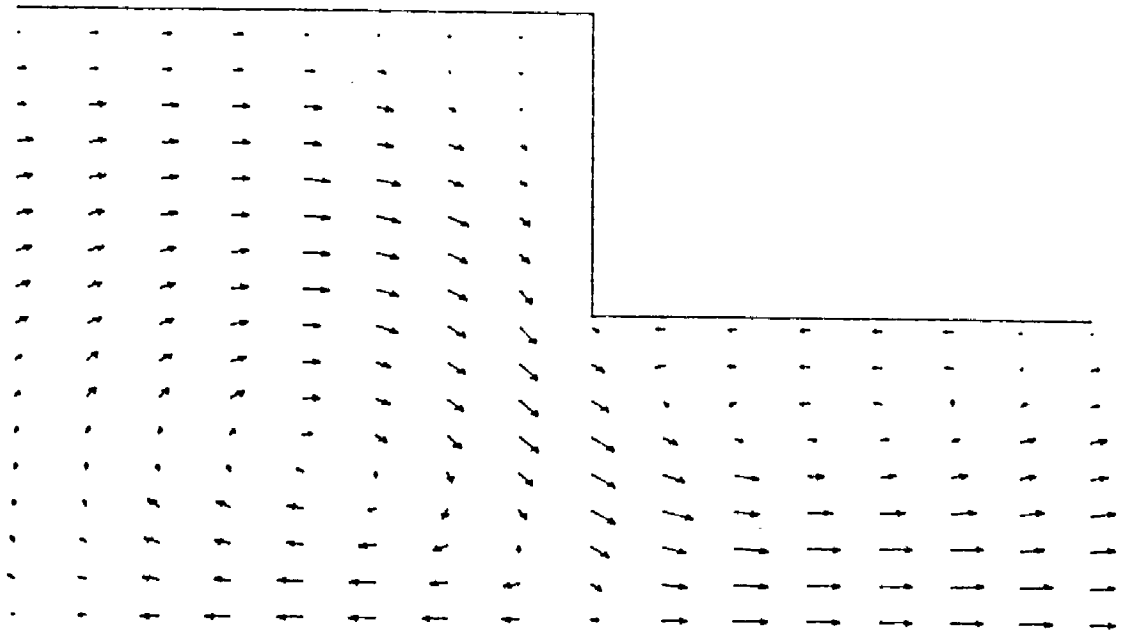

Figure 5-70. Flowfield for t = 0.00336 seconds
This is 4pi/10 radians after the end of the previous cycle
The velocity of the large piston is -7.73 meters/second
The velocity of the small piston is 47.55 meters/second

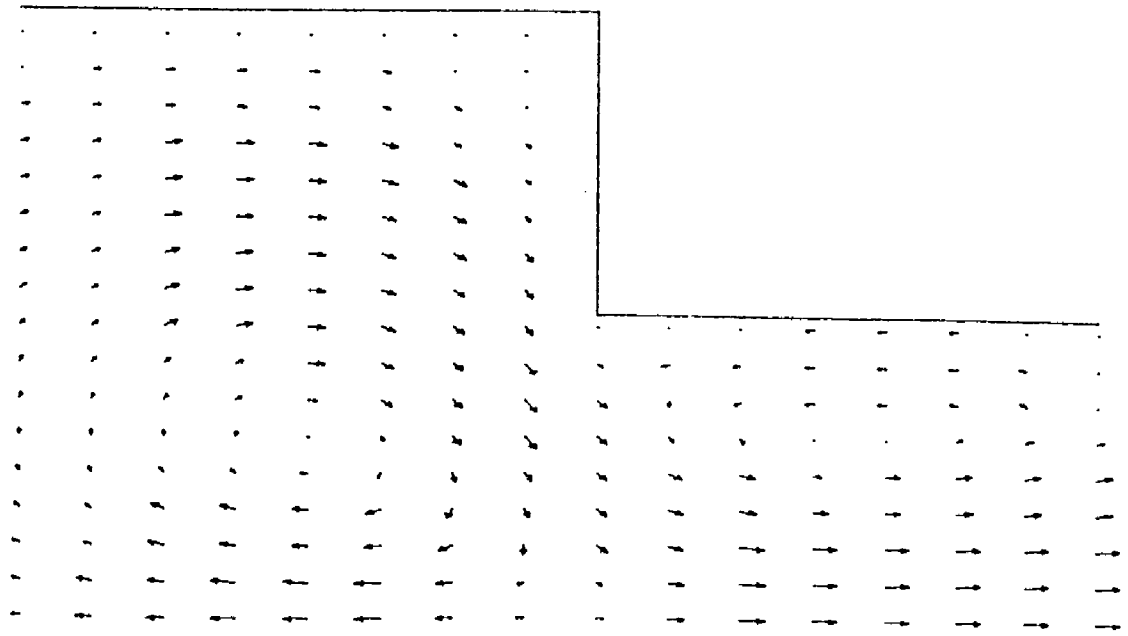

Figure 5-71. Flowfield for t = 0.00340 seconds
This is 5pi/10 radians after the end of the previous cycle
The velocity of the large piston is 0.00 meters/second
The velocity of the small piston is 50.00 meters/second

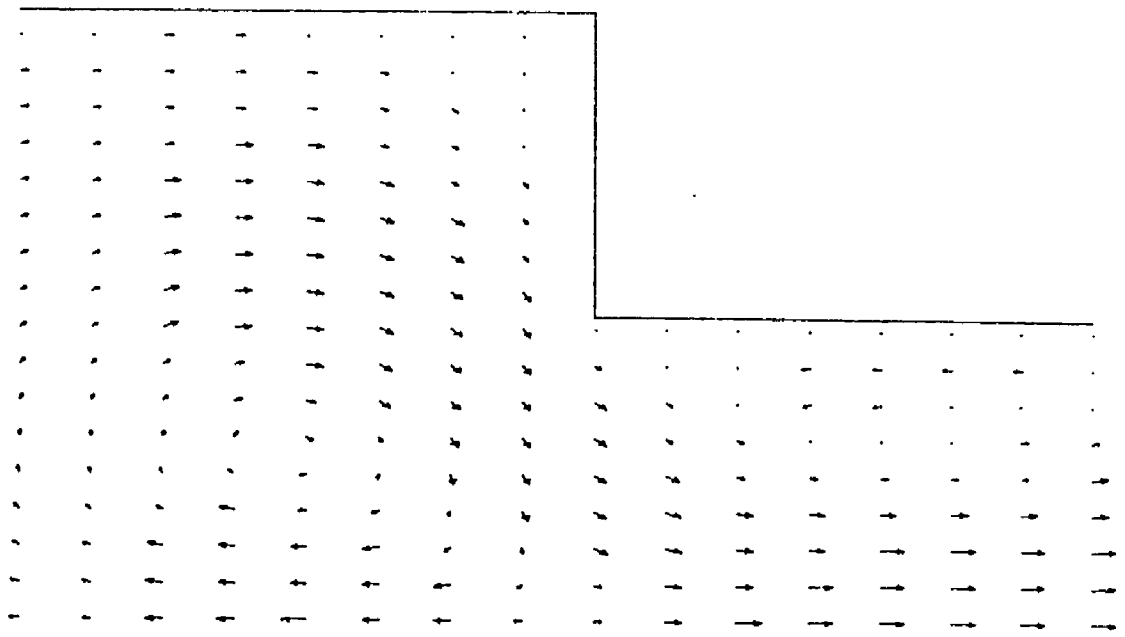

Figure 5-72. Flowfield for t = 0.00344 seconds
This is 6pi/10 radians after the end of the previous cycle
The velocity of the large piston is 7.73 meters/second
The velocity of the small piston is 47.55 meters/second

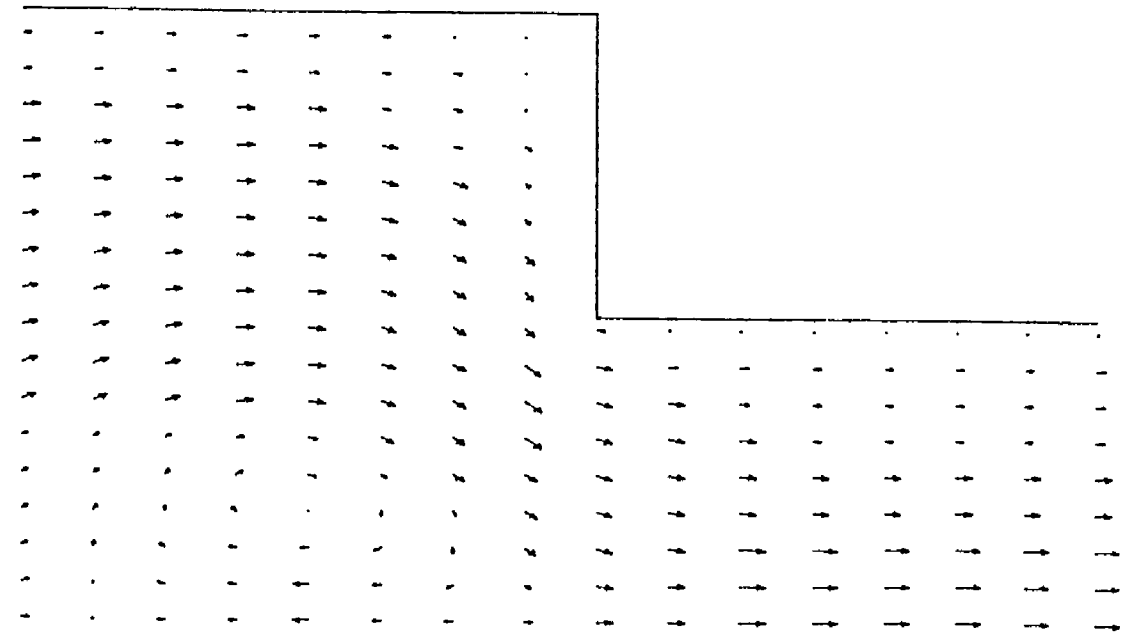

Figure 5-73. Flowfield for t = 0.00348 seconds
This is 7pi/10 radians after the end of the previous cycle
The velocity of the large piston is 14.69 meters/second
The velocity of the small piston is 40.45 meters/second

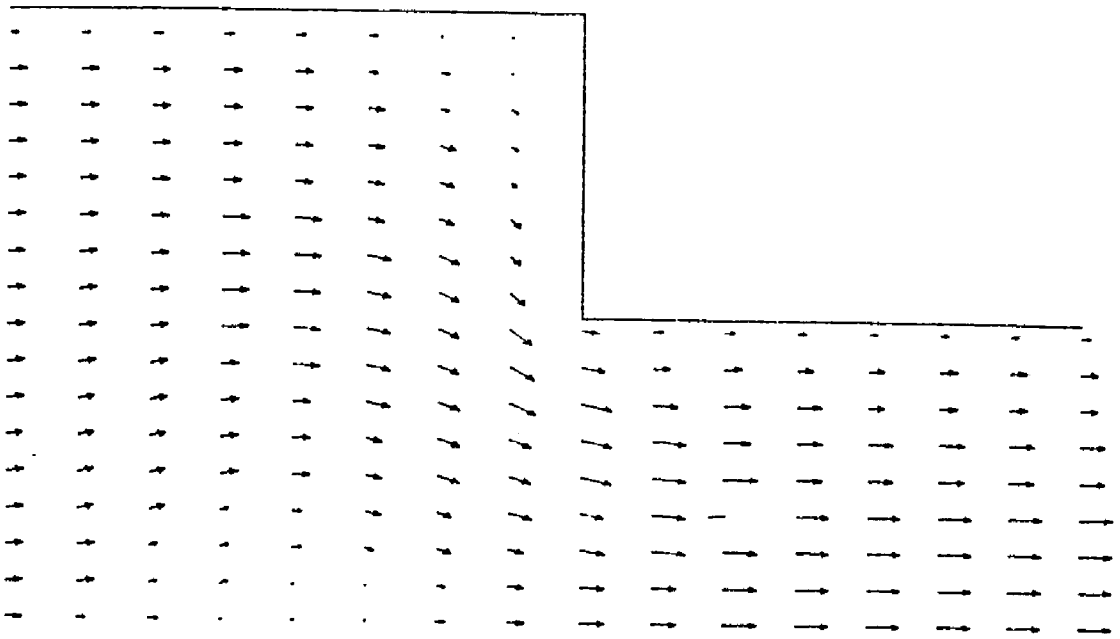

Figure 5-74. Flowfield for t = 0.00352 seconds
This is 8pi/10 radians after the end of the previous cycle
The velocity of the large piston is 20.23 meters/second
The velocity of the small piston is 29.39 meters/second

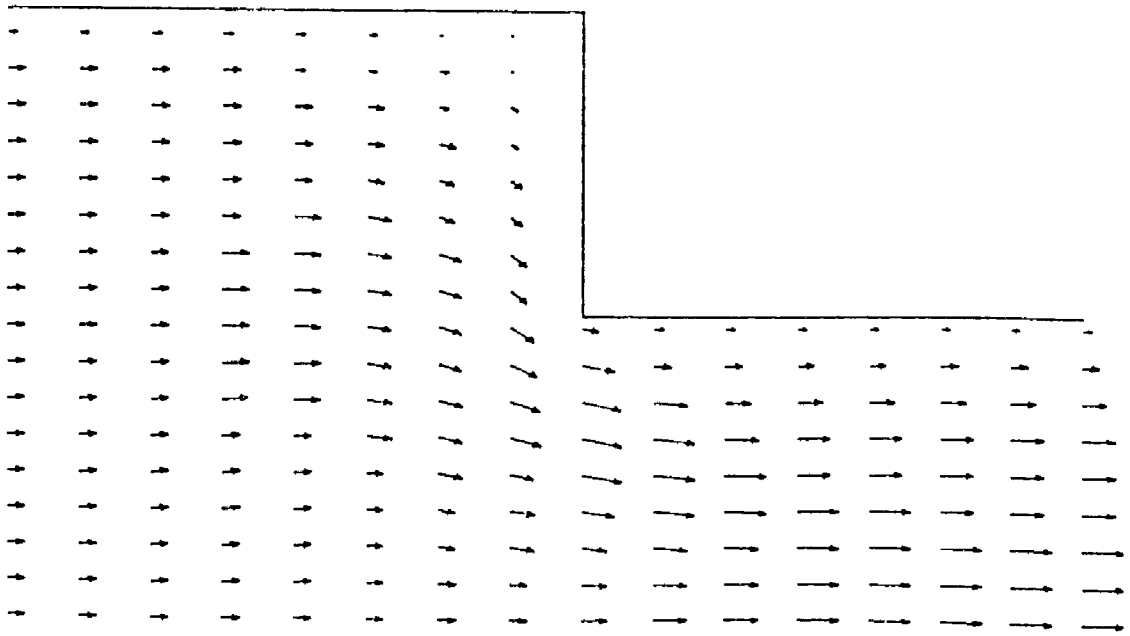

Figure 5-75. Flowfield for t = 0.00356 seconds
This is 9pi/10 radians after the end of the previous cycle
The velocity of the large piston is 23.78 meters/second
The velocity of the small piston is 15.45 meters/second

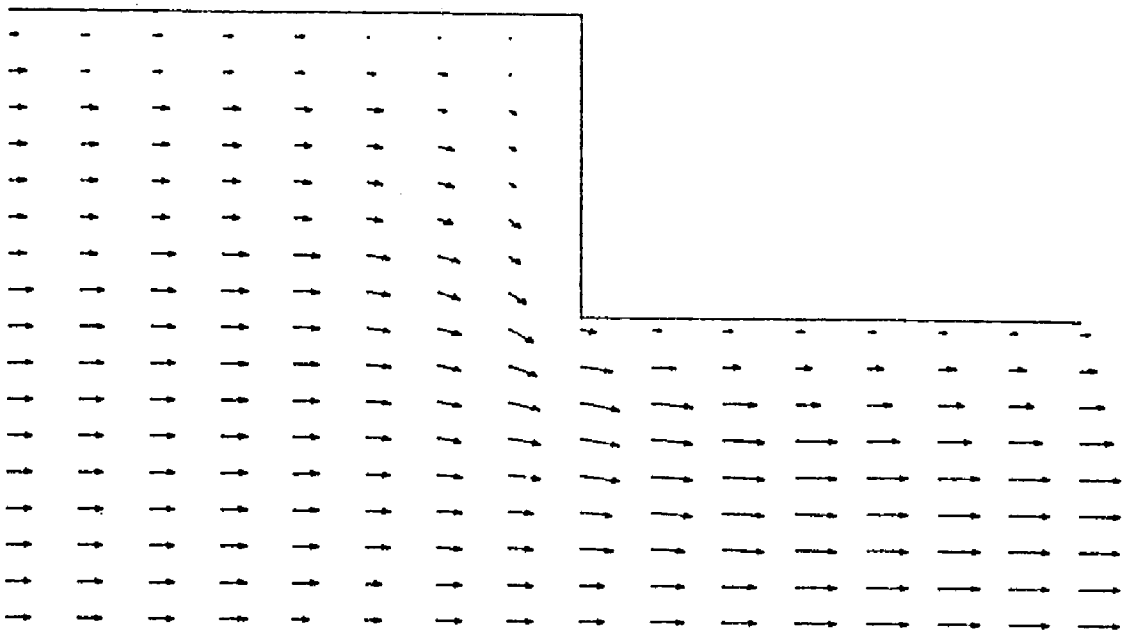

Figure 5-76. Flowfield for t = 0.00360 seconds
This is 10pi/10 radians after the end of the previous cycle
The velocity of the large piston is 25.0 meters/second
The velocity of the small piston is 0.0 meters/second

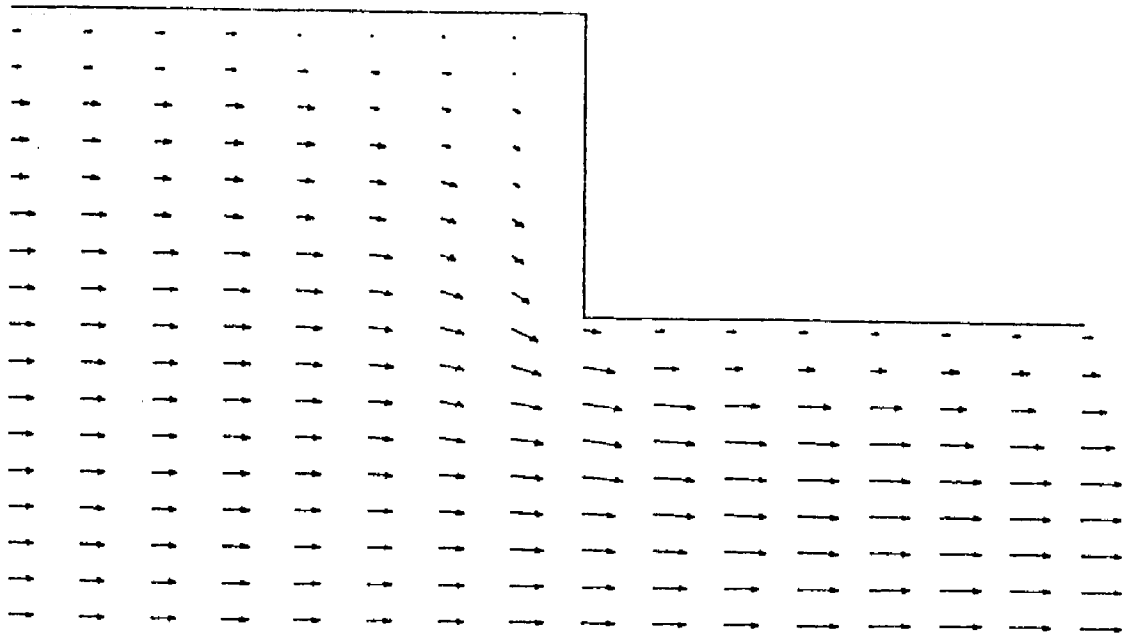

Figure 5-77. Flowfield for t = 0.00364 seconds
This is 11pi/10 radians after the end of the previous cycle
The velocity of the large piston is 23.78 meters/second
The velocity of the small piston is -15.45 meters/second

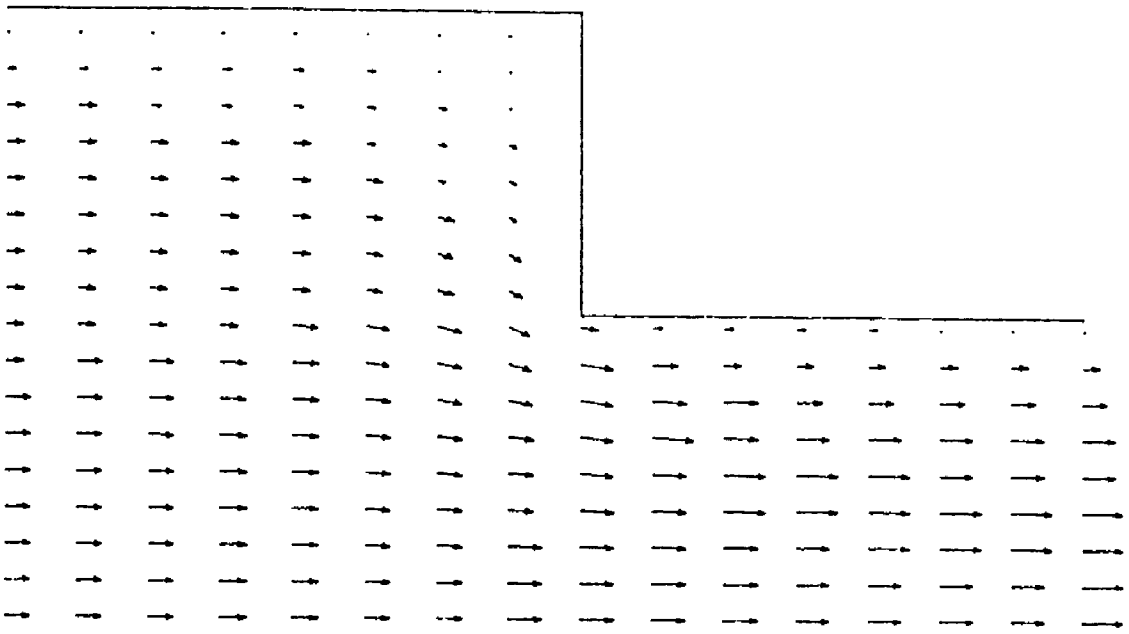

Figure 5-78. Flowfield for t = 0.00368 seconds
This is 12pi/10 radians after the end of the previous cycle
The velocity of the large piston is 20.23 meters/second
The velocity of the small piston is -29.39 meters/second

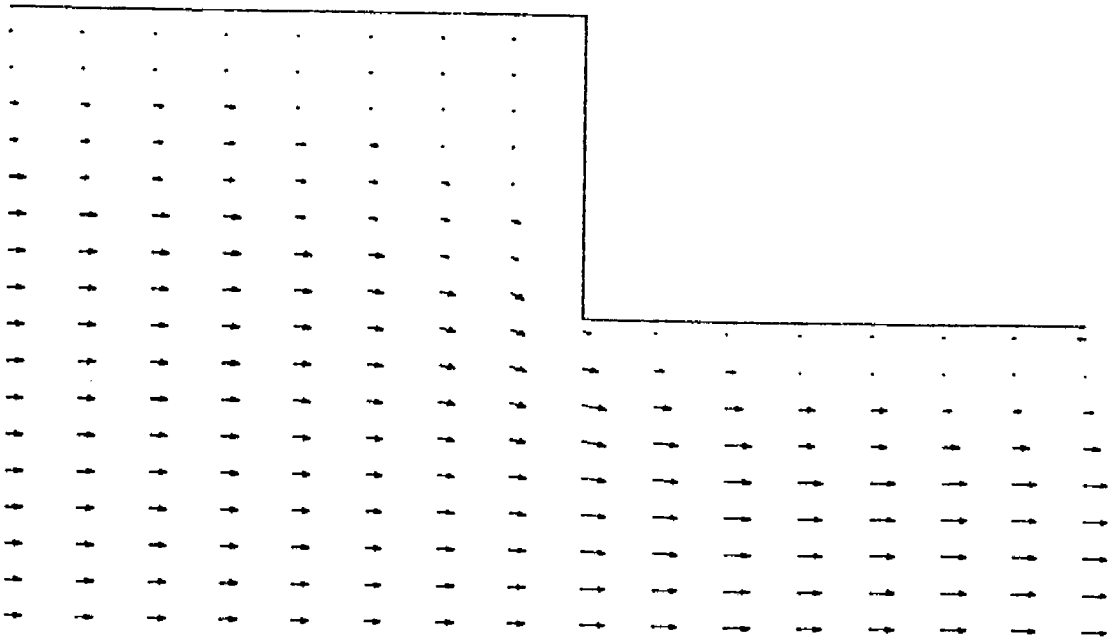

Figure 5-79. Flowfield for t = 0.00372 seconds
This is 13pi/10 radians after the end of the previous cycle
The velocity of the large piston is 14.69 meters/second
The velocity of the small piston is -40.45 meters/second

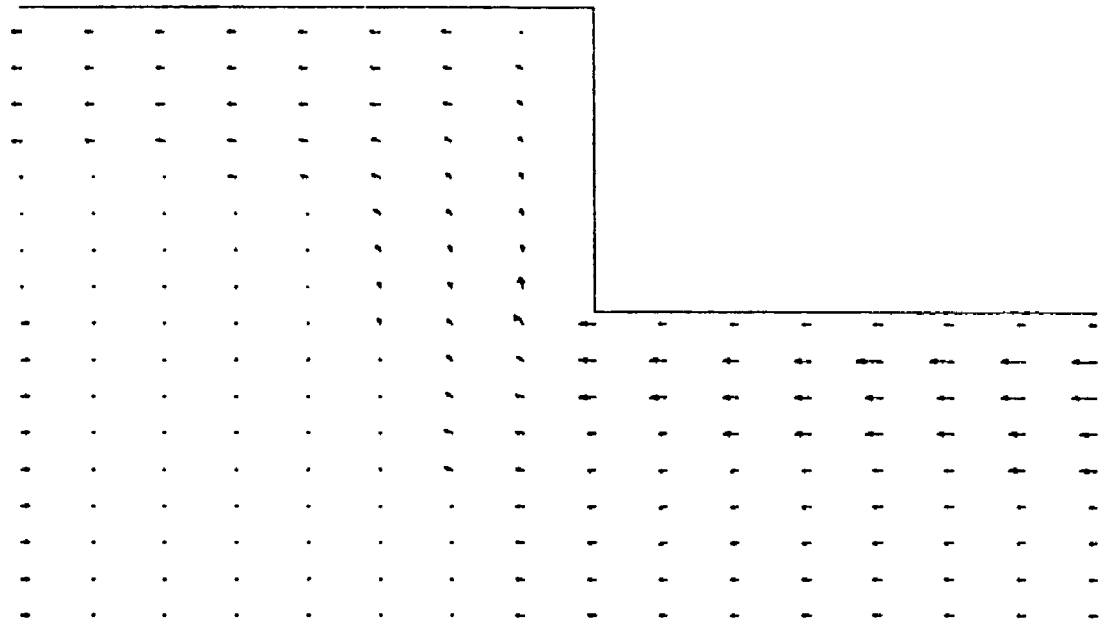

Figure 5-80. Flowfield for t = 0.00376 seconds
This is 14pi/10 radians after the end of the previous cycle
The velocity of the large piston is 7.73 meters/second
The velocity of the small piston is -47.55 meters/second

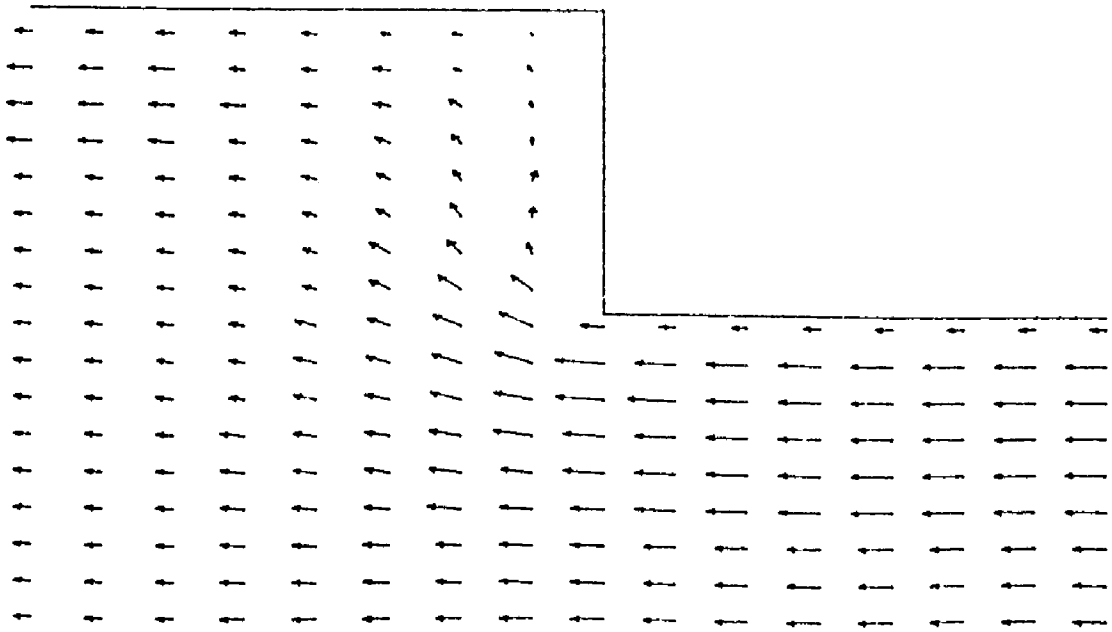

Figure 5-81. Flowfield for t = 0.00380 seconds
This is 15pi/10 radians after the end of the previous cycle
The velocity of the large piston is 0.00 meters/second
The velocity of the small piston is -50.00 meters/second

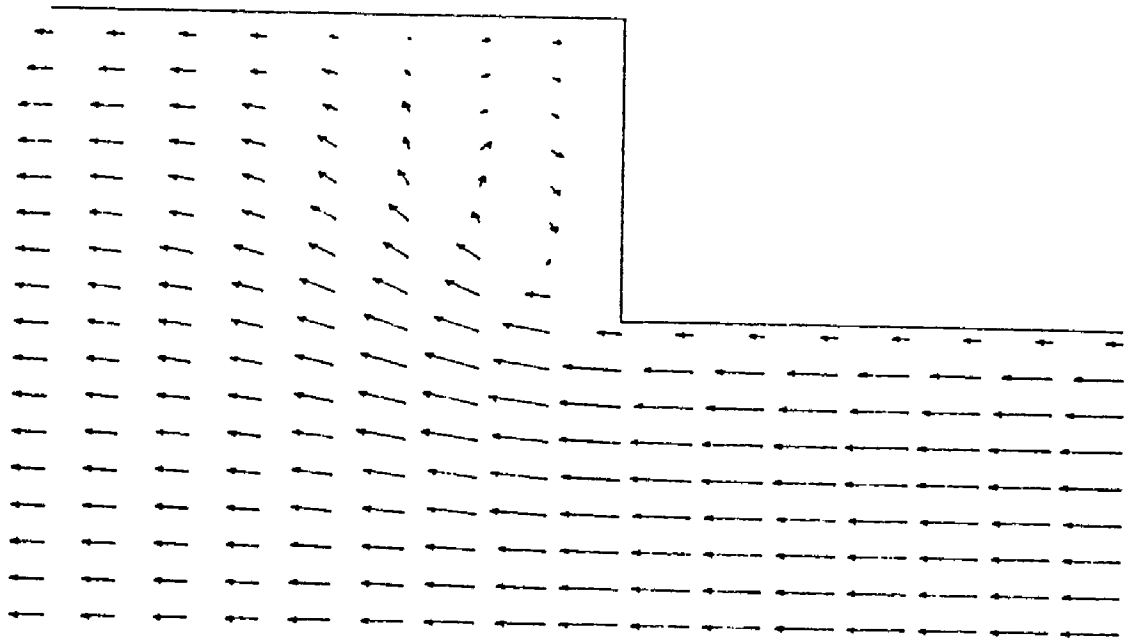

Figure 5-82. Flowfield for t = 0.00384 seconds
This is 16pi/10 radians after the end of the previous cycle
The velocity of the large piston is -7.73 meters/second
The velocity of the small piston is -47.55 meters/second

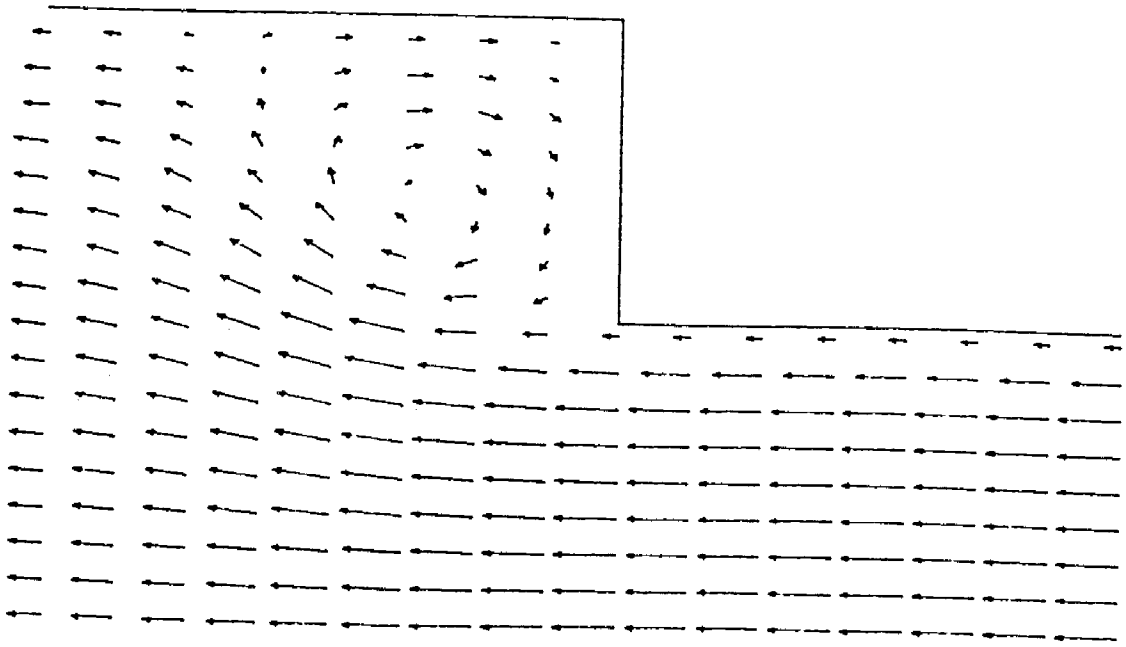

Figure 5-83. Flowfield for t = 0.00388 seconds
This is 17pi/10 radians after the end of the previous cycle
The velocity of the large piston is -14.69 meters/second
The velocity of the small piston is -40.45 meters/second

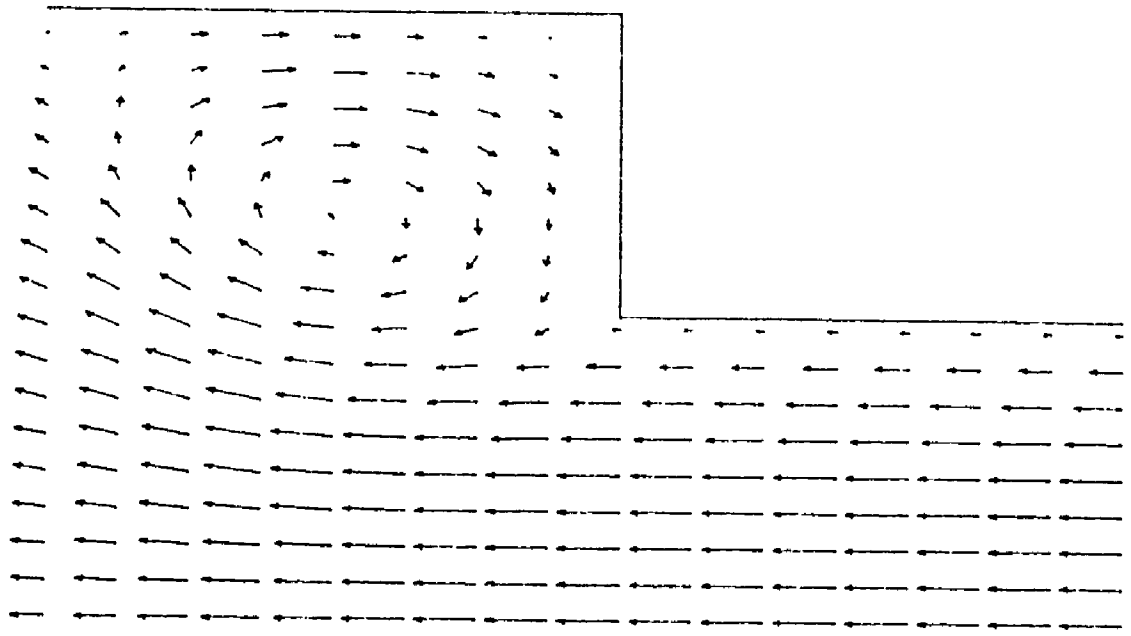

Figure 5-84. Flowfield for t = 0.00392 seconds
This is 18pi/10 radians after the end of the previous cycle
The velocity of the large piston is -20.23 meters/second
The velocity of the small piston is -29.39 meters/second

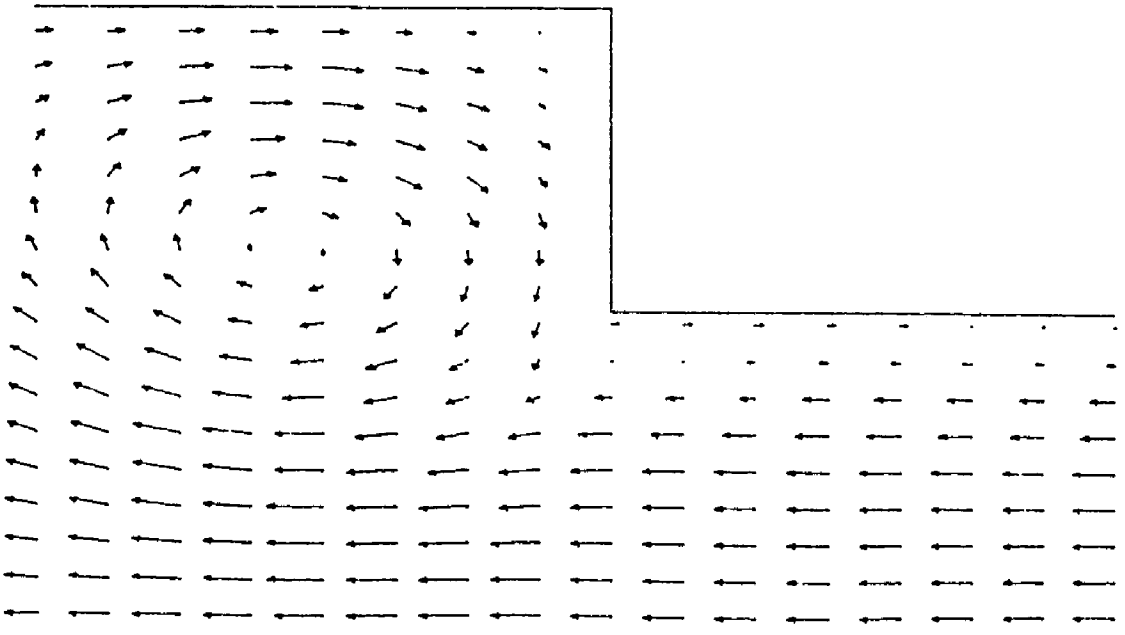

Figure 5-85. Flowfield for t = 0.00396 seconds
This is 19pi/10 radians after the end of the previous cycle
The velocity of the large piston is -23.78 meters/second
The velocity of the small piston is -15.45 meters/second

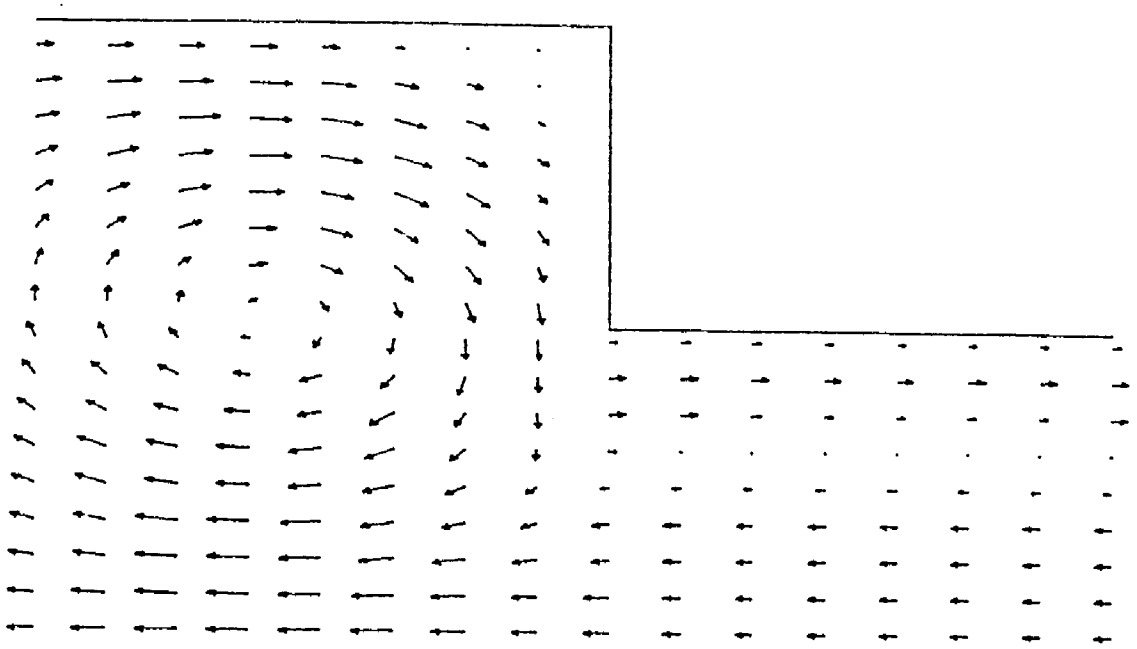

Figure 5-86. Flowfield for t = 0.00400 seconds
This is 20pi/10 radians after the end of the previous cycle
The velocity of the large piston is -25.0 meters/second
The velocity of the small piston is 0.0 meters/second

CHAPTER VI

SUMMARY

A computer program was developed, using MacCormack's time-split method, to find numerical solutions for the conservation equations of mass, momentum, and total energy. The conservation equations used were those valid for two-dimensional, unsteady, laminar flow of an ideal gas. The program was written in generalized coordinates so that it could be easily applied to a variety of problems by using the appropriate coordinate transformations.

The computer program was then used to study oscillating flows over a step where the oscillation was induced by two oscillating pistons, one on each side of the step. To demonstrate the usefulness of the computer program for studying oscillating flows over a two-dimensional step, the computer program was used to generate the velocity fields for three types of flows past a step. The three types of flows studied were

1. Steady flows past a step
2. Oscillating flows past a step with the pistons oscillating in phase
3. Oscillating flows past a step with the pistons oscillating out of phase

The velocity fields generated for each case studied were presented in graphical form.

The velocity fields generated for the oscillating flows over a step had several interesting features. Some of these interesting features are summarized as follows:

1. When the direction of piston motion reversed, the gas in the boundary layer changed direction before the gas outside the boundary layer changed direction
2. Recirculating flow patterns similar to those occuring in steady flow over a backstep occured when the gas moved from the smaller side of the region to the larger side of the region
3. Separation bubbles formed in the inlet to the smaller side of the region for the lower velocity cases
4. Two areas of recirculating flow formed when the gas moved from the smaller side of the region to the larger side of the region in the higher velocity case
5. Separation bubbles did not form in the entrance to the smaller side of the region for the higher velocity case due to the second area of recirculting flow

REFERENCES

1. Schlichting, H., Boundary-Layer Theory, Sixth Edition, McGraw-Hill Book Co., New York, 1968, pp. 85-86.

2. Rayleigh, J.W.S., "On the Circulation of Air Observed in Kundt's Tubes, and on Some Allied Acoustical Problems," Philosophical Transactions of the Royal Society of London, Vol. 175, 1884, pp. 1-21.

3. Andrade, E.N., "On the Circulation Caused by the Vibration of Air in Tubes," Proceedings of the Royal Society, Series A, Vol. 134, 1931, pp. 447-470.

4. Schlichting, H., Boundary-Layer Theory, Sixth Edition, McGraw-Hill Book Co., New York, 1968, pp. 441-415.

5. Davidson, B.J., "Heat Transfer from a Vibrating Circular Cylinder," International Journal of Heat and Mass Transfer, Vol. 16, 1973, pp. 1703-1727.

6. Roy, D., "Nonsteady Periodic Boundary Layer," Journal of Applied Mathematical Physics, Vol. XII, 1961, pp. 363-366.

7. Lin, C.C., "Motion in the Boundary Layer with a Rapidly Oscillating External Flow," Proceedings of the Ninth International Congress of Applied Mechanics, Brussels, Vol. 4, 1957, pp. 155-167.

8. Steger, J.L., "Implicit Finite-Difference Simulation of Flow about Arbitrary Two-Dimensional Geometries," AIAA Journal, Vol. 16, 1978, pp. 679-686.

9. Chyu, W.J., Davis, S.S., and Chang, K.S., "Calculation of Unsteady Transonic Flow over an Airfoil," AIAA Journal, Vol. 19, 1981, pp. 684-690.

10. Sexl, Th., "Urber den von E. G. Richardson entdeckten Annulareffekt'," Z. Phys., Vol. 61, 1930, p. 349.

11. Uchida, S., "The Pulsating Viscous Flow Superposed on the Steady Laminar Motion of Incompressible Fluid in a Circular Pipe," ZAMP, Vol. 7, 1950, pp. 403-422.

12. Brocher, E., "Oscillating Flows in Tubes," Journal of Fluid Mechanics, Vol. 79, 1977, pp. 113-126.

13. Watson, E.J., "Diffusion in Oscillating Pipe Flows," Journal of Fluid Mechanics, Vol. 133, 1983, pp. 233-244.

14. Kurzweg, U.H. and Zhao, L.D., "Heat Transfer by High Frequency Oscillations; a New Hydrodynamic Technique for Achieving Large Effective Thermal Conductivities," Physics of Fluids, Vol. 27, 1984, pp. 2624-2627.

15. Kurzweg, U.H., "Enhanced Heat Conduction in Fluids Subjected to Sinusoidal Oscillations," Journal of Heat Transfer, Vol. 107, 1985, pp. 459-462.

16. Chong, M.S., Milkins, E.E., and Watson, H.C., "Predictions of Heat and Mass Transfer during Compression and Expansion in I.C. Engines," SAE Paper No. 760761, Society of Automotive Engineers, Warrendale, PA, 1976.

17. Boni, A.A., "Numerical Simulation of Flame Propagation in Internal Combustion Engines, a Status Report," SAE Paper No. 780316, Society of Automotive Engineers, Warrendale, PA, 1978.

18. Boni, A.A., Chapman, M., and Schmeyer, G.P., "Computer Simulation of Combustion Processes in a Stratified Charge Engine," Acta Astronautica, Vol. 3, 1976, pp. 293-307.

19. Sod, G.A., "Automotive Engine Modeling with a Hybrid Random Choice Method," SAE Paper No. 790242, Society of Automotive Engineers, Warrendale, PA, 1979.

20. Sod, G.A., "A Hybrid Random Choice Method with Application to Internal Combustion Engines II," LBL-9423, Lawrence Berkeley Laboratory, The University of California, Berkeley, 1979.

21. Ashurst, W.T., "Vortex Dynamic Calculation of Fluid Motion in a Four Stroke Piston 'Cylinder' - Planar and Axisymmetric Geometry," SAND 78-8229, Sandia Laboratories, Livermore, CA, 1978.

22. Diwaker, R., Anderson, Jr., J.D., Griffin, M.D., and Jones E., "Inviscid Solutions of the Flowfield in an Internal Combustion Engine," AIAA Journal, Vol. 14, 1976, pp. 1667-1668.

23. Griffin, M.D., Anderson, Jr., J.D., and Diwaker, R., "Navier-Stokes in an Internal Combustion Engine," AIAA Journal, Vol. 14, 1976, pp. 1665-1666.

24. Griffin, M.D., Diwaker, R., Anderson, Jr., J.D., and Jones, E., "Computational Fluid Dynamics Applied to the Flow in an Internal Combustion Engine," AIAA Paper No. 78-57, American Institute of Aeronautics and Astronautics, New York, NY, 1978.

25. Griffin, M.D., Anderson, Jr., J.D., and Jones, E., "Computational Fluid Dynamics Applied to Three-Dimensional Nonreacting Inviscid Flows in an Internal Combustion Engine," Journal of Fluids Engineering, Vol. 101, 1979, pp. 367-372.

26. Ramos, J.I., Humphrey, J.A.C., and Sirignano, W.A., "Laminar Flow Calculations in Internal Combustion Engines," MAE Report No. 1409, Department of Mechanical and Aerospace Engineering, Princeton University, Princeton, NJ, October, 1975.

27. Ramos, J.I., Humphrey, J.A.C., and Sirignano, W.A., "Turbulent Flow Calculations in Internal Combustion Engines," MAE Report No. 1410, Department of Mechanical and Aerospace Engineering, Princeton University, Princeton, NJ, October, 1978.

28. Ramos, J.I., Humphrey, J.A.C., and Sirignano, W.A., "Numerical Prediction of Axisymmetric Laminar and Turbulent Flows in Motored, Reciprocating Internal Combustion Engines," SAE Paper No. 790356 Society of Automotive Engineers, Warrendale, PA, 1979.

29. Ramos, J.I., and Sirignano, W.A., "Axisymmetric Flow Model with and without Swirl in a Piston-Cylinder Arrangement with Idealized Value Operation," SAE Paper No. 800284, Society of Automotive Engineers, Warrendale, PA, 1980.

30. Ramos, J.I., and Sirignano, W.A., "Axisymmetric Flow Model in a Piston Cylinder Arrangement with Detailed Analysis of the Valve Region," SAE Paper No. 800286, Society of Automotive Engineers, Warrendale, PA, 1980.

31. Ramos, J.I., "Axisymmetric Flows in Spark-Ignition Engines," Report CO/80/2, Department of Mechanical Engineering, Carnegie-Mellon University, Pittsburgh, PA, 1980.

32. Gosman, A.D., Johns, R.J.R., and Watkins, A.P., "Development of Prediction Methods for In-Cylinder Processes in Reciprocating Engines," Combustion Modeling in Reciprocating Engines, J.N. Mattavi and C.A. Amann, Eds., Plenum Press, New York, 1980, pp. 69-129.

33. Ahmadi-Befrui, B., Gosman, A.D., Lockwood, F.C., and Watkins, A.P., "Multidimensional Calculation of Combustion in an Idealized Homogeneous Charge Engine: a Progress Report," SAE Paper No. 810151 Society of Automotive Engineers, Warrendale, PA, 1981.

34. Gosman, A.D. and Johns, R.J.R., "Development of a Predictive Tool for In-Cylinder Gas Motion in Engines," SAE Paper No. 780315, Society of Automotive Engineers, Warrendale, PA, 1978.

35. Gosman, A.D. and Johns, R.J.R., "Computer Analysis of Fuel-Air Mixing in Direct-Injection Engines," SAE Paper No. 800091, Society of Automotive Engineers, Warrendale, PA, 1980.

36. Shih, T. I-P., Smith, G.E., and Springer, G.S., "Numerical Simulation of the Flow and Fuel-Air Mixing in an Axisymmetric Piston-Cylinder Arrangement," NASA TM 83011, 1982.

37. Shih, T. I-P., Smith, G.E., and Springer, G.S., "Vortex Motion in Axisymmetric Piston-Cylinder Configurations," AIAA Journal, Vol. 22, 1984, pp. 512-513.

38. Armaly, B.F., and Durst, F., Pereira, J.C.F. and Schonung, B., "Experimental and Theoretical Investigations of Backward-Facing Step Flow," Journal of Fluid Mechanics, Vol. 127, 1983, pp. 473-496.

39. Roberts, G.O., "Computational Meshes for Boundary Layer Problems," Lecture Notes in Physics, Proc. Second Int. Conf. Num. Methods Fluid Dyn., Springer-Verlag, New York, NY, Vol. 8, 1971, pp. 171-177.

40. Anderson, D.A., Tannehill, J.C. and Pletcher, R.H., Computational Fluid Mechanics and Heat Transfer, Hemisphere, New York, 1984.

41. MacCormack, R.W. and Paullay, A.J.,"Computational Efficiency Achieved by Time Splitting of Finite Difference Operators," AIAA Paper 72-154, San Diego, CA, 1972.

42. Stone, H.S., Introduction to Computer Architecture, 2nd Ed., Science Research Associates, Chicago, IL, 1980.

43. Koggi, P.M., The Architecture of Pipelined Computers, Hemisphere Publishing Corp., Washington, DC, 1981.

44. Sydow, P.J., Cray Computer Systems Technical Note Optimization Guide, SN-0220, 1982.

45. Denham, M.K. and Patrick, M.A., "Laminar Flow Over a Downstream-Facing Step in a Two-Dimensional Flow Channel," Trans. Instn Chem. Engrs, Vol. 52, 1974, pp. 361-367.

BIOGRAPHICAL SKETCH

Douglas Hofer is a graduate of the University of Florida with a bachelor's degree in mechanical engineering. He is currently pursuing a Ph.D. at Purdue University. He is 23 years old, married, with no children.

I certify that I have read this study and that in my opinion it conforms to acceptable standards of scholarly presentation and is fully adequate, in scope and quality, as a thesis for the degree of Master of Science.

Tom I-P. Shih, Chairman
Assistant Professor of Mechanical Engineering

I certify that I have read this study and that in my opinion it conforms to acceptable standards of scholarly presentation and is fully adequate, in scope and quality, as a thesis for the degree of Master of Science.

Roger A. Gater
Associate Professor of Mechanical Engineering

I certify that I have read this study and that in my opinion it conforms to acceptable standards of scholarly presentation and is fully adequate, in scope and quality, as a thesis for the degree of Master of Science.

Ulrich H. Kurzweg
Professor of Engineering Sciences

This thesis was submitted to the Graduate Faculty of the College of Engineering and to the Graduate School and was accepted as partial fulfillment of the requirements for the degree of Master of Science.

December 1987

Dean, College of Engineering

Dean, Graduate School